Modeling and analysis of chemical reactions in catalytic pellets with non-uniform catalyst distribution

Zhanar Marx, BS Oil and Gas Engineering

Submitted in fulfilment of the requirements for the degree of Master of Science in Chemical & Materials Engineering

School of Engineering and Digital Sciences

Department of Chemical & Materials Engineering

Nazarbayev University

53 Kabanbay Batyr Avenue,

Astana, Kazakhstan, 010000

Supervisors: Prof. Boris Golman

Co-Supervisor: Prof. Piotr Skrzypacz

April 2024

Declaration form

I hereby, declare that this manuscript, entitled “Modeling and analysis of chemical reactions in catalytic pellets with non-uniform catalyst distribution”, is the result of my own work except for quotations and citations which have been duly acknowledged.

I also declare that, to the best of my knowledge and belief, it has not been previously or concurrently submitted, in whole or in part, for any other degree or diploma at Nazarbayev University or any other national or international institution.

Name: Zhanar Marx
Date: April 30, 2024

Abstract

This thesis explores the modeling and analysis of chemical reactions in catalytic pellets with non-uniform catalyst distribution, focusing mainly on core-shell structures with an inert shell. Recognizing the critical role of heterogeneous catalysis in various industrial processes, this study delves into how the spatial distribution of the active catalytic material within the pellets influences reaction efficiency and catalyst performance. Utilizing a combination of analytical and numerical methods, this research addresses the distribution of active material following a Gaussian profile within a spherical and slab-type pellet, a scenario less explored in existing literature. The study conducted modeling of core-shell catalytic pellets with an inert shell, examining two particle shapes: sphere and slab. Analytical solutions for the intra-particle reactant concentration were obtained by solving reaction-diffusion equations for an isothermal irreversible first-order reaction. Then, the mass balance equations were solved numerically and compared with the corresponding analytical solutions. Consequently, the mathematical model and its numerical solution were developed to include a Gaussian distribution of catalytic material in the active layer, and the equations are derived to account for non-isothermal reactions with arbitrary kinetics. The findings highlight the impact of the distribution of active material on the catalytic reaction rates, demonstrating that non-uniform distribution, particularly the Gaussian profile, can enhance catalyst performance compared to uniform distribution. Additionally, the parametric analysis on the effect of process and reaction parameters on catalyst effectiveness factor is carried out.

Keywords: heterogeneous catalysis, core-shell pellets, Gaussian activity distribution, power-law kinetics, numerical analysis, parametric study.

Acknowledgments

Firstly, I would like to express my uttermost gratitude to my supervisors, Professor Boris Golman and Professor Piotr Skrzypacz. Their supervision and direction throughout the duration of my studies have allowed me to successfully complete this Master's program. I am grateful for all the hours of discussion they have offered me. I am also immensely grateful to Professor Vsevolod Andreev, who provided significant assistance and advice during the preparation of this thesis.

Secondly, I extend my appreciation to the university for providing the necessary resources and software that enabled me to conduct the analytical simulations. The access to these tools has been vital in achieving the research objectives.

I wish to express my gratitude to my family members for their support and encouragement throughout the duration of this thesis. Their belief in my capabilities has been my constant source of strength and motivation.

Table of Contents

List of Abbreviations & Symbols

$a(\underline{x})$	=	dimensionless catalyst distribution	[-]
B	=	normalizing factor	[-]
Bi_h	=	Biot number for heat transfer	[-]
Bi_m	=	Biot number for mass transfer	[-]
$\underline{c}_i$	=	dimensionless intra-particle reactant concentration in i^{th} region	[-]
$C_i(x,t)$	=	reactant concentration in i^{th} region	[mol m^{-3}]
C_b	=	reactant concentration in bulk phase surrounding pellet	[mol m^{-3}]
$\tilde{C}_b$	=	time-independent bulk concentration	[mol m^{-3}]
c_{pi}	=	effective specific heat capacity in pores in i^{th} region	[J kg^{-1} K^{-1}]
D_{ei}	=	effective diffusivity of i^{th} region	[m^2 s^{-1}]
F	=	area of the slab surface perpendicular to x-axis	[m^2]
$f(\underline{c}_2,\theta_2)$	=	dimensionless reaction rate	[-]
g_0	=	catalyst density	[kg m^{-3}]
$g(x)$	=	catalyst distribution function	[-]
h	=	heat transfer coefficient	[W m^{-2} K^{-1}]
$h_I,\ h_{II},\ h_{III}$	=	mesh spacing in each region	[m]
$(-\Delta H_{r_A})$	=	heat of reaction per mole of reactant A	[J mol^{-1}]
J_A	=	productivity of species A	[mol s^{-1}]
J_b	=	pellet productivity at bulk concentration and temperature	[mol s^{-1}]
k	=	kinetic constant	[s^{-1}]
$k_{2,1}$	=	ratio of effective conductivities in regions ii and i	[-]

$k_{2,3}$	=	ratio of effective conductivities in regions ii and iii	[-]
k_{ei}	=	effective conductivity in i^{th} region	[W m^{-1} K^{-1}]
k_f	=	mass transfer coefficient	[m s^{-1}]
K	=	number of interior mesh points in region 3	[-]
M	=	number of interior mesh points in region 2	[-]
N	=	number of interior mesh points in region 1	[-]
R	=	pellet radius for cylindrical and spherical geometries or half-thickness for planar geometry	[m]
r_1	=	dimensionless distance from center to inner radius of intermediate active shell	[-]
r_2	=	dimensionless distance from center to outer radius of intermediate active shell	[-]
r_A	=	rate of reaction of species A	[m s^{-1}]
t	=	time	[s]
t_{d2}	=	characteristic diffusion time of reactant in i^{th} layer of porous pellet	[-]
t_{hi}	=	characteristic heat conduction time in i^{th} region	[-]
T_i	=	temperature in i^{th} region	[K]
T_b	=	bulk phase temperature	[K]
$\tilde{T}_b$	=	time-independent bulk temperature	[K]
V_0	=	volume	[m^3]
x_1	=	center of Gaussian distribution function	[m]
x	=	distance	[m]
$\underline{x}_1$	=	dimensionless center of Gaussian function	[-]
x_I	=	inner radius of intermediate active shell	[m]
x_{II}	=	outer radius of intermediate active shell	[m]
$\underline{x}$	=	dimensionless distance	[-]

z	=	geometric factor	[-]
ζ	=	ratio of effective diffusivities of 2 and 3 regions	[-]
ζ'	=	ratio of effective diffusivities of 1 and 2 regions	[-]
ε_i	=	porosity of i^{th} region	[-]
τ	=	dimensionless time	[-]
ϕ	=	Thiele modulus	[-]
Δ_{x_1}	=	width of Gaussian distribution	[m]
Δ	=	dimensionless width of Gaussian distribution	[-]
θ_i	=	dimensionless temperature in i^{th} region	[-]
ρ_i	=	effective density of porous pellet in i^{th} region	[kg m^{-3}]
ψ_i	=	ratio of characteristic times of diffusion and heat conduction for i^{th} region	[-]
β	=	energy generation function	[-]
ε_g	=	factor for each shape of pellet	[-]
η	=	dimensionless effectiveness factor	[-]
γ	=	Arrhenius number	[-]

List of Figures

List of Tables

Chapter 1 – Introduction

Heterogeneous catalysis plays a crucial role in chemical engineering and industrial processes and finds applications ranging from chemical synthesis to pollution control. The efficiency of catalytic reactions depends not only on the nature of the active material but also on its spatial distribution within porous supports. While conventional approaches often assume uniform catalyst distribution, many researchers have paid attention to non-uniformly distributed active material in the pellet.

The core-shell structure refers to a catalyst particle with a core material surrounded by a shell of a different material. It has been demonstrated that tailoring the structure to suit a specific catalytic application can yield superior performance compared to conventional catalysts [7]. For example, to study the effectiveness factor of the pellet and performance of fixed bed reactor, core-shell spherical pellets with inert core were designed by Li et al [12]. However, core-shell pellets with inert shells have been studied rarely. Core-shell catalyst pellets with inert shells can be considered as non-uniformly distributed since active material is concentrated in the center while the inert shell is deactivated part near the surface of the pellet. Hence, another possible way to predict reactor's performance is to develop a modeling of core-shell pellets with inert shells.

In a previous study, Cho derived reaction-diffusion equations for a core-shell pellet with an inert shell for different morphologies with step-distribution of active material [5]. The concentration profiles of a reactant in three regions were predicted by solving the coupled ordinary differential equations (ODEs) analytically. The effectiveness factor was investigated by varying reaction parameters such as Biot number, the peak and width of the Gaussian distribution function, and active core radius.

The present work is an attempt to analyze the impact of the active material distribution, specifically following a Gaussian distribution, on the catalyst performance in the case of slab-type and spherical pellets. For this purpose, the distribution of active material inside a core-shell catalyst pellet with an inert shell will be discussed. The mass and heat balances will be derived for the catalytic chemical reaction with power-law kinetics in the slab-type and spherical pellets with Gaussian distribution of active sites in the intermediate layer. The numerical algorithm and computer program will be developed to solve the model equation using the method of lines with finite difference approximation of derivatives. The numerical algorithm and computer program will be verified by comparison with analytical solution

derived by Cho for the first-order reaction in a core-shell pellet with step distribution of active material in an intermediate layer [5]. The concentration and temperature profiles in the catalytic pellets with Gaussian distribution of active material will be calculated and plotted for various process parameters. Additionally, the impact of activity distribution on the effectiveness factor for different process parameters will be discussed.

1.1 Objectives

The objectives of this thesis are:

- To derive an expression for the effectiveness factor that accounts for the Gaussian distribution of catalytic active material within the pellet.
- To investigate the effect of the Gaussian distribution on catalyst effectiveness factor in a core-shell pellet structure.
- To demonstrate the enhanced performance of catalysts with non-uniform distribution compared to those with uniform distribution.

Chapter 2 - Literature review

Heterogeneous catalysis finds extensive application in chemical, refinery, and pollution control processes. Consequently, the optimization of catalyst performance is a critical concern for chemical engineers, aiming to maximize reaction rates, reduce energy consumption, and enhance product yields.

The distribution of active material within a pellet is one of the methods to improve the catalyst performance in chemical reactions. The way in which the catalytic material is distributed impacts key factors that determine the efficiency and effectiveness of the catalytic process, including the movement of reactants and products to and from the active sites and thermal management within the pellet. Hence, identifying the best conditions for executing specific non-stationary reaction-diffusion processes in porous granules with non-uniform catalyst distribution requires not only experimental studies but also numerical analyses using a mathematical model.

Researchers have been investigating the impact of non-uniform catalyst distribution since the 1960s. For instance, Kasaoka and Sakata analytically expressed the relationship between the effectiveness factor and catalyst activity distribution [11]. Another early study by Verykios et al. demonstrated higher selectivity and yield in a fixed bed reactor with a non-uniform distribution of catalytic pellets compared to uniform catalysts [21]. These pioneering studies provided the groundwork for subsequent research.

In [18], a model featuring different nonuniform active site profiles (eggshell, egg white, egg yolk) to optimize conditions for specific chemical substances is introduced. They discussed how the morphological properties of heterogeneous catalysts, particularly non-uniform active phase distribution, can significantly enhance catalytic system performance. This research focuses on the impact of the active phase's distribution and thickness within catalytic particles and demonstrates that such attributes can critically influence catalyst synthesis strategies. The study uses a modeling approach in a batch reactor with various catalytic particle types (egg shell, egg white, and egg yolk) to explore how the location of the active zone affects reaction outcomes, particularly aiming to improve selectivity for a desired intermediate product.

In [17], the authors examine the influence of active phase distribution within spherical catalytic particles on the yield and selectivity for a series of reactions where the intermediate is the main product. The study highlights different active phase distributions, such as egg-shell,

egg-yolk, and egg-white, and uses intraparticle mass and energy balances to identify optimal conditions for maximizing the intermediate yield. It suggests that egg-shell catalysts can maximize this yield with lower active-phase usage, providing a notable example of how non-uniform distribution can enhance catalyst performance.

In [8], it was shown that egg-shell distribution allows to save 30 % of catalytically active material compared to conventional uniform distribution for methane steam reforming. In this study, the authors investigated three kinetic expressions for methane steam reforming, each with different dependencies on methane and water partial pressures. Subsequently, two methane steam reforming reactors were simulated, utilizing pelletized catalysts with uniform and eggshell configurations to achieve consistent nomenclature for active site distributions.

Thuy et al. examined egg-shell and core-shell distribution of zeolite catalysts in hydrocarbon processing. Experiments conducted with catalytic testing utilizing the methanol-to-hydrocarbon (MTH) reaction revealed that core–shell zeolites demonstrate extended lifetimes, increased total turnovers, and an unforeseen enhancement of the aromatic cycle within the hydrocarbon pool mechanism. Acid titration conducted in a time-resolved manner on both core and core–shell catalysts verified that the siliceous shell introduces a hydrophobic exterior, thereby affecting molecular diffusion [12].

Recently, Bizon et al. distributed active material uniformly and on the outer surface of the catalyst pellet, observing enhanced selectivity with the second catalyst profile [4]. Moreover, the utilization of an eggshell distribution of nickel, serving as the catalyst's active material, proved to be more effective and economically advantageous for steam methane reforming reactions [20][18]. In a related context, Boukezoula et al. explored the benefits of nonuniform catalyst activity distribution in fixed bed reactors, particularly in naphtha catalytic reforming [3].

Distribution of active material on the other surface to achieve better performance was also examined by Xu et al. The authors prepared egg-shell type catalyst with the Ag-shell. They showed that optimized thickness of the Ag shell in the egg-shell-type pellet catalyst would lead to improved hydrogenation activity and selectivity towards methyl glycolate [24].

These studies underscore the potential benefits of non-uniform catalyst distributions, including improved selectivity and efficiency, offering valuable insights for optimizing catalytic processes in the chemical industry.

More recently, there has been a focus on modeling core-shell spherical pellets featuring an inert core. This modeling has been conducted to analyze fixed bed reactors in the context of isothermal first-order reactions. The investigation aims to understand the impact of inert-core thickness on the effectiveness factor and overall reactor performance, as explored by Li et al. [14]. Lately, researchers have extended their consideration to core-shell catalytic pellets with inert cores. This extension includes the modeling of series reactions, particularly relevant to petrochemical industries. The analysis involves evaluating the secondary effectiveness factor of intermittent products across various reactors employing core-shell structured catalysts. This research, conducted by Cho [6][7], Peters [16], and Zadeh and Peters [25], helps to enhance understanding of these complex systems.

While core-shell pellets with inert cores have been investigated in this systematic manner, core-shell pellets with inert shells have received comparatively less attention. These micro-structured catalysts, although rarely studied, show promise for applications such as CO_2 methanation due to their high selectivity and thermal stability, as highlighted by Zimmermann et al. [26].

Expanding the scope, not only core-shell pellets with inert shells but also core-shell adsorbents with protective shells have been synthesized. In these cases, an inert component is coated onto the core of activated carbon, serving as an adsorbent for endocrine-disrupting chemicals (EDCs). This suggests that core-shell particles with inert shells play a crucial role in both catalyst engineering and separation technology, as indicated by Ndagijimana et al. [15]. Therefore, it becomes imperative to advance the modeling of core-shell catalytic pellets with inert shells to predict reactor performance in chemical industries. This is crucial since an inert-shell catalyst can essentially be regarded as catalytic pellets with a deactivated portion near the surface of the pellets.

This study introduces a novel approach by focusing on non-isothermal catalytic reactions in core-shell pellets with non-uniformly distributed active material, that has not been considered by previous studies.

Chapter 3 – Modeling Equations

In this chapter, mathematical models are formulated to describe catalytic reactions within pellets of various geometries, considering the non-uniform distribution of active catalytic material throughout the pellet. Initially, the mass balance equations are derived for catalytic pellets with a step distribution of active material. Subsequently, the model is expanded to include a Gaussian distribution of catalytic material in the active layer, and the equations are derived to account for non-isothermal reactions with arbitrary kinetics. Finally, the model is established to describe catalytic reactions occurring under forced unsteady-state conditions.

3.1 Modeling of catalytic pellets with step distribution of active material

The reaction-diffusion processes are considered within isothermal porous catalyst pellets exhibiting planar, cylindrical, and spherical symmetries while also accounting for resistance to mass transfer in the boundary layer surrounding the pellet.

A porous pellet consists of three distinct regions, as illustrated in **Figure 3.1**. The first region constitutes a catalytically inactive core located in the central part of the pellet. The second region comprises a catalytically active porous shell situated in direct contact with the outer surface of the central core. Catalyst is assumed to be uniformly distributed in this region. The third external region is also composed of catalytically inactive material.

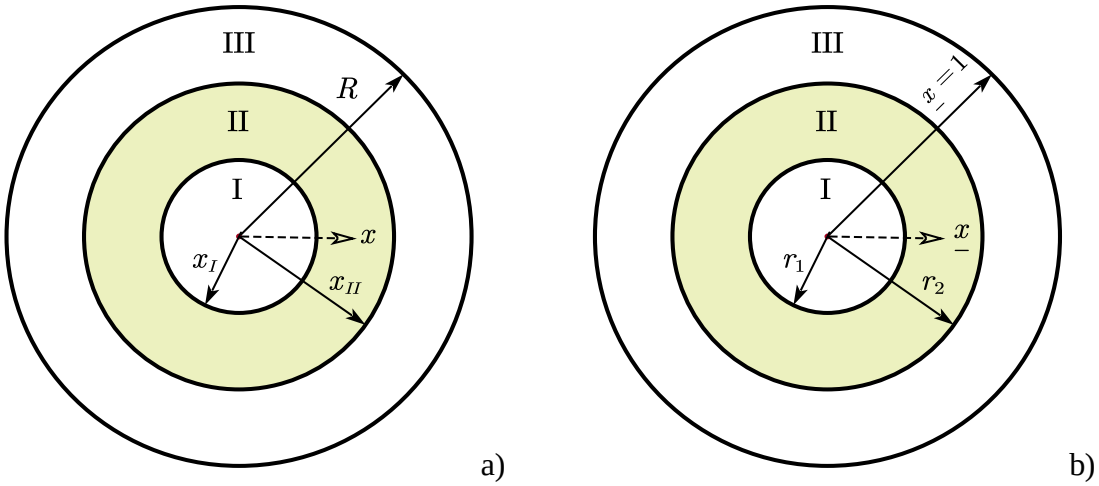

Figure 3.1: Schematic representation of catalytic pellet with step-distributed active component. The regions within the pellet are labeled as I, II, and III, corresponding to the inert core, active layer, and outer inert layer, respectively: a) dimension, b) dimensionless.

The reactant concentration, temperature, and model parameters in the first region are denoted by the subscript 1. Similarly, for the second and third regions, the subscripts 2 and 3 are used for designation, respectively.

The unsteady-state material balance equations for each region are derived by considering the first-order irreversible reaction and diffusion in the second region, as well as diffusion in the first and third regions.

$$\text{Region } 1,\ 0<\underline{x}<r_1:\ \ \varepsilon_1\zeta'\frac{\partial \underline{c}_1}{\partial\tau}=\frac{1}{\underline{x}^z}\frac{d}{d\underline{x}}\left(\underline{x}^z\frac{d\underline{c}_1}{d\underline{x}}\right), \tag{1}$$

$$\text{Region } 2,\ r_1<\underline{x}<r_2:\ \ \varepsilon_2\frac{\partial \underline{c}_2}{\partial\tau}=\frac{1}{\underline{x}^z}\frac{d}{d\underline{x}}\left(\underline{x}^z\frac{d\underline{c}_2}{d\underline{x}}\right)-\phi^2\cdot\underline{c}_2, \tag{2}$$

$$\text{Region } 3,\ r_2<\underline{x}<1:\ \ \varepsilon_3\zeta\frac{\partial \underline{c}_3}{\partial\tau}=\frac{1}{\underline{x}^z}\frac{d}{d\underline{x}}\left(\underline{x}^z\frac{d\underline{c}_3}{d\underline{x}}\right). \tag{3}$$

A symmetry boundary condition is imposed at the pellet center.

$$\text{Pellet center, } \underline{x}=0:\frac{\partial \underline{c}_1}{\partial\underline{x}}(0,\tau)=0. \tag{4}$$

The external mass transfer resistance on the outer pellet surface is taken into account.

$$\text{Pellet surface, } \underline{x}=1:\frac{\partial \underline{c}_3}{\partial\underline{x}}(1,\tau)=Bi_m(1-\underline{c}_3(1,\tau)). \tag{5}$$

The boundary conditions on the inner and outer boundaries of the intermediate layer are formulated by considering the continuity of the concentration profile in the pellet and the equality of fluxes at the boundaries.

$$\text{Inner boundary of intermediate layer, } \underline{x}=r_1:\ \underline{c}_1(r_1,\tau)=\underline{c}_2(r_1,\tau), \tag{6}$$

$$\frac{\partial \underline{c}_1}{\partial\underline{x}}(r_1,\tau)=\zeta'\frac{\partial \underline{c}_2}{\partial\underline{x}}(r_1,\tau) \tag{7}$$

$$\text{Outer boundary of intermediate layer, } \underline{x}=r_2:\ \underline{c}_2(r_2,\tau)=\underline{c}_3(r_2,\tau) \tag{8}$$

$$\zeta\frac{\partial \underline{c}_2}{\partial\underline{x}}(r_2,\tau)=\frac{\partial \underline{c}_3}{\partial\underline{x}}(r_2,\tau) \tag{9}$$

Here, $\underline{c}_i$ refers to the dimensionless intra-particle reactant concentration in the i^{th} region, defined as $\underline{c}_i(\underline{x},\tau) = \frac{C_i(x,t)}{C_b}$, where $C_i(x,t)$ represents the reactant concentration in the i^{th} region, and C_b is the reactant concentration in the bulk phase surrounding the pellet. The dimensionless distance $\underline{x}$ is specified as $\underline{x} = \frac{x}{R}$, where R is the pellet radius for cylindrical and spherical geometries or half-thickness for planar geometry. The dimensionless distances from the center to the inner and outer radii of the intermediate active shell are defined in units of R as $r_1 = \frac{x_I}{R}$ and $r_2 = \frac{x_{II}}{R}$, where x_I and x_{II} are the inner and outer radius of intermediate active shell, respectively. The geometric factor z defines the pellet geometry with $z = 0$, $z = 1$ and $z = 2$ for planar, cylindrical and spherical geometries, respectively. The ratios of effective diffusivities in adjacent regions ζ and ζ' are denoted as $\zeta = \frac{D_{e2}}{D_{e3}}$ and $\zeta' = \frac{D_{e2}}{D_{e1}}$, respectively. The porosity of the i^{th} region is denoted as ε_i. The dimensionless time τ is specified as $\tau = \frac{t}{t_{d2}}$, where $t_{di} = \frac{R^2}{D_{ei}}$ represents the characteristic diffusion time of reactant in the i^{th} layer of a porous pellet and t is the time. The Biot number for mass transfer Bi_m and the Thiele modulus for the first-order irreversible reaction are defined as $Bi_m = \frac{R \cdot k_f}{D_{e3}}$ and $\phi = \sqrt{\frac{R^2 \cdot k}{D_{e2}}}$, where k_f represents the mass transfer coefficient and k denotes the kinetic constant, respectively.

3.2 Modeling of non-uniform distribution of active catalytic sites in porous pellet

The reaction-diffusion processes are considered within non-isothermal porous pellet with the non-uniform profile of catalyst distribution throughout its depth. A porous pellet consists of three regions, with the second region being an active shell with a Gaussian spatial distribution of catalytically active material, while the other regions comprise an inactive internal core and an external layer. To compare the productivity and effectiveness of catalyst pellets

with different sizes of catalytically active porous shells and various distributions of active material, it is assumed that the amount of catalyst in a pellet is the same in all cases.

The density of the catalyst per unit volume of V_0 is denoted by g_0. If the total amount of catalyst is equal to $g_0 V_0$, then the catalyst distribution function for Gaussian profile in the active region is given as:

$$g(x) = B \cdot \exp\left(-\frac{(x - x_1)^2}{\Delta_{x_1}^2}\right), \tag{10}$$

where Δ_{x_1} is the width of the distribution, x_1 is the center of the Gaussian function, x is the distance, and B is the normalizing factor. Thus, the normalization condition for a constant amount of catalyst in porous pellets can be derived as follows:

$$B\int_{x_I}^{x_{II}} \exp\left(-\frac{(x - x_1)^2}{\Delta_{x_1}^2}\right) x^z dx = g_0 \frac{R^{z+1}}{z+1}. \tag{11}$$

The dimensionless parameters of Gaussian function are defined as $\underline{x}_1 = \frac{x_1}{R}$ and $\Delta = \frac{\Delta_{x_1}}{R}$. Equations (10) and (11) are transformed into dimensionless form as follows:

$$a\left(\underline{x}\right) = \frac{g(x)}{g_0} = B \cdot \exp\left(-\frac{\left(\underline{x} - \underline{x}_1\right)^2}{\Delta^2}\right), \tag{12}$$

$$B = \frac{1}{(z+1)\int_{r_1}^{r_2} \exp\left(-\frac{\left(\underline{x} - \underline{x}_1\right)^2}{\Delta^2}\right) \underline{x}^z d\underline{x}}. \tag{13}$$

Here, $a\left(\underline{x}\right)$ is the dimensionless catalyst distribution function for $\underline{x} \in [r_1; r_2]$. If $\underline{x} \in [0; r_1)$ or $\underline{x} \in (r_2; 1]$, then

$$a\left(\underline{x}\right) \equiv 0. \tag{14}$$

The integral in Eq. (13) is analytically evaluated for each pellet geometry. Subsequently, analytical expressions are derived for Gaussian activity distribution profiles in the active layer. The final expressions are summarized in **Table 3.1**, and the detailed derivations are presented in **Appendix A**. The Gaussian distributions of active material in slab-type and spherical pellets are illustrated in **Figure 3.2** and **Figure 3.3**, respectively. Comparison of activity distribution

and normalized activity distribution functions in both slab-type and spherical pellets are demonstrated in **Figure 3.4** and **Figure 3.5**, respectively.

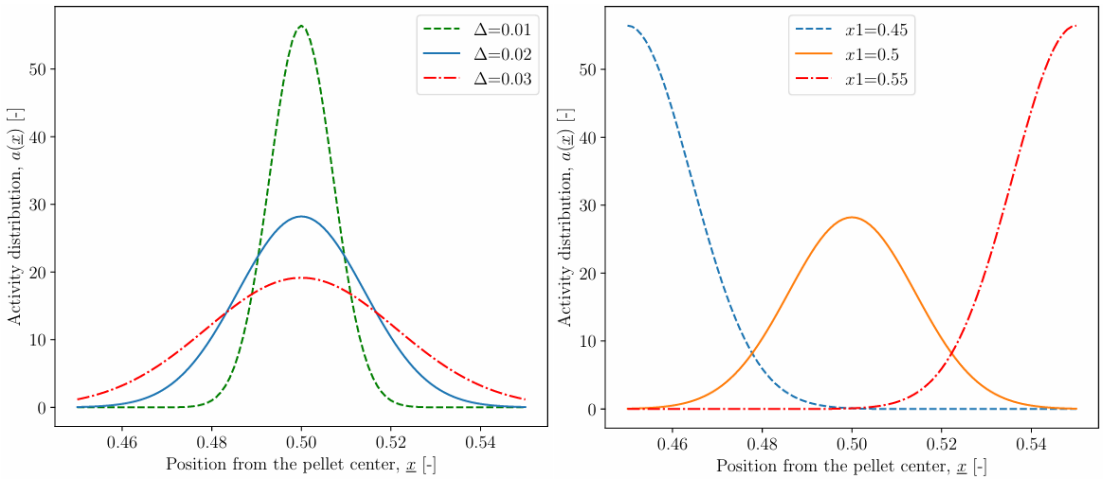

(a) (b)

Figure 3.2: Gaussian activity distributions in slab-type pellet for different distribution parameters:

(a) $\underline{x}_1 = 0.5$, $r_1 = 0.45$, $r_2 = 0.55$, ***(b)*** $\Delta = 0.02$, $r_1 = 0.45$, $r_2 = 0.55$.

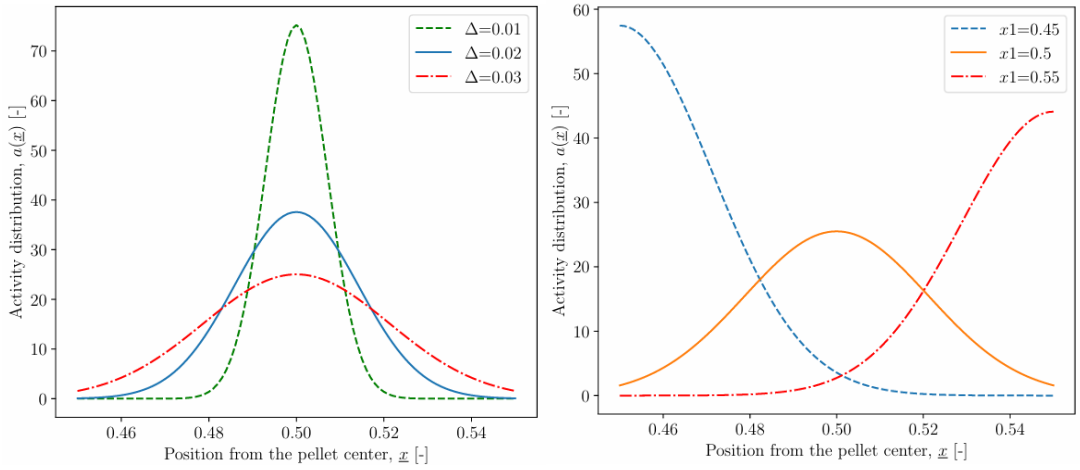

(a) (b)

Figure 3.3: Gaussian activity distributions in spherical pellet for different distribution parameters:

(a) $\underline{x}_1 = 0.5$, $r_1 = 0.45$, $r_2 = 0.55$, ***(b)*** $\Delta = 0.02$, $r_1 = 0.45$, $r_2 = 0.55$.

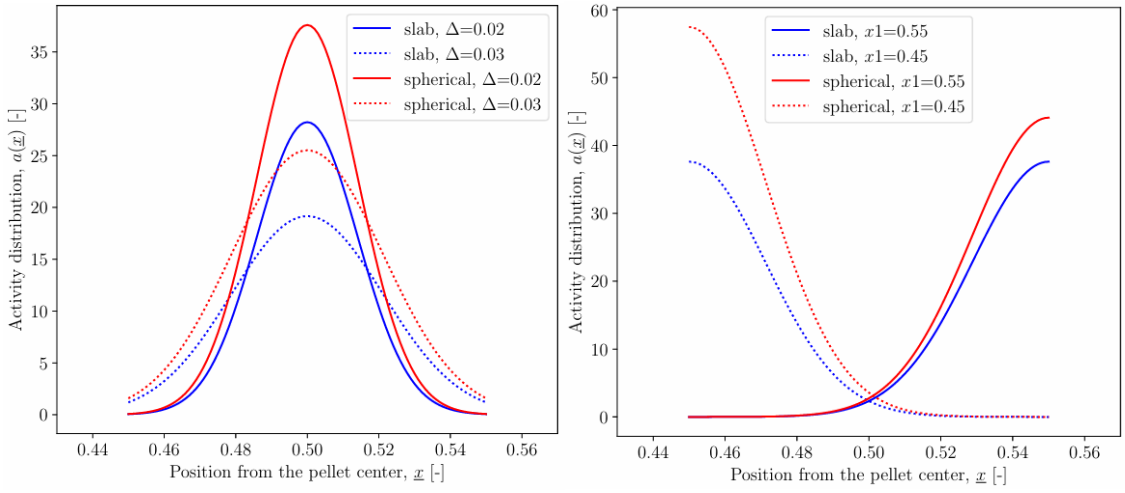

a) b)

Figure 3.4: Gaussian activity distributions in slab-type and spherical pellet for different distribution parameters:

(a) $\underline{x}_1 = 0.5$, $r_1 = 0.45$, $r_2 = 0.55$, ***(b)*** $\Delta = 0.03$, $r_1 = 0.45$, $r_2 = 0.55$.

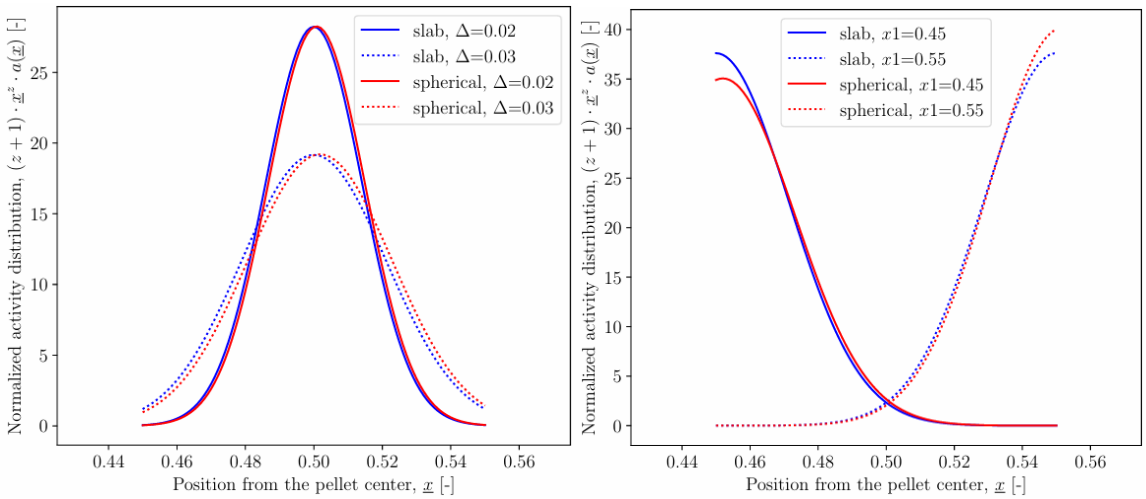

a) b)

Figure 3.5: Normalized activity distributions in slab-type and spherical pellet for different distribution parameters:

(a) $\underline{x}_1 = 0.5$, $r_1 = 0.45$, $r_2 = 0.55$, ***(b)*** $\Delta = 0.03$, $r_1 = 0.45$, $r_2 = 0.55$.

Table 3.1: Gaussian activity distribution profiles

Pellet geometry	Activity distribution
Plain, $z=0$	$a\left(\underline{x}\right)=\dfrac{\exp\left(-\dfrac{\left(\underline{x}-\underline{x}_1\right)^2}{\Delta^2}\right)}{\Delta\dfrac{\sqrt{\pi}}{2}\left(erf\left(\dfrac{r_2-\underline{x}_1}{\Delta}\right)-erf\left(\dfrac{r_1-\underline{x}_1}{\Delta}\right)\right)}$ (15)
Sphere, $z=2$	$a\left(\underline{x}\right)=\dfrac{\exp\left(-\dfrac{\left(\underline{x}-\underline{x}_1\right)^2}{\Delta^2}\right)}{\left(\begin{array}{c}\dfrac{3\sqrt{\pi}}{4}\left(\Delta^3+2\underline{x}_1^2\Delta\right)\left(erf\left(\dfrac{r_2-\underline{x}_1}{\Delta}\right)-erf\left(\dfrac{r_1-\underline{x}_1}{\Delta}\right)\right)- \\ \dfrac{3}{2}\Delta^2\left(\underline{x}_1+r_2\right)\cdot\exp\left(-\dfrac{\left(r_2-\underline{x}_1\right)^2}{\Delta^2}\right)+\dfrac{3}{2}\Delta^2\left(r_1+\underline{x}_1\right)\cdot\exp\left(-\dfrac{\left(r_1-\underline{x}_1\right)^2}{\Delta^2}\right)\end{array}\right)}$ (16)

A catalytic reaction occurring within the second intermediate porous shell of the pellet is expressed as follows:

$$A \xrightarrow{r_A} Products\,. \tag{17}$$

The dimensionless mass and heat balance equations for the unsteady-state case in the shell with a non-uniformly distributed catalyst are derived through a pseudo-homogeneous approach as follows:

$$\varepsilon_2\frac{\partial \underline{c}_2(\underline{x},\tau)}{\partial\tau}=\frac{1}{\underline{x}^z}\frac{\partial}{\partial\underline{x}}\left(\underline{x}^z\frac{\partial c_2(\underline{x},\tau)}{\partial\underline{x}}\right)-a\left(\underline{x}\right)\phi^2 f(\underline{c}_2,\theta_2) \tag{18}$$

$$\frac{1}{\psi_2}\frac{\partial\theta_2(\underline{x},\tau)}{\partial\tau}=\frac{1}{\underline{x}^z}\frac{\partial}{\partial\underline{x}}\left(\underline{x}^z\frac{\partial\theta_2(\underline{x},\tau)}{\partial\underline{x}}\right)+a\left(\underline{x}\right)\beta\phi^2 f(\underline{c}_2,\theta_2) \tag{19}$$

In the inactive central core of the pellet, the following mass and heat balances are developed:

$$\varepsilon_1\zeta'\frac{\partial \underline{c}_1(\underline{x},\tau)}{\partial\tau}=\frac{1}{\underline{x}^z}\frac{\partial}{\partial\underline{x}}\left(\underline{x}^z\frac{\partial \underline{c}_1(\underline{x},\tau)}{\partial\underline{x}}\right) \tag{20}$$

$$\frac{\zeta'}{\psi_1}\frac{\partial\theta_1(\underline{x},\tau)}{\partial\tau}=\frac{1}{\underline{x}^z}\frac{\partial}{\partial\underline{x}}\left(\underline{x}^z\frac{\partial\theta_1(\underline{x},\tau)}{\partial\underline{x}}\right) \tag{21}$$

In the inactive external shell, the mass and heat balances are given as:

$$\varepsilon_3 \zeta \frac{\partial \underline{c}_3(\underline{x},\tau)}{\partial \tau} = \frac{1}{\underline{x}^z} \frac{\partial}{\partial \underline{x}} \left(\underline{x}^z \frac{\partial \underline{c}_3(\underline{x},\tau)}{\partial \underline{x}} \right) \tag{22}$$

$$\frac{\zeta}{\psi_3} \frac{\partial \theta_3(\underline{x},\tau)}{\partial \tau} = \frac{1}{\underline{x}^z} \frac{\partial}{\partial \underline{x}} \left(\underline{x}^z \frac{\partial \theta_3(\underline{x},\tau)}{\partial \underline{x}} \right) \tag{23}$$

The boundary conditions in dimensionless form at the pellet center (i.e. $\underline{x} = 0$) and on the external surface of the pellet (i.e. $\underline{x} = 1$) are written as follows:

$$\left. \frac{\partial \underline{c}_1(\underline{x},\tau)}{\partial \underline{x}} \right|_{\underline{x}=0} = 0 \tag{24}$$

$$\left. \frac{\partial \theta_1(\underline{x},\tau)}{\partial \underline{x}} \right|_{\underline{x}=0} = 0 \tag{25}$$

$$\left. \frac{\partial \underline{c}_3(\underline{x},\tau)}{\partial \underline{x}} \right|_{\underline{x}=1} = Bi_m \left(1 - \underline{c}_3(1,\tau)\right) \tag{26}$$

$$\left. \frac{\partial \theta_3(\underline{x},\tau)}{\partial \underline{x}} \right|_{\underline{x}=1} = Bi_h \left(1 - \theta_3(1,\tau)\right) \tag{27}$$

The boundary conditions at the inner and outer boundaries of intermediate layer are specified in a manner similar to Eqs. (6) - (9) as follows:

Inner boundary of intermediate layer, $\underline{x} = r_1$: $\underline{c}_1(r_1,\tau) = \underline{c}_2(r_1,\tau)$ (28)

$$\left. \frac{\partial \underline{c}_1(\underline{x},\tau)}{\partial \underline{x}} \right|_{\underline{x}=r_1} = \zeta' \left. \frac{\partial \underline{c}_2(\underline{x},\tau)}{\partial \underline{x}} \right|_{\underline{x}=r_1} \tag{29}$$

$$\theta_1(r_1,\tau) = \theta_2(r_1,\tau) \tag{30}$$

$$\left. \frac{\partial \theta_1(\underline{x},\tau)}{\partial \underline{x}} \right|_{\underline{x}=r_1} = k_{2,1} \left. \frac{\partial \theta_2(\underline{x},\tau)}{\partial \underline{x}} \right|_{\underline{x}=r_1} \tag{31}$$

Outer boundary of intermediate layer, $\underline{x} = r_2$: $\underline{c}_2(r_2,\tau) = \underline{c}_3(r_2,\tau)$ (32)

$$\zeta \left. \frac{\partial \underline{c}_2(x,\tau)}{\partial \underline{x}} \right|_{\underline{x}=r_2} = \left. \frac{\partial \underline{c}_3(x,\tau)}{\partial \underline{x}} \right|_{\underline{x}=r_2} \tag{33}$$

$$\theta_2(r_2,\tau) = \theta_3(r_2,\tau) \tag{34}$$

$$k_{2,3} \left. \frac{\partial \theta_2(\underline{x},\tau)}{\partial \underline{x}} \right|_{\underline{x}=r_2} = \left. \frac{\partial \theta_3(\underline{x},\tau)}{\partial \underline{x}} \right|_{\underline{x}=r_2} \tag{35}$$

Here, $\theta_i(\underline{x},\tau) = \frac{T_i(x,t)}{T_b}$ denotes the dimensionless temperature in the i^{th} region, $T_i(x,t)$ is the temperature in the i^{th} region, T_b is the bulk phase temperature, $t_{hi} = \frac{R^2 \rho_i c_{pi}}{k_{ei}}$ is the characteristic heat conduction time in the i^{th} region, k_{ei} is the effective conductivity in the i^{th} region, c_{pi} and ρ_i are the effective specific heat capacity and effective density of the porous pellet with gas in the pores in the i^{th} region, respectively. The ratio of effective conductivities in regions II and I is denoted as $k_{2,1} = \frac{k_{e2}}{k_{e1}}$, while the ratio of effective conductivities in regions II and III is denoted as $k_{2,3} = \frac{k_{e2}}{k_{e3}}$. The ratio of characteristic times of diffusion and heat conduction for the i^{th} region is represented as $\psi_i = \frac{t_{di}}{t_{hi}}$. The Biot number for heat transfer is defined as $Bi_h = \frac{R \cdot h}{k_{e3}}$, where h is the heat transfer coefficient. The energy generation function is given as $\beta = \frac{(-\Delta H_{r_A}) C_b D_{e2}}{T_b \; k_{e2}}$, where $(-\Delta H_{r_A})$ is the heat of reaction per mole of reactant A. The dimensionless reaction rate is denoted as $f(\underline{c}_2, \theta_2) = \frac{r_A(C_2,T_2)}{r_A(C_b,T_b)}$ and the Thiele modulus is defined as $\phi^2 = \frac{R^2 r_A(C_b,T_b)\, g_0}{D_{e2}\; C_b}$. $\tilde{C}_b$ and $\tilde{T}_b$ represent the time-independent bulk concentration and bulk temperature, respectively. All dimensionless concentrations, temperatures and other parameters in Eqs. (18) - (35) are defined in units of $\tilde{C}_b$

and $\tilde{T}_b$, i.e. $\underline{c}_i(\underline{x},\tau)=\frac{C_i(x,t)}{\tilde{C}_b}$, $\theta_i(\underline{x},\tau)=\frac{T_i(x,t)}{\tilde{T}_b}$, $f(\underline{c}_2,\theta_2)=\frac{r_A(C_2,T_2)}{r_A(\tilde{C}_b,\tilde{T}_b)}$,

$\beta=\frac{(-\Delta H_{r_A})\tilde{C}_b D_{e2}}{\tilde{T}_b\ k_{e2}}$ and $\phi^2=\frac{R^2 r_A(\tilde{C}_b,\tilde{T}_b)\,g_0}{D_{e2}\tilde{C}_b}$.

The reaction described by scheme Eq. (17) is assumed to follow power-law kinetics with Arrhenius dependence on temperature, and the reaction rate in the dimensionless form is given as follows:

$$f(\underline{c},\theta)=\underline{c}^{\,n}\exp\left(\gamma\left(1-\frac{1}{\theta}\right)\right). \tag{36}$$

The productivity of species A in terms of physical quantities is determined as:

$$J_A=-\varepsilon_g R^z D_{e3}\left.\frac{\partial C_3}{\partial x}\right|_{x=R}. \tag{37}$$

When utilizing dimensionless concentration, distance, and time, the productivity can be expressed as follows:

$$J_A=-\varepsilon_g R^{z-1} D_{e3}\tilde{C}_b\left.\frac{\partial \underline{c}_3}{\partial \underline{x}}\right|_{\underline{x}=1} \tag{38}$$

Here, the factor ε_g is determined for each shape of the pellet: $\varepsilon_g=4\pi$ for a sphere, $\varepsilon_g=2\pi l$ for a cylinder with height l, $\varepsilon_g=2F$ for a slab, where F is the area of the slab surface perpendicular to the x-axis.

Since a single reaction is discussed in this paper, the performance of the catalyst is directly related to the effectiveness factor. The dimensionless effectiveness factor, particularly for pellets of various geometries containing catalytically active material, is a critical parameter that measures the efficiency of a catalyst. It is defined as the ratio of the actual reaction rate within the catalyst pellet to the reaction rate if the entire pellet were to react at the surface reaction rate, assuming no mass transfer limitations.

The dimensionless effectiveness factor for steady-state, applicable to pellets of various geometries containing catalytically active material within the second region, is defined in terms of productivities as follows:

$$\eta=\frac{J_A}{J_b} \tag{39}$$

The productivity of a porous catalyst pellet for species A at steady state refers to the rate at which species A is converted into product within the catalyst pellet. If we denote r_A as the rate of reaction of species A per unit volume of catalyst, the productivity of the catalyst for species A over the entire pellet can be calculated by integrating the rate of reaction over the volume of the pellet:

$$J_A = \int_{V_g} r_A dV \tag{40}$$

The productivity of species A is expressed in Eq. (38), while J_b represents the productivity of a pellet with non-uniform catalyst distributions at constant bulk concentration and temperature, i.e., $C_2 = \tilde{C}_b,\ T_2 = \tilde{T}_b$.

$$J_b = -\varepsilon_g g_0 r_A(\tilde{C}_b, \tilde{T}_b) R \int_{x_I}^{x_{II}} g(x) x^z dx \tag{41}$$

and in the dimensionless form as

$$J_b = -\varepsilon_g g_0 r_A(\tilde{C}_b, \tilde{T}_b) R^{z+1} \int_{r1}^{r2} a\left(\underline{x}\right) \underline{x}^z d\underline{x} \tag{42}$$

Since the total amount of catalyst is constant, the following expression is obtained:

$$\int_{r1}^{r2} a\left(\underline{x}\right) \underline{x}^z d\underline{x} = \frac{1}{z+1} \tag{43}$$

Inserting Eq. (43) into Eq. (42) will result in:

$$J_b = \frac{-\varepsilon_g g_0 r_A(\tilde{C}_b, \tilde{T}_b) R^{z+1}}{z+1} \tag{44}$$

Substituting Eqs. (38) and (44) into the Eq. (39) yields:

$$\eta = \frac{J_A}{J_b} = \frac{-\varepsilon_g R^{z-1} D_{e3} \tilde{C}_b \frac{\partial \underline{c}_3}{\partial \underline{x}}\left(\underline{x}, \tau\right)\Big|_{\underline{x}=1}}{\frac{-\varepsilon_g g_0 r_A(\tilde{C}_b, \tilde{T}_b) R^{z+1}}{z+1}} = \frac{D_{e3} \tilde{C}_b}{\frac{g_0 r_A(\tilde{C}_b, \tilde{T}_b) R^2}{z+1}} \frac{\partial \underline{c}_3}{\partial \underline{x}}\left(\underline{x}, \tau\right)\Big|_{\underline{x}=1}, \tag{45}$$

$$\eta = \frac{z+1}{\phi^2} \frac{\partial \underline{c}_3}{\partial \underline{x}}\left(\underline{x}, \tau\right)\Big|_{\underline{x}=1}$$

The effectiveness factor can also be calculated through integration as follows:

$$\eta = \frac{\int_{x_I}^{x_{II}} g(x) r_A(C_2, T_2) x^z dx}{\int_{x_I}^{x_{II}} g(x) r_A(\tilde{C}_b, \tilde{T}_b) x^z dx}. \tag{46}$$

When utilizing dimensionless concentration, temperature, and distance, the effectiveness factor can be expressed as follows:

$$\eta = \frac{\int_{r1}^{r2} f\left(\underline{c}, \theta\right) a\left(\underline{x}\right) \underline{x}^z d\underline{x}}{\int_{r1}^{r2} a\left(\underline{x}\right) \underline{x}^z d\underline{x}}. \tag{47}$$

Here, $f(\underline{c}, \theta) = \frac{r(C,T)}{r(C_b, T_b)}$ is described by Eq. (36).

Inserting Eq. (43) into Eq. (47) will result in:

$$\eta = (z+1) \int_{r1}^{r2} f\left(\underline{c}, \theta\right) a\left(\underline{x}\right) \underline{x}^z d\underline{x} \tag{48}$$

Chapter 4 – Solution of Model Equations

In this chapter, numerical methods are formulated to solve the mathematical model equations introduced in the previous chapter for slab-type and spherical pellets with a non-uniform distribution of active material. To validate the numerical scheme, analytical solutions are derived for the mass balance equations governing catalytic pellets with a step distribution of active material, and these analytical results are then compared with the corresponding numerical solutions. Subsequently, the model equations incorporating a Gaussian distribution of catalytic material in the active layer are solved numerically under isothermal conditions. Finally, the numerical solutions of the model equations for non-isothermal reactions are demonstrated.

4.1 Solution of steady-state mass balance equation in catalytic pellets with step distribution of active material

4.1.1 Analytical solution

The analytical solutions of steady-state mass balance equations for the first-order reaction in catalytic pellets with step distribution of active material were derived by solving Eqs. (1), (2), and (3) using the method of separation of variables [**18**]. The detail derivations are provided in **Appendix B**, and the results are summarized in **Table 4.1**.

4.1.2 Numerical solution

The numerical solution of steady-state mass balance equations governing the first-order reaction in catalytic pellets, characterized by a step distribution of active material, was obtained as the steady-state solution of the unsteady-state mass balance Eqs. (1) - (3). The method of lines was employed to solve the system of partial differential equations, utilizing a finite difference approximation for spatial derivatives [10, 11, 18]. The resulting system of ordinary differential equations is solved using the Python '*solve_ivp*' solver for stiff systems from the SciPy library [21].

Table 4.1: Analytical solution of steady-state mass balance equations in catalytic pellets with step distribution of active material

Pellet geometry	Normalized activity distribution	
Plain, $z=0$	$\underline{c}_1 = \dfrac{1}{cosh(\phi(r_2-r_1)) + \zeta\,\phi\,sinh(\phi(r_2-r_1))\left(1-r_2+\frac{1}{Bi}\right)}$ $\underline{c}_2(\underline{x}) = \dfrac{cosh(\phi r_1)\cdot cosh(\phi \underline{x}) - sinh(\phi r_1)\cdot sinh(\phi \underline{x})}{cosh(\phi(r_2-r_1)) + \zeta\,\phi\,sinh(\phi(r_2-r_1))\left(1-r_2+\frac{1}{Bi}\right)}$ $\underline{c}_3(\underline{x}) = 1 - \dfrac{\zeta\,\phi\,sinh(\phi(r_2-r_1))\left(1-\underline{x}+\frac{1}{Bi}\right)}{cosh(\phi(r_2-r_1)) + \zeta\,\phi\,sinh(\phi(r_2-r_1))\left(1-r_2+\frac{1}{Bi}\right)}$	(49)
Sphere, $z=2$	$\underline{c}_1 = \dfrac{\phi r_2 \;/\; cosh(\phi(r_2-r_1))}{((tanh(\phi(r_2-r_1))(\phi^2 r_1 r_2 - 1) + \phi(r_2-r_1))\,\zeta\left(1-r_2+\frac{r_2}{Bi}\right) + (\phi r_1 + tanh(\phi(r_2-r_1))))}$ $\underline{c}_2(x) = \dfrac{r_2}{cosh(\phi(r_2-r_1))} \dfrac{cosh(\phi \underline{x})(\phi r_1 cosh(\phi r_1) - sinh(\phi r_1)) + sinh(\phi \underline{x})(cosh(\phi r_1) - \phi r_1 sinh(\phi r_1))}{\underline{x}(tanh(\phi(r_2-r_1))(\phi^2 r_1 r_2 - 1) + \phi(r_2-r_1))\,\zeta\left(1-r_2+\frac{r_2}{Bi}\right) + (\phi r_1 + tanh(\phi(r_2-r_1)))}$ $\underline{c}_3(x) = 1 - \dfrac{\zeta r_2 (tanh(\phi(r_2-r_1))(\phi^2 r_1 r_2 - 1) + \phi(r_2-r_1))}{(tanh(\phi(r_2-r_1))(\phi^2 r_1 r_2 - 1) + \phi(r_2-r_1))\,\zeta\left(1-r_2+\frac{r_2}{Bi}\right) + (\phi r_1 + tanh(\phi(r_2-r_1)))} \left(\dfrac{1}{Bi} + \dfrac{1}{\underline{x}} - 1\right)$	(50)

Slab-type pellet

Introduce the uniform mesh with $N+M+K$ interior points, where N is the number of interior mesh points in the region 1, M is the number of interior mesh points in the region 2, and K is the number of interior mesh points in the region 3. The mesh spacing in each region is given as $h_I = \frac{r_1}{N+1}, h_{II} = \frac{r_2 - r_1}{M+1}$, $h_{III} = \frac{1-r_2}{K+1}$.

Figure 4.1 illustrates the interior mesh point with boundaries of all regions.

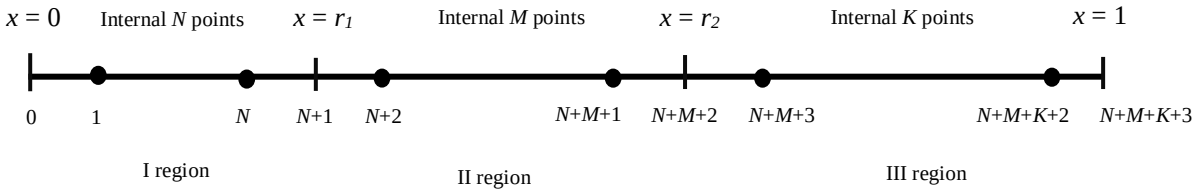

Figure 4.1: Illustration of finite-difference mesh in a pellet

Using the second-order central finite-difference approximations for the spatial derivatives in PDEs results in the following system of ODEs at the internal mesh points:

$$\frac{d\underline{c}_i}{d\tau} = \frac{1}{\varepsilon_1 \zeta'} \cdot \left[\frac{\underline{c}_{i+1} - 2\underline{c}_i + \underline{c}_{i-1}}{h_I^2} \right], \; i = 1, \cdots, N \tag{51}$$

$$\frac{d\underline{c}_i}{d\tau} = \frac{1}{\varepsilon_2} \cdot \left[\frac{\underline{c}_{i+1} - 2\underline{c}_i + \underline{c}_{i-1}}{h_{II}^2} - \phi^2 \cdot \underline{c}_i \right], \; i = N+2, \cdots, N+M+1 \tag{52}$$

$$\frac{d\underline{c}_i}{d\tau} = \frac{1}{\varepsilon_3 \zeta} \cdot \left[\frac{\underline{c}_{i+1} - 2\underline{c}_i + \underline{c}_{i-1}}{h_{III}^2} \right], \; i = N+M+3, \cdots, N+M+K+2. \tag{53}$$

The boundary condition, as described by Eqs. (4) - (9) are transformed into algebraic equations using the corresponding second-order finite difference approximations for the spatial derivatives. The formulas for calculating the concentration at the boundaries are derived as follows:

$$\underline{x} = 0 : \frac{-3\underline{c}_0 + 4\underline{c}_1 - \underline{c}_2}{2h_I} = 0$$

$$\underline{c}_0 = \frac{4\underline{c}_1}{3} - \frac{\underline{c}_2}{3} \tag{54}$$

$$\underline{x}=1:\frac{3\underline{c}_{N+M+K+3}-4\underline{c}_{N+M+K+2}+\underline{c}_{N+M+K+1}}{2h_{III}}=Bi\left(1-\underline{c}_{N+M+K+3}\right),$$

$$\underline{c}_{N+M+K+3}=\frac{2h_{III}Bi+4\underline{c}_{N+M+K+2}-\underline{c}_{N+M+K+1}}{3+2h_{III}Bi} \tag{55}$$

$$\underline{x}=r_1:\ \frac{3\underline{c}_{N+1}-4\underline{c}_{N}+\underline{c}_{N-1}}{2h_I}=\zeta'\frac{-3\underline{c}_{N+1}+4\underline{c}_{N+2}-\underline{c}_{N+3}}{2h_{II}} \tag{56}$$

$$\underline{c}_{N+1}\left(\frac{3}{2h_I}+\frac{3\zeta'}{2h_{II}}\right)=\zeta'\frac{4\underline{c}_{N+2}-\underline{c}_{N+3}}{2h_{II}}-\frac{-4\underline{c}_{N}+\underline{c}_{N-1}}{2h_I};$$

$$\underline{c}_{N+1}=\frac{\left(4\underline{c}_{N+2}-\underline{c}_{N+3}\right)\zeta' h_I-\left(\underline{c}_{N-1}-4\underline{c}_{N}\right)h_{II}}{3(h_I\zeta'+h_{II})} \tag{57}$$

$$\underline{x}=r_2:\ \zeta\frac{3\underline{c}_{N+M+2}-4\underline{c}_{N+M+1}+\underline{c}_{N+M}}{2h_{II}}=\frac{-3\underline{c}_{N+M+2}+4\underline{c}_{N+M+3}-\underline{c}_{N+M+4}}{2h_{III}}$$

(58)

$$\underline{c}_{N+M+2}\left(\frac{3\zeta}{2h_{II}}+\frac{3}{2h_{III}}\right)=\frac{4\underline{c}_{N+M+3}-\underline{c}_{N+M+4}}{2h_{III}}-\zeta\frac{-4\underline{c}_{N+M+1}+\underline{c}_{N+M}}{2h_{II}};$$

$$\underline{c}_{N+M+2}=\frac{\left(4\underline{c}_{N+M+3}-\underline{c}_{N+M+4}\right)h_{II}-\left(\underline{c}_{N+M}-4\underline{c}_{N+M+1}\right)h_{III}\zeta}{3(h_{II}+h_{III}\zeta)} \tag{59}$$

The boundary conditions defined by Eqs. (6) and (8) are automatically satisfied, assuming the continuity of concentration and temperature as functions of distance.

The overall system of ODEs is presented in Eq. (60). The concentrations at boundary points are calculated by corresponding equations and then substituted into the system of ODEs. Specifically, $\underline{c}_0$ by Eq. (54) is substituted into the first equation, $\underline{c}_{N+1}$ by Eq. (57) is employed in the third and fourth equations, $\underline{c}_{N+M+2}$ by Eq. (59) is utilized in the sixth and seventh equations, and $\underline{c}_{N+M+K+3}$ by Eq. (55) is applied in the last equation within the system of ODEs.

$$\frac{d\underline{c}_1}{d\tau} = \frac{1}{\varepsilon_1 \zeta'} \cdot \left[\frac{\underline{c}_2 - 2\underline{c}_2 + \underline{c}_0}{h_I^2} \right] \tag{1}$$

$$\frac{d\underline{c}_i}{d\tau} = \frac{1}{\varepsilon_1 \zeta'} \cdot \left[\frac{\underline{c}_{i+1} - 2\underline{c}_i + \underline{c}_{i-1}}{h_I^2} \right],\ i = 2, \cdots, N-1 \tag{2}$$

$$\frac{d\underline{c}_N}{d\tau} = \frac{1}{\varepsilon_1 \zeta'} \cdot \left[\frac{\underline{c}_{N+1} - 2\underline{c}_N + \underline{c}_{N-1}}{h_I^2} \right] \tag{3}$$

$$\frac{d\underline{c}_{N+2}}{d\tau} = \frac{1}{\varepsilon_2} \cdot \left[\frac{\underline{c}_{N+3} - 2\underline{c}_{N+2} + \underline{c}_{N+1}}{h_{II}^2} - \phi^2 \cdot \underline{c}_{N+2} \right] \tag{4}$$

$$\frac{d\underline{c}_i}{d\tau} = \frac{1}{\varepsilon_2} \cdot \left[\frac{\underline{c}_{i+1} - 2\underline{c}_i + \underline{c}_{i-1}}{h_{II}^2} - \phi^2 \cdot \underline{c}_i \right],\ \ i = N+3, \cdots, N+M \tag{5}$$

$$\frac{d\underline{c}_{N+M+1}}{d\tau} = \frac{1}{\varepsilon_2} \cdot \left[\frac{\underline{c}_{N+M+2} - 2\underline{c}_{N+M+1} + \underline{c}_{N+M}}{h_{II}^2} - \phi^2 \cdot \underline{c}_{N+M+1} \right] \tag{6}$$

$$\frac{d\underline{c}_{N+M+3}}{d\tau} = \frac{1}{\varepsilon_3 \zeta} \cdot \left[\frac{\underline{c}_{N+M+4} - 2\underline{c}_{N+M+3} + \underline{c}_{N+M+2}}{h_{III}^2} \right] \tag{7}$$

$$\frac{d\underline{c}_i}{d\tau} = \frac{1}{\varepsilon_3 \zeta} \cdot \left[\frac{\underline{c}_{i+1} - 2\underline{c}_i + \underline{c}_{i-1}}{h_{III}^2} \right],\ \ i = N+M+4, \cdots, N+M+K+1 \tag{8}$$

$$\frac{d\underline{c}_{N+M+K+2}}{d\tau} = \frac{1}{\varepsilon_3 \zeta} \cdot \left[\frac{\underline{c}_{N+M+K+3} - 2\underline{c}_{N+M+K+2} + \underline{c}_{N+M+K+1}}{h_{III}^2} \right] \tag{9}$$

(60)

In the Python computer program, the concentrations at boundary points are represented by variables $c0 = \underline{c}_0$, $cN1 = \underline{c}_{N+1}$, $cNM1 = \underline{c}_{N+M+2}$, and $cNMK1 = \underline{c}_{N+M+K+3}$. Additionally, an array denoted as $c[0,...,N+M+K-1]$ is utilized to store the concentration at the internal mesh points as follows:

$c[0] = \underline{c}_1, ..., c[N-1] = \underline{c}_N, c[N] = \underline{c}_{N+2}, ..., c[N+M-1] = \underline{c}_{N+M+1}$,

$c[N+M] = \underline{c}_{N+M+3}, ..., c[N+M+K-1] = \underline{c}_{N+M+K+2}$.

Spherical pellet

The uniform mesh illustrated in **Figure 4.1** is employed for the finite-difference approximation of spatial derivatives. Second-order central finite difference approximations are utilized for both the first and second-order spatial derivatives in partial differential equations (PDEs) and boundary conditions. The system of PDEs is transformed into a system of ODEs using the method of lines, as follows:

$$\frac{d\underline{c}_i}{d\tau} = \frac{1}{\varepsilon_1 \zeta'} \cdot \left[\frac{\underline{c}_{i+1} - 2\underline{c}_i + \underline{c}_{i-1}}{h_I^2} + \frac{2}{\underline{x}_i} \frac{\underline{c}_{i+1} - \underline{c}_{i-1}}{2h_I} \right], \quad i = 1, \cdots, N \tag{61}$$

$$\frac{d\underline{c}_i}{d\tau} = \frac{1}{\varepsilon_2} \cdot \left[\frac{\underline{c}_{i+1} - 2\underline{c}_i + \underline{c}_{i-1}}{h_{II}^2} + \frac{2}{\underline{x}_i} \frac{\underline{c}_{i+1} - \underline{c}_{i-1}}{2h_{II}} - \phi^2 \cdot \underline{c}_i \right], \quad i = N+2, \cdots, N+M+1 \tag{62}$$

$$\frac{d\underline{c}_i}{d\tau} = \frac{1}{\varepsilon_3 \zeta} \cdot \left[\frac{\underline{c}_{i+1} - 2\underline{c}_i + \underline{c}_{i-1}}{h_{III}^2} + \frac{2}{\underline{x}_i} \frac{\underline{c}_{i+1} - \underline{c}_{i-1}}{2h_{III}} \right], \quad i = N+M+3, \cdots, N+M+K+2 \tag{63}$$

The concentrations at boundary points are calculated using Eqs. (54) - (59) and the resulting overall system of ODEs is given as follows:

$$\frac{d\underline{c}_1}{d\tau} = \frac{1}{\varepsilon_1 \zeta'} \cdot \left[\frac{\underline{c}_2 - 2\underline{c}_1 + \underline{c}_0}{h_I^2} + \frac{2}{\underline{x}_i} \frac{\underline{c}_2 - \underline{c}_0}{2h_I} \right]$$

$$\frac{d\underline{c}_i}{d\tau} = \frac{1}{\varepsilon_1 \zeta'} \cdot \left[\frac{\underline{c}_{i+1} - 2\underline{c}_i + \underline{c}_{i-1}}{h_I^2} + \frac{2}{\underline{x}_i} \frac{\underline{c}_{i+1} - \underline{c}_{i-1}}{2h_I} \right], \; i = 2, \cdots, N-1$$

$$\frac{d\underline{c}_N}{d\tau} = \frac{1}{\varepsilon_1 \zeta'} \cdot \left[\frac{\underline{c}_{N+1} - 2\underline{c}_N + \underline{c}_{N-1}}{h_I^2} + \frac{2}{\underline{x}_i} \frac{\underline{c}_{N+1} - \underline{c}_{N-1}}{2h_I} \right]$$

$$\frac{d\underline{c}_{N+2}}{d\tau} = \frac{1}{\varepsilon_2} \cdot \left[\frac{\underline{c}_{N+3} - 2\underline{c}_{N+2} + \underline{c}_{N+1}}{h_{II}^2} + \frac{2}{\underline{x}_i} \frac{\underline{c}_{N+3} - \underline{c}_{N+1}}{2h_{II}} - \phi^2 \cdot \underline{c}_{N+2} \right],$$

$$\frac{d\underline{c}_i}{d\tau} = \frac{1}{\varepsilon_2} \cdot \left[\frac{\underline{c}_{i+1} - 2\underline{c}_i + \underline{c}_{i-1}}{h_{II}^2} + \frac{2}{\underline{x}_i} \frac{\underline{c}_{i+1} - \underline{c}_{i-1}}{2h_{II}} - \phi^2 \cdot \underline{c}_i \right], \quad i = N+3, \cdots, N+M \tag{64}$$

$$\frac{d\underline{c}_{N+M+1}}{d\tau} = \frac{1}{\varepsilon_2} \cdot \left[\frac{\underline{c}_{N+M+2} - 2\underline{c}_{N+M+1} + \underline{c}_{N+M}}{h_{II}^2} + \frac{2}{\underline{x}_i} \frac{\underline{c}_{N+M+2} - \underline{c}_{N+M}}{2h_{II}} - \phi^2 \cdot \underline{c}_{N+M+1} \right],$$

$$\frac{d\underline{c}_{N+M+3}}{d\tau} = \frac{1}{\varepsilon_3 \zeta} \cdot \left[\frac{\underline{c}_{N+M+4} - 2\underline{c}_{N+M+3} + \underline{c}_{N+M+2}}{h_{III}^2} + \frac{2}{\underline{x}_i} \frac{\underline{c}_{N+M+4} - \underline{c}_{N+M+2}}{2h_{III}} \right]$$

$$\frac{d\underline{c}_i}{d\tau} = \frac{1}{\varepsilon_3 \zeta} \cdot \left[\frac{\underline{c}_{i+1} - 2\underline{c}_i + \underline{c}_{i-1}}{h_{III}^2} + \frac{2}{\underline{x}_i} \frac{\underline{c}_{i+1} - \underline{c}_{i-1}}{2h_{III}} \right],$$

$$i = N+M+4, \cdots, N+M+K+2$$

$$\frac{d\underline{c}_{N+M+K+2}}{d\tau} = \frac{1}{\varepsilon_3 \zeta} \cdot \left[\begin{array}{c} \frac{\underline{c}_{N+M+K+3} - 2\underline{c}_{N+M+K+2} + \underline{c}_{N+M+K+1}}{h_{III}^2} + \\ \frac{2}{\underline{x}_i} \frac{\underline{c}_{N+M+K+3} - \underline{c}_{iN+M+K+1}}{2h_{III}} \end{array} \right]$$

4.2 Numerical solution of mass balance equations for isothermal pellets with non-uniform catalyst distribution

The numerical solution for the steady-state mass balance equations governing the first-order reaction in isothermal pellets with a Gaussian spatial distribution of catalytically active material was derived as the steady-state solution of the transient mass balance Eqs. (18), (20), and (22). The method of lines was employed to solve the system of partial differential equations, utilizing a finite difference approximation for spatial derivatives [8, 9, 18]. The resulting system of ordinary differential equations is solved using the Python '*solve_ivp*' solver for stiff systems from the SciPy library [21].

Slab-type pellet

The finite-difference approximation of spatial derivatives utilizes the uniform mesh depicted in **Figure 4.1**. Using the second-order central finite-difference approximations for the spatial derivatives in PDEs results in the following system of ODEs at the internal mesh points:

$$\frac{d\underline{c}_i}{d\tau} = \frac{1}{\varepsilon_1 \zeta'} \cdot \left[\frac{\underline{c}_{i+1} - 2\underline{c}_i + \underline{c}_{i-1}}{h_I^2} \right], \; i = 1, \cdots, N \tag{65}$$

$$\frac{d\underline{c}_i}{d\tau} = \frac{1}{\varepsilon_2} \cdot \left[\frac{\underline{c}_{i+1} - 2\underline{c}_i + \underline{c}_{i-1}}{h_{II}^2} - \frac{exp\left(- \frac{\left(\underline{x}_i - \underline{x}_1 \right)^2}{\Delta^2} \right)}{\frac{\sqrt{\pi}}{2} \Delta \left(\left(\frac{r_2 - \underline{x}_1}{\Delta} \right) - \left(\frac{r_1 - \underline{x}_1}{\Delta} \right) \right)} \phi^2 \cdot \underline{c}_i \right], \tag{66}$$

$$i = N+2, \cdots, N+M+1$$

$$\frac{d\underline{c}_i}{d\tau} = \frac{1}{\varepsilon_3 \zeta} \cdot \left[\frac{\underline{c}_{i+1} - 2\underline{c}_i + \underline{c}_{i-1}}{h_{III}^2} \right], \quad i = N+M+3, \cdots, N+M+K+2. \tag{67}$$

The boundary condition, as described by Eqs. (24), (26), (29), and (33) are transformed to the algebraic equations using the corresponding second-order finite difference approximations for the spatial derivatives. The formulas for calculating the concentration at the boundaries are derived as follows:

$$\underline{x}=0:\frac{-3\underline{c}_0+4\underline{c}_1-\underline{c}_2}{2h_I}=0$$

$$\underline{c}_0=\frac{4\underline{c}_1}{3}-\frac{\underline{c}_2}{3} \tag{68}$$

$$\underline{x}=1:\frac{3\underline{c}_{N+M+K+3}-4\underline{c}_{N+M+K+2}+\underline{c}_{N+M+K+1}}{2h_{III}}=Bi_m\left(1-\underline{c}_{N+M+K+3}\right),$$

$$\underline{c}_{N+M+K+3}=\frac{2h_{III}Bi+4\underline{c}_{N+M+K+2}-\underline{c}_{N+M+K+1}}{3+2h_{III}Bi} \tag{69}$$

$$\underline{x}=r_1:\ \frac{3\underline{c}_{N+1}-4\underline{c}_N+\underline{c}_{N-1}}{2h_I}=\zeta'\frac{-3\underline{c}_{N+1}+4\underline{c}_{N+2}-\underline{c}_{N+3}}{2h_{II}} \tag{70}$$

$$\underline{c}_{N+1}\left(\frac{3}{2h_I}+\frac{3\zeta'}{2h_{II}}\right)=\zeta'\frac{4\underline{c}_{N+2}-\underline{c}_{N+3}}{2h_{II}}-\frac{-4\underline{c}_N+\underline{c}_{N-1}}{2h_I};$$

$$\underline{c}_{N+1}=\frac{\left(4\underline{c}_{N+2}-\underline{c}_{N+3}\right)\zeta'h_I-\left(\underline{c}_{N-1}-4\underline{c}_N\right)h_{II}}{3(h_I\zeta'+h_{II})} \tag{71}$$

$$\underline{x}=r_2:\ \zeta\frac{3\underline{c}_{N+M+2}-4\underline{c}_{N+M+1}+\underline{c}_{N+M}}{2h_{II}}=\frac{-3\underline{c}_{N+M+2}+4\underline{c}_{N+M+3}-\underline{c}_{N+M+4}}{2h_{III}}$$

(72)

$$\underline{c}_{N+M+2}\left(\frac{3\zeta}{2h_{II}}+\frac{3}{2h_{III}}\right)=\frac{4\underline{c}_{N+M+3}-\underline{c}_{N+M+4}}{2h_{III}}-\zeta\frac{-4\underline{c}_{N+M+1}+\underline{c}_{N+M}}{2h_{II}};$$

$$\underline{c}_{N+M+2}=\frac{\left(4\underline{c}_{N+M+3}-\underline{c}_{N+M+4}\right)h_{II}-\left(\underline{c}_{N+M}-4\underline{c}_{N+M+1}\right)h_{III}\zeta}{3(h_{II}+h_{III}\zeta)} \tag{73}$$

Assuming continuity of concentration and temperature as functions of distance, the boundary conditions specified by Eqs. (28) and (32) are automatically met. The complete system of ODEs is outlined in Eq.(74). Concentrations at boundary points are computed using their respective equations and subsequently inserted into the ODE system. Precisely, $\underline{c}_0$ by

Eq. (68) is substituted into the first equation, $\underline{c}_{N+1}$ by Eq. (71) is utilized for the third and fourth equations, $\underline{c}_{N+M+2}$ by Eq. (73) is employed in the sixth and seventh equations, and finally, $\underline{c}_{N+M+K+3}$ by Eq. (69) is applied in the last equation within the ODE system.

$$\frac{d\underline{c}_1}{d\tau} = \frac{1}{\varepsilon_1 \zeta'} \cdot \left[\frac{\underline{c}_2 - 2\underline{c}_1 + \underline{c}_0}{h_I^2} \right] \tag{1}$$

$$\frac{d\underline{c}_i}{d\tau} = \frac{1}{\varepsilon_1 \zeta'} \cdot \left[\frac{\underline{c}_{i+1} - 2\underline{c}_i + \underline{c}_{i-1}}{h_I^2} \right],\ i = 2, \cdots, N-1 \tag{2}$$

$$\frac{d\underline{c}_N}{d\tau} = \frac{1}{\varepsilon_1 \zeta'} \cdot \left[\frac{\underline{c}_{N+1} - 2\underline{c}_N + \underline{c}_{N-1}}{h_I^2} \right] \tag{3}$$

$$\frac{d\underline{c}_{N+2}}{d\tau} = \frac{1}{\varepsilon_2} \cdot \left[\frac{\underline{c}_{N+3} - 2\underline{c}_{N+2} + \underline{c}_{N+1}}{h_{II}^2} - \frac{exp\left(- \frac{\left(\underline{x}_{N+2} - \underline{x}_1 \right)^2}{\Delta^2} \right)}{\frac{\sqrt{\pi}}{2} \Delta \left(\left(\frac{r_2 - \underline{x}_1}{\Delta} \right) - \left(\frac{r_1 - \underline{x}_1}{\Delta} \right) \right)} \phi^2 \cdot \underline{c}_{N+2} \right] \tag{4}$$

$$\frac{d\underline{c}_i}{d\tau} = \frac{1}{\varepsilon_2} \cdot \left[\frac{\underline{c}_{i+1} - 2\underline{c}_i + \underline{c}_{i-1}}{h_{II}^2} - \frac{exp\left(- \frac{\left(\underline{x}_i - \underline{x}_1 \right)^2}{\Delta^2} \right)}{\frac{\sqrt{\pi}}{2} \Delta \left(\left(\frac{r_2 - \underline{x}_1}{\Delta} \right) - \left(\frac{r_1 - \underline{x}_1}{\Delta} \right) \right)} \phi^2 \cdot \underline{c}_i \right],\ i = N+3, \cdots, N+M \tag{5}$$

$$\frac{d\underline{c}_{N+M+1}}{d\tau} = \frac{1}{\varepsilon_2} \cdot \left[\frac{\underline{c}_{N+M+2} - 2\underline{c}_{N+M+1} + \underline{c}_{N+M}}{h_{II}^2} - \frac{exp\left(- \frac{\left(\underline{x}_{N+M+1} - \underline{x}_1 \right)^2}{\Delta^2} \right)}{\frac{\sqrt{\pi}}{2} \Delta \left(\left(\frac{r_2 - \underline{x}_1}{\Delta} \right) - \left(\frac{r_1 - \underline{x}_1}{\Delta} \right) \right)} \phi^2 \cdot \underline{c}_{N+M+1} \right] \tag{6}$$

$$\frac{d\underline{c}_{N+M+3}}{d\tau} = \frac{1}{\varepsilon_3 \zeta} \cdot \left[\frac{\underline{c}_{N+M+4} - 2\underline{c}_{N+M+3} + \underline{c}_{N+M+2}}{h_{III}^2} \right] \tag{7}$$

$$\frac{d\underline{c}_i}{d\tau} = \frac{1}{\varepsilon_3 \zeta} \cdot \left[\frac{\underline{c}_{i+1} - 2\underline{c}_i + \underline{c}_{i-1}}{h_{III}^2} \right],\ i = N+M+4, \cdots, N+M+K+1 \tag{8}$$

$$\frac{d\underline{c}_{N+M+K+2}}{d\tau} = \frac{1}{\varepsilon_3 \zeta} \cdot \left[\frac{\underline{c}_{N+M+K+3} - 2\underline{c}_{N+M+K+2} + \underline{c}_{N+M+K+1}}{h_{III}^2} \right] \tag{9}$$

(74)

In the Python computer program, the concentrations at boundary points are represented by variables $c0 = \underline{c}_0$, $cN1 = \underline{c}_{N+1}$, $cNM1 = \underline{c}_{N+M+2}$, and $cNMK1 = \underline{c}_{N+M+K+3}$. Additionally, an array denoted as $c[0,...,N+M+K-1]$ is utilized to store the concentration at the internal mesh points as follows:

$$c[0]=\underline{c}_1,...,c[N-1]=\underline{c}_N,c[N]=\underline{c}_{N+2},...,c[N+M-1]=\underline{c}_{N+M+1},$$

$$c[N+M]=\underline{c}_{N+M+3},...,c[N+M+K-1]=\underline{c}_{N+M+K+2}.$$

Spherical pellet

The uniform mesh illustrated in **Figure 4.1** is employed for the finite-difference approximation of spatial derivatives. Second-order central finite difference approximations are utilized for both the first and second-order spatial derivatives in partial differential equations (PDEs) and boundary conditions as described above for the case of slab-type pellet. The system of PDEs is transformed into a system of ODEs using the method of lines, as follows:

$$\frac{d\underline{c}_i}{d\tau}=\frac{1}{\varepsilon_1\zeta'}\cdot\left[\frac{\underline{c}_{i+1}-2\underline{c}_i+\underline{c}_{i-1}}{h_I^2}+\frac{2}{\underline{x}_i}\frac{\underline{c}_{i+1}-\underline{c}_{i-1}}{2h_I}\right],\qquad i=1,\cdots,N \tag{75}$$

$$\frac{d\underline{c}_i}{d\tau}=\frac{1}{\varepsilon_2}\cdot\left[\frac{\dfrac{\underline{c}_{i+1}-2\underline{c}_i+\underline{c}_{i-1}}{h_{II}^2}+\dfrac{2}{\underline{x}_i}\dfrac{\underline{c}_{i+1}-\underline{c}_{i-1}}{2h_{II}}-\exp\left(-\dfrac{\left(\underline{x}_i-\underline{x}_1\right)^2}{\Delta^2}\right)}{\left(\begin{array}{c}\dfrac{3\sqrt{\pi}}{4}\left(\Delta^3+2\underline{x}_1^2\Delta\right)\left(erf\left(\dfrac{r_2-\underline{x}_1}{\Delta}\right)-erf\left(\dfrac{r_1-\underline{x}_1}{\Delta}\right)\right)-\\ \dfrac{3}{2}\left(\underline{x}_1+r_2\right)\cdot\exp\left(-\dfrac{\left(r_2-\underline{x}_1\right)^2}{\Delta^2}\right)+\dfrac{3}{2}\left(r_1+\underline{x}_1\right)\cdot\exp\left(-\dfrac{\left(r_1-\underline{x}_1\right)^2}{\Delta^2}\right)\end{array}\right)}\phi^2\cdot\underline{c}_i\right], \tag{76}$$

$$i=N+2,\cdots,N+M+1$$

$$\frac{d\underline{c}_i}{d\tau}=\frac{1}{\varepsilon_3\zeta}\cdot\left[\frac{\underline{c}_{i+1}-2\underline{c}_i+\underline{c}_{i-1}}{h_{III}^2}+\frac{2}{\underline{x}_i}\frac{\underline{c}_{i+1}-\underline{c}_{i-1}}{2h_{III}}\right],\qquad i=N+M+3,\cdots,N+M+K+2 \tag{77}$$

The concentrations at boundary points are calculated using Eqs. (68) - (73) and the resulting overall system of ODEs is given as follows:

$$\frac{d\underline{c}_1}{d\tau}=\frac{1}{\varepsilon_1\zeta'}\cdot\left[\frac{\underline{c}_2-2\underline{c}_1+\underline{c}_0}{h_I^2}+\frac{2}{\underline{x}_1}\frac{\underline{c}_2-\underline{c}_0}{2h_I}\right]$$

$$\frac{d\underline{c}_i}{d\tau}=\frac{1}{\varepsilon_1\zeta'}\cdot\left[\frac{\underline{c}_{i+1}-2\underline{c}_i+\underline{c}_{i-1}}{h_I^2}+\frac{2}{\underline{x}_i}\frac{\underline{c}_{i+1}-\underline{c}_{i-1}}{2h_I}\right],\ i=2,\cdots,N-1$$

$$\frac{d\underline{c}_N}{d\tau}=\frac{1}{\varepsilon_1\zeta'}\cdot\left[\frac{\underline{c}_{N+1}-2\underline{c}_N+\underline{c}_{N-1}}{h_I^2}+\frac{2}{\underline{x}_N}\frac{\underline{c}_{N+1}-\underline{c}_{N-1}}{2h_I}\right]$$

$$\frac{d\underline{c}_{N+2}}{d\tau}=\frac{1}{\varepsilon_2}\cdot\left[\frac{\dfrac{\underline{c}_{N+3}-2\underline{c}_{N+2}+\underline{c}_{N+1}}{h_{II}^2}+\dfrac{2}{\underline{x}_{N+2}}\dfrac{\underline{c}_{N+3}-\underline{c}_{N+1}}{2h_{II}}-\exp\left(-\dfrac{\left(x_{N+2}-\underline{x}_1\right)^2}{\Delta^2}\right)}{\left(\dfrac{3\sqrt{\pi}}{4}\left(\Delta^3+2\underline{x}_1^2\Delta\right)\left(erf\left(\dfrac{r_2-\underline{x}_1}{\Delta}\right)-erf\left(\dfrac{r_1-\underline{x}_1}{\Delta}\right)\right)-\dfrac{3}{2}\left(\underline{x}_1+r_2\right)\cdot\exp\left(-\dfrac{\left(r_2-\underline{x}_1\right)^2}{\Delta^2}\right)+\dfrac{3}{2}\left(r_1+\underline{x}_1\right)\cdot\exp\left(-\dfrac{\left(r_1-\underline{x}_1\right)^2}{\Delta^2}\right)\right)\phi^2}\cdot\underline{c}_{N+2}\right],$$

$$\frac{d\underline{c}_i}{d\tau}=\frac{1}{\varepsilon_2}\cdot\left[\frac{\dfrac{\underline{c}_{i+1}-2\underline{c}_i+\underline{c}_{i-1}}{h_{II}^2}+\dfrac{2}{\underline{x}_i}\dfrac{\underline{c}_{i+1}-\underline{c}_{i-1}}{2h_{II}}-\exp\left(-\dfrac{\left(\underline{x}_i-\underline{x}_1\right)^2}{\Delta^2}\right)}{\left(\dfrac{3\sqrt{\pi}}{4}\left(\Delta^3+2\underline{x}_1^2\Delta\right)\left(erf\left(\dfrac{r_2-\underline{x}_1}{\Delta}\right)-erf\left(\dfrac{r_1-\underline{x}_1}{\Delta}\right)\right)-\dfrac{3}{2}\left(\underline{x}_1+r_2\right)\cdot\exp\left(-\dfrac{\left(r_2-\underline{x}_1\right)^2}{\Delta^2}\right)+\dfrac{3}{2}\left(r_1+\underline{x}_1\right)\cdot\exp\left(-\dfrac{\left(r_1-\underline{x}_1\right)^2}{\Delta^2}\right)\right)\phi^2}\cdot\underline{c}_i\right],\ i=N+3,\cdots,N+M$$

$$\frac{d\underline{c}_{N+M+1}}{d\tau}=\frac{1}{\varepsilon_2}\cdot\left[\frac{\dfrac{\underline{c}_{N+M+2}-2\underline{c}_{N+M+1}+\underline{c}_{N+M}}{h_{II}^2}+\dfrac{2}{\underline{x}_{N+M+1}}\dfrac{\underline{c}_{N+M+2}-\underline{c}_{N+M}}{2h_{II}}-\exp\left(-\dfrac{\left(x_{N+M+1}-\underline{x}_1\right)^2}{\Delta^2}\right)}{\left(\dfrac{3\sqrt{\pi}}{4}\left(\Delta^3+2\underline{x}_1^2\Delta\right)\left(erf\left(\dfrac{r_2-\underline{x}_1}{\Delta}\right)-erf\left(\dfrac{r_1-\underline{x}_1}{\Delta}\right)\right)-\dfrac{3}{2}\left(\underline{x}_1+r_2\right)\cdot\exp\left(-\dfrac{\left(r_2-\underline{x}_1\right)^2}{\Delta^2}\right)+\dfrac{3}{2}\left(r_1+\underline{x}_1\right)\cdot\exp\left(-\dfrac{\left(r_1-\underline{x}_1\right)^2}{\Delta^2}\right)\right)\phi^2}\cdot\underline{c}_{N+M+1}\right],$$

(78)

$$\frac{d\underline{c}_{N+M+3}}{d\tau} = \frac{1}{\varepsilon_3\zeta}\cdot\left[\frac{\underline{c}_{N+M+4} - 2\underline{c}_{N+M+3} + \underline{c}_{N+M+2}}{h_{III}^2} + \frac{2}{\underline{x}_{N+M+3}}\frac{\underline{c}_{N+M+4} - \underline{c}_{N+M+2}}{2h_{III}}\right]$$

$$\frac{d\underline{c}_i}{d\tau} = \frac{1}{\varepsilon_3\zeta}\cdot\left[\frac{\underline{c}_{i+1} - 2\underline{c}_i + \underline{c}_{i-1}}{h_{III}^2} + \frac{2}{\underline{x}_i}\frac{\underline{c}_{i+1} - \underline{c}_{i-1}}{2h_{III}}\right],$$

$$i = N+M+4, \cdots, N+M+K+2$$

$$\frac{d\underline{c}_{N+M+K+2}}{d\tau} = \frac{1}{\varepsilon_3\zeta}\cdot\left[\begin{array}{c}\frac{\underline{c}_{N+M+K+3} - 2\underline{c}_{N+M+K+2} + \underline{c}_{N+M+K+1}}{h_{III}^2} + \\ \frac{2}{\underline{x}_{N+M+K+2}}\frac{\underline{c}_{N+M+K+3} - \underline{c}_{iN+M+K+1}}{2h_{III}}\end{array}\right]$$

4.3 Numerical solutions of mass and heat balance equations for non-isothermal pellets with non-uniform distribution of catalyst

The steady-state solution of the numerical solution for the mass balance equations, which govern the first-order reaction in non-isothermal catalytic pellets with a Gaussian spatial distribution of catalytically active material, was derived from the steady-state solution of the transient mass balance Eqs. (18) - (23). Similarly, the method of lines was utilized for solving the system of partial differential equations, employing a finite difference approximation for spatial derivatives. The resultant system of ordinary differential equations was then solved using the Python 'solve_ivp' solver specifically designed for stiff systems, which is available in the SciPy library.

Slab-type pellet

Employing second-order central finite-difference approximations for spatial derivatives in PDEs yields the subsequent system of ODEs at the internal mesh points:

$$\begin{aligned}\frac{d\underline{c}_i}{d\tau} &= \frac{1}{\varepsilon_1\zeta'}\cdot\left[\frac{\underline{c}_{i+1} - 2\underline{c}_i + \underline{c}_{i-1}}{h_I^2}\right] \\ \frac{d\theta_i}{d\tau} &= \frac{\psi_1}{\zeta'}\left[\frac{\theta_{i+1} - 2\theta_i + \theta_{i-1}}{h_I^2}\right],\ i = 1, \cdots, N\end{aligned} \tag{79}$$

$$\frac{d\underline{c}_i}{d\tau} = \frac{1}{\varepsilon_2} \cdot \left[\frac{\underline{c}_{i+1} - 2\underline{c}_i + \underline{c}_{i-1}}{h_{II}^2} - \frac{exp\left(- \frac{\left(\underline{x}_i - \underline{x}_1\right)^2}{\Delta^2} \right)}{\frac{\sqrt{\pi}}{2}\Delta\left(\left(\frac{r_2 - \underline{x}_1}{\Delta}\right) - \left(\frac{r_1 - \underline{x}_1}{\Delta}\right)\right)} \phi^2 \underline{c}_i^n exp\left(\gamma\left(1 - \frac{1}{\theta_i}\right)\right) \right]$$

$$\frac{d\theta_i}{d\tau} = \psi_2 \left[\frac{\theta_{i+1} - 2\theta_i + \theta_{i-1}}{h_{II}^2} - \frac{\exp\left(- \frac{\left(\underline{x}_i - \underline{x}_1\right)^2}{\Delta^2} \right)}{\frac{\sqrt{\pi}}{2}\Delta\left(\left(\frac{r_2 - \underline{x}_1}{\Delta}\right) - \left(\frac{r_1 - \underline{x}_1}{\Delta}\right)\right)} \beta\phi^2 \underline{c}_i^n \exp\left(\gamma\left(1 - \frac{1}{\theta_i}\right)\right) \right],$$

$$i = N+2, \cdots, N+M+1$$

(80)

$$\begin{aligned} &\frac{d\underline{c}_i}{d\tau} = \frac{1}{\varepsilon_3 \zeta} \cdot \left[\frac{\underline{c}_{i+1} - 2\underline{c}_i + \underline{c}_{i-1}}{h_{III}^2} \right] \\ &\frac{d\theta_i}{d\tau} = \frac{\psi_3}{\zeta} \left[\frac{\theta_{i+1} - 2\theta_i + \theta_{i-1}}{h_{III}^2} \right], \quad i = N+M+3, \cdots, N+M+K+2 \end{aligned} \quad . \tag{81}$$

The boundary condition, as described by Eqs. (24) - (35) are transformed into algebraic equations using the corresponding second-order finite difference approximations for the spatial derivatives. The formulas for calculating the concentration at the boundaries are derived as follows:

$$\underline{x} = 0 : \frac{-3\underline{c}_0 + 4\underline{c}_1 - \underline{c}_2}{2h_I} = 0$$

$$\underline{c}_0 = \frac{4\underline{c}_1}{3} - \frac{\underline{c}_2}{3} \tag{82}$$

$$\frac{-3\theta_0 + 4\theta_1 - \theta_2}{2h_I} = 0$$

$$\theta_0 = \frac{4\theta_1}{3} - \frac{\theta_2}{3} \tag{83}$$

$$\underline{x} = 1 : \frac{3\underline{c}_{N+M+K+3} - 4\underline{c}_{N+M+K+2} + \underline{c}_{N+M+K+1}}{2h_{III}} = Bi_m\left(1 - \underline{c}_{N+M+K+3}\right),$$

$$\underline{c}_{N+M+K+3} = \frac{2h_{III}Bi + 4\underline{c}_{N+M+K+2} - \underline{c}_{N+M+K+1}}{3 + 2h_{III}Bi} \tag{84}$$

$$\frac{3\theta_{N+M+K+3}-4\theta_{N+M+K+2}+\theta_{N+M+K+1}}{2h_{III}}=Bi_m(1-\theta_{N+M+K+3}),$$

$$\theta_{N+M+K+3}=\frac{2h_{III}Bi+4\theta_{N+M+K+2}-\theta_{N+M+K+1}}{3+2h_{III}Bi} \tag{85}$$

$$\underline{x}=r_1:\ \ \frac{3\underline{c}_{N+1}-4\underline{c}_{N}+\underline{c}_{N-1}}{2h_I}=\zeta'\frac{-3\underline{c}_{N+1}+4\underline{c}_{N+2}-\underline{c}_{N+3}}{2h_{II}} \tag{86}$$

$$\underline{c}_{N+1}\left(\frac{3}{2h_I}+\frac{3\zeta'}{2h_{II}}\right)=\zeta'\frac{4\underline{c}_{N+2}-\underline{c}_{N+3}}{2h_{II}}-\frac{-4\underline{c}_{N}+\underline{c}_{N-1}}{2h_I};$$

$$\underline{c}_{N+1}=\frac{\left(4\underline{c}_{N+2}-\underline{c}_{N+3}\right)\zeta' h_I-\left(\underline{c}_{N-1}-4\underline{c}_{N}\right)h_{II}}{3(h_I\zeta'+h_{II})} \tag{87}$$

$$\frac{3\theta_{N+1}-4\theta_N+\theta_{N-1}}{2h_I}=k_{2,1}\frac{-3\theta_{N+1}+4\theta_{N+2}-\theta_{N+3}}{2h_{II}} \tag{88}$$

$$\theta_{N+1}\left(\frac{3}{2h_I}+\frac{3k_{2,1}}{2h_{II}}\right)=k_{2,1}\frac{4\theta_{N+2}-\theta_{N+3}}{2h_{II}}-\frac{-4\theta_N+\theta_{N-1}}{2h_I};$$

$$\theta_{N+1}=\frac{(4\theta_{N+2}-\theta_{N+3})k_{2,1}h_I-(\theta_{N-1}-4\theta_N)h_{II}}{3(h_Ik_{2,1}+h_{II})} \tag{89}$$

$$\underline{x}=r_2:\ \ \zeta\frac{3\underline{c}_{N+M+2}-4\underline{c}_{N+M+1}+\underline{c}_{N+M}}{2h_{II}}=\frac{-3\underline{c}_{N+M+2}+4\underline{c}_{N+M+3}-\underline{c}_{N+M+4}}{2h_{III}} \tag{90}$$

$$\underline{c}_{N+M+2}\left(\frac{3\zeta}{2h_{II}}+\frac{3}{2h_{III}}\right)=\frac{4\underline{c}_{N+M+3}-\underline{c}_{N+M+4}}{2h_{III}}-\zeta\frac{-4\underline{c}_{N+M+1}+\underline{c}_{N+M}}{2h_{II}};$$

$$\underline{c}_{N+M+2}=\frac{\left(4\underline{c}_{N+M+3}-\underline{c}_{N+M+4}\right)h_{II}-\left(\underline{c}_{N+M}-4\underline{c}_{N+M+1}\right)h_{III}\zeta}{3(h_{II}+h_{III}\zeta)} \tag{91}$$

$$k_{2,3}\frac{3\underline{c}_{N+M+2}-4\underline{c}_{N+M+1}+\underline{c}_{N+M}}{2h_{II}}=\frac{-3\underline{c}_{N+M+2}+4\underline{c}_{N+M+3}-\underline{c}_{N+M+4}}{2h_{III}} \tag{92}$$

$$\theta_{N+M+2}\left(\frac{3k_{2,3}}{2h_{II}}+\frac{3}{2h_{III}}\right)=\frac{4\theta_{N+M+3}-\theta_{N+M+4}}{2h_{III}}-k_{2,3}\frac{-4\theta_{N+M+1}+\theta_{N+M}}{2h_{II}};$$

$$\theta_{N+M+2}=\frac{(4\theta_{N+M+3}-\theta_{N+M+4})h_{II}-(\theta_{N+M}-4\theta_{N+M+1})k_{2,3}\cdot h_{III}}{3(h_{II}+k_{2,3}h_{III})} \tag{93}$$

Equation (94) presents the complete system of ODEs. Concentrations at boundary points are computed using their respective equations and then inserted into the ODE system.

Specifically, $\underline{c}_0$ by Eq. (82) and θ_0 by Eq. (83) are substituted into the first equation, , $\underline{c}_{N+1}$ by Eq. (87) and θ_{N+1} by Eq. (89) are employed in the third and fourth equations, $\underline{c}_{N+M+2}$ by Eq. (91) and θ_{N+M+2} by Eq. (93) are utilized in the sixth and seventh equations, and finally, $\underline{c}_{N+M+K+3}$ by Eq. (84) and $\theta_{N+M+K+3}$ by Eq. (85) are applied in the last equation within the system of ODEs.

$$\frac{d\underline{c}_1}{d\tau} = \frac{1}{\varepsilon_1 \zeta'} \cdot \left[\frac{\underline{c}_2 - 2\underline{c}_1 + \underline{c}_0}{h_I^2} \right] \tag{1}$$

$$\frac{d\theta_1}{d\tau} = \frac{\psi_1}{\zeta'} \left[\frac{\theta_2 - 2\theta_1 + \theta_0}{h_I^2} \right] \tag{2}$$

$$\frac{d\underline{c}_i}{d\tau} = \frac{1}{\varepsilon_1 \zeta'} \cdot \left[\frac{\underline{c}_{i+1} - 2\underline{c}_i + \underline{c}_{i-1}}{h_I^2} \right] \tag{3}$$

$$\frac{d\theta_i}{d\tau} = \frac{\psi_1}{\zeta'} \left[\frac{\theta_{i+1} - 2\theta_i + \theta_{i-1}}{h_I^2} \right],\ i = 2, \cdots, N-1 \tag{4}$$

$$\frac{d\underline{c}_N}{d\tau} = \frac{1}{\varepsilon_1 \zeta'} \cdot \left[\frac{\underline{c}_{N+1} - 2\underline{c}_N + \underline{c}_{N-1}}{h_I^2} \right] \tag{5}$$

$$\frac{d\theta_N}{d\tau} = \frac{\psi_1}{\zeta'} \left[\frac{\theta_{N+1} - 2\theta_N + \theta_{N-1}}{h_I^2} \right] \tag{6}$$

$$\frac{d\underline{c}_{N+2}}{d\tau} = \frac{1}{\varepsilon_2} \cdot \left[\frac{\dfrac{\underline{c}_{N+3} - 2\underline{c}_{N+2} + \underline{c}_{N+1}}{h_{II}^2} - exp\left(- \dfrac{\left(\underline{x}_{N+2} - \underline{x}_1 \right)^2}{\Delta^2} \right)}{\dfrac{\sqrt{\pi}}{2} \Delta \left(\left(\dfrac{r_2 - \underline{x}_1}{\Delta} \right) - \left(\dfrac{r_1 - \underline{x}_1}{\Delta} \right) \right)} \phi^2 \underline{c}_{N+2}^{\,n} exp\left(\gamma \left(1 - \frac{1}{\theta_{N+2}} \right) \right) \right] \tag{7}$$

$$\frac{d\theta_{N+2}}{d\tau} = \psi_2 \left[\frac{\dfrac{\theta_{N+3} - 2\theta_{N+2} + \theta_{N+1}}{h_{II}^2} - \exp\left(- \dfrac{\left(\underline{x}_{N+2} - \underline{x}_1 \right)^2}{\Delta^2} \right)}{\dfrac{\sqrt{\pi}}{2} \Delta \left(\left(\dfrac{r_2 - \underline{x}_1}{\Delta} \right) - \left(\dfrac{r_1 - \underline{x}_1}{\Delta} \right) \right)} \beta \phi^2 \underline{c}_{N+2}^{\,n} \exp\left(\gamma \left(1 - \frac{1}{\theta_{N+2}} \right) \right) \right], \tag{8}$$

$$\frac{dc_{i}}{d\tau}=\frac{1}{\varepsilon_2}\cdot\left[\frac{\frac{c_{i+1}-2c_{i}+c_{i-1}}{h_{II}^2}-exp\left(-\frac{\left(x_{i}-x_{1}\right)^2}{\Delta^2}\right)}{\frac{\sqrt{\pi}}{2}\Delta\left(\left(\frac{r_2-x_{1}}{\Delta}\right)-\left(\frac{r_1-x_{1}}{\Delta}\right)\right)}\phi^2\,c_{i}^{n}exp\left(\gamma\left(1-\frac{1}{\theta}\right)\right)\right] \tag{9}$$

$$\frac{d\theta_i}{d\tau}=\psi_2\left[\frac{\frac{\theta_{i+1}-2\theta_i+\theta_{i-1}}{h_{II}^2}-\exp\left(-\frac{\left(x_{i}-x_{1}\right)^2}{\Delta^2}\right)}{\frac{\sqrt{\pi}}{2}\Delta\left(\left(\frac{r_2-x_{1}}{\Delta}\right)-\left(\frac{r_1-x_{1}}{\Delta}\right)\right)}\beta\phi^2\,c_{i}^{n}\exp\left(\gamma\left(1-\frac{1}{\theta_i}\right)\right)\right],$$

$$i=N+3,\cdots,N+M \tag{10}$$

$$\frac{dc_{N+M+1}}{d\tau}=\frac{1}{\varepsilon_2}\cdot\left[\frac{\frac{c_{N+M+2}-2c_{N+M+1}+c_{N+M}}{h_{II}^2}-exp\left(-\frac{\left(x_{N+M+1}-x_{1}\right)^2}{\Delta^2}\right)}{\frac{\sqrt{\pi}}{2}\Delta\left(\left(\frac{r_2-x_{1}}{\Delta}\right)-\left(\frac{r_1-x_{1}}{\Delta}\right)\right)}\phi^2\cdot c_{N+M+1}\right] \tag{11}$$

$$\frac{dc_{N+M+3}}{d\tau}=\frac{1}{\varepsilon_3\zeta}\cdot\left[\frac{c_{N+M+4}-2c_{N+M+3}+c_{N+M+2}}{h_{III}^2}\right] \tag{12}$$

$$\frac{dc_{i}}{d\tau}=\frac{1}{\varepsilon_3\zeta}\cdot\left[\frac{c_{i+1}-2c_{i}+c_{i-1}}{h_{III}^2}\right],\quad i=N+M+4,\cdots,N+M+K+1 \tag{13}$$

$$\frac{dc_{N+M+K+2}}{d\tau}=\frac{1}{\varepsilon_3\zeta}\cdot\left[\frac{c_{N+M+K+3}-2c_{N+M+K+2}+c_{N+M+K+1}}{h_{III}^2}\right] \tag{14}$$

(94)

Spherical pellet

The system of PDEs is transformed into a system of ODEs using the method of lines and the second-order central finite difference approximations for both the first and second-order spatial derivatives, as follows:

$$\frac{dc_{i}}{d\tau}=\frac{1}{\varepsilon_1\zeta'}\cdot\left[\frac{c_{i+1}-2c_{i}+c_{i-1}}{h_I^2}+\frac{2}{x_{i}}\frac{c_{i+1}-c_{i-1}}{2h_I}\right]$$

$$\frac{d\theta_i}{d\tau}=\frac{\psi_1}{\zeta'}\left[\frac{\theta_{i+1}-2\theta_i+\theta_{i-1}}{h_I^2}+\frac{2}{x_{i}}\frac{\theta_{i+1}-\theta_{i-1}}{2h_I}\right],\ i=1,\cdots,N \tag{95}$$

$$\frac{d\underline{c}_i}{d\tau}=\frac{1}{\varepsilon_2}\cdot\left[\frac{\frac{\underline{c}_{i+1}-2\underline{c}_i+\underline{c}_{i-1}}{h_{II}^2}+\frac{2}{\underline{x}_i}\frac{\underline{c}_{i+1}-\underline{c}_{i-1}}{2h_{II}}-\exp\left(-\frac{\left(\underline{x}_i-\underline{x}_1\right)^2}{\Delta^2}\right)}{\left(\begin{array}{c}\frac{3\sqrt{\pi}}{4}\left(\Delta^3+2\underline{x}_1^2\Delta\right)\left(erf\left(\frac{r_2-\underline{x}_1}{\Delta}\right)-erf\left(\frac{r_1-\underline{x}_1}{\Delta}\right)\right)-\\ \frac{3}{2}\left(\underline{x}_1+r_2\right)\cdot\exp\left(-\frac{\left(r_2-\underline{x}_1\right)^2}{\Delta^2}\right)+\frac{3}{2}\left(r_1+\underline{x}_1\right)\cdot\exp\left(-\frac{\left(r_1-\underline{x}_1\right)^2}{\Delta^2}\right)\end{array}\right)}\right],$$

$$\frac{d\theta_i}{d\tau}=\psi_2\left[\frac{\frac{\theta_{i+1}-2\theta_i+\theta_{i-1}}{h_{II}^2}+\frac{2}{\underline{x}_i}\frac{\theta_{i+1}-\theta_{i-1}}{2h_{II}}-\exp\left(-\frac{\left(\underline{x}_i-\underline{x}_1\right)^2}{\Delta^2}\right)}{\left(\begin{array}{c}\frac{3\sqrt{\pi}}{4}\left(\Delta^3+2\underline{x}_1^2\Delta\right)\left(erf\left(\frac{r_2-\underline{x}_1}{\Delta}\right)-erf\left(\frac{r_1-\underline{x}_1}{\Delta}\right)\right)-\\ \frac{3}{2}\left(\underline{x}_1+r_2\right)\cdot\exp\left(-\frac{\left(r_2-\underline{x}_1\right)^2}{\Delta^2}\right)+\frac{3}{2}\left(r_1+\underline{x}_1\right)\cdot\exp\left(-\frac{\left(r_1-\underline{x}_1\right)^2}{\Delta^2}\right)\end{array}\right)}\right], \tag{96}$$

$$\beta\phi^2\,\underline{c}_i^{\,n}\exp\left(\gamma\left(1-\frac{1}{\theta_i}\right)\right)$$

$$i=N+2,\cdots,N+M+1$$

$$\begin{aligned}\frac{d\underline{c}_i}{d\tau}&=\frac{1}{\varepsilon_3\zeta}\cdot\left[\frac{\underline{c}_{i+1}-2\underline{c}_i+\underline{c}_{i-1}}{h_{III}^2}+\frac{2}{\underline{x}_i}\frac{\underline{c}_{i+1}-\underline{c}_{i-1}}{2h_{III}}\right]\\ \frac{d\theta_i}{d\tau}&=\frac{\psi_3}{\zeta}\left[\frac{\theta_{i+1}-2\theta_i+\theta_{i-1}}{h_{III}^2}+\frac{2}{\underline{x}_i}\frac{\theta_{i+1}-\theta_{i-1}}{2h_{III}}\right],\qquad\cdot\\ i&=N+M+3,\cdots,N+M+K+2\end{aligned} \tag{97}$$

The concentrations at boundary points are calculated using Eqs. (82) - (93) and the resulting overall system of ODEs is given as follows:

$$\frac{d\underline{c}_1}{d\tau}=\frac{1}{\varepsilon_1\zeta'}\cdot\left[\frac{\underline{c}_2-2\underline{c}_1+\underline{c}_0}{h_I^2}+\frac{2}{\underline{x}_1}\frac{\underline{c}_2-\underline{c}_0}{2h_I}\right]$$

$$\frac{d\theta_1}{d\tau}=\frac{\psi_1}{\zeta'}\left[\frac{\theta_2-2\theta_1+\theta_0}{h_I^2}+\frac{2}{\underline{x}_1}\frac{\theta_2-\theta_0}{2h_I}\right]$$

$$\frac{d\underline{c}_i}{d\tau}=\frac{1}{\varepsilon_1\zeta'}\cdot\left[\frac{\underline{c}_{i+1}-2\underline{c}_i+\underline{c}_{i-1}}{h_I^2}+\frac{2}{\underline{x}_i}\frac{\underline{c}_{i+1}-\underline{c}_{i-1}}{2h_I}\right]$$

$$\frac{d\theta_i}{d\tau}=\frac{\psi_1}{\zeta'}\left[\frac{\theta_{i+1}-2\theta_i+\theta_{i-1}}{h_I^2}+\frac{2}{\underline{x}_i}\frac{\theta_{i+1}-\theta_{i-1}}{2h_I}\right],\ i=2,\cdots,N-1$$

$$\frac{d\underline{c}_N}{d\tau}=\frac{1}{\varepsilon_1\zeta'}\cdot\left[\frac{\underline{c}_{N+1}-2\underline{c}_N+\underline{c}_{N-1}}{h_I^2}+\frac{2}{\underline{x}_N}\frac{\underline{c}_{N+1}-\underline{c}_{N-1}}{2h_I}\right]$$

$$\frac{d\theta_N}{d\tau}=\frac{\psi_1}{\zeta'}\left[\frac{\theta_{N+1}-2\theta_N+\theta_{N-1}}{h_I^2}+\frac{2}{\underline{x}_N}\frac{\theta_{N+1}-\theta_{N-1}}{2h_I}\right]$$

$$\frac{d\underline{c}_{N+2}}{d\tau}=\frac{1}{\varepsilon_2}\cdot\left[\frac{\frac{\underline{c}_{N+3}-2\underline{c}_{N+2}+\underline{c}_{N+1}}{h_{II}^2}+\frac{2}{\underline{x}_{N+2}}\frac{\underline{c}_{N+3}-\underline{c}_{N+1}}{2h_{II}}-\exp\left(-\frac{\left(\underline{x}_{N+2}-\underline{x}_1\right)^2}{\Delta^2}\right)}{\left(\begin{array}{c}\frac{3\sqrt{\pi}}{4}\left(\Delta^3+2\underline{x}_1^2\Delta\right)\left(erf\left(\frac{r_2-\underline{x}_1}{\Delta}\right)-erf\left(\frac{r_1-\underline{x}_1}{\Delta}\right)\right)-\\ \frac{3}{2}\left(\underline{x}_1+r_2\right)\cdot\exp\left(-\frac{\left(r_2-\underline{x}_1\right)^2}{\Delta^2}\right)+\frac{3}{2}\left(r_1+\underline{x}_1\right)\cdot\exp\left(-\frac{\left(r_1-\underline{x}_1\right)^2}{\Delta^2}\right)\end{array}\right)}\phi^2\cdot\underline{c}_{N+2}^{\,n}exp\left(\gamma\left(1-\frac{1}{\theta_{N+2}}\right)\right)\right],$$

$$\frac{d\theta_{N+2}}{d\tau}=\psi_2\cdot\left[\frac{\frac{\theta_{N+3}-2\theta_{N+2}+\theta_{N+1}}{h_{II}^2}+\frac{2}{\underline{x}_{N+2}}\frac{\theta_{N+3}-\theta_{N+1}}{2h_{II}}-\exp\left(-\frac{\left(\underline{x}_{N+2}-\underline{x}_1\right)^2}{\Delta^2}\right)}{\left(\begin{array}{c}\frac{3\sqrt{\pi}}{4}\left(\Delta^3+2\underline{x}_1^2\Delta\right)\left(erf\left(\frac{r_2-\underline{x}_1}{\Delta}\right)-erf\left(\frac{r_1-\underline{x}_1}{\Delta}\right)\right)-\\ \frac{3}{2}\left(\underline{x}_1+r_2\right)\cdot\exp\left(-\frac{\left(r_2-\underline{x}_1\right)^2}{\Delta^2}\right)+\frac{3}{2}\left(r_1+\underline{x}_1\right)\cdot\exp\left(-\frac{\left(r_1-\underline{x}_1\right)^2}{\Delta^2}\right)\end{array}\right)}\beta\phi^2\cdot\underline{c}_{N+2}^{\,n}exp\left(\gamma\left(1-\frac{1}{\theta_{N+2}}\right)\right)\right]$$

$$\frac{d\underline{c}_i}{d\tau}=\frac{1}{\varepsilon_2}\cdot\left[\frac{\frac{\underline{c}_{i+1}-2\underline{c}_i+\underline{c}_{i-1}}{h_{II}^2}+\frac{2}{\underline{x}_i}\frac{\underline{c}_{i+1}-\underline{c}_{i-1}}{2h_{II}}-\exp\left(-\frac{\left(\underline{x}_i-\underline{x}_1\right)^2}{\Delta^2}\right)}{\left(\begin{array}{c}\frac{3\sqrt{\pi}}{4}\left(\Delta^3+2\underline{x}_1^2\Delta\right)\left(erf\left(\frac{r_2-\underline{x}_1}{\Delta}\right)-erf\left(\frac{r_1-\underline{x}_1}{\Delta}\right)\right)-\\ \frac{3}{2}\left(\underline{x}_1+r_2\right)\cdot\exp\left(-\frac{\left(r_2-\underline{x}_1\right)^2}{\Delta^2}\right)+\frac{3}{2}\left(r_1+\underline{x}_1\right)\cdot\exp\left(-\frac{\left(r_1-\underline{x}_1\right)^2}{\Delta^2}\right)\end{array}\right)}\phi^2\cdot\underline{c}_i^{\,n}exp\left(\gamma\left(1-\frac{1}{\theta_i}\right)\right)\right]$$

$$\frac{d\theta_i}{d\tau}=\psi_2\cdot\left[\frac{\frac{\theta_{i+1}-2\theta_i+\theta_{i-1}}{h_{II}^2}+\frac{2}{\underline{x}_i}\frac{\theta_{i+1}-\theta_{i-1}}{2h_{II}}-\exp\left(-\frac{\left(\underline{x}_i-\underline{x}_1\right)^2}{\Delta^2}\right)}{\left(\begin{array}{c}\frac{3\sqrt{\pi}}{4}\left(\Delta^3+2\underline{x}_1^2\Delta\right)\left(erf\left(\frac{r_2-\underline{x}_1}{\Delta}\right)-erf\left(\frac{r_1-\underline{x}_1}{\Delta}\right)\right)-\\ \frac{3}{2}\left(\underline{x}_1+r_2\right)\cdot\exp\left(-\frac{\left(r_2-\underline{x}_1\right)^2}{\Delta^2}\right)+\frac{3}{2}\left(r_1+\underline{x}_1\right)\cdot\exp\left(-\frac{\left(r_1-\underline{x}_1\right)^2}{\Delta^2}\right)\end{array}\right)}\beta\phi^2\cdot\underline{c}_i^{\,n}exp\left(\gamma\left(1-\frac{1}{\theta_i}\right)\right)\right]$$

$,i=N+3,\cdots,N+M$

$$\frac{dc_{N+M+1}}{d\tau}=\frac{1}{\varepsilon_2}\cdot\left[\begin{array}{c}\frac{c_{N+M+2}-2c_{N+M+1}+c_{N+M}}{h_{II}^2}+\frac{2}{x_{N+M+1}}\frac{c_{N+M+2}-c_{N+M}}{2h_{II}}-\\ \exp\left(-\frac{\left(x_{N+M+1}-x_1\right)^2}{\Delta^2}\right)\\ \hline \left(\begin{array}{c}\frac{3\sqrt{\pi}}{4}\left(\Delta^3+2x_1^2\Delta\right)\left(erf\left(\frac{r_2-x_1}{\Delta}\right)-erf\left(\frac{r_1-x_1}{\Delta}\right)\right)-\\ \frac{3}{2}\left(x_1+r_2\right)\cdot\exp\left(-\frac{\left(r_2-x_1\right)^2}{\Delta^2}\right)+\frac{3}{2}\left(r_1+x_1\right)\cdot\exp\left(-\frac{\left(r_1-x_1\right)^2}{\Delta^2}\right)\end{array}\right)\end{array}\right]\phi^2\cdot c_{N+M+1}^n exp\left(\gamma\left(1-\frac{1}{\theta_{N+M+1}}\right)\right)$$

$$\frac{d\theta_{N+M+1}}{d\tau}=\psi_2\cdot\left[\begin{array}{c}\frac{\theta_{N+M+2}-2\theta_{N+M+1}+\theta_{N+M}}{h_{II}^2}+\frac{2}{x_{N+M+1}}\frac{\theta_{N+M+2}-\theta_{N+M}}{2h_{II}}-\\ \exp\left(-\frac{\left(x_{N+M+1}-x_1\right)^2}{\Delta^2}\right)\\ \hline \left(\begin{array}{c}\frac{3\sqrt{\pi}}{4}\left(\Delta^3+2x_1^2\Delta\right)\left(erf\left(\frac{r_2-x_1}{\Delta}\right)-erf\left(\frac{r_1-x_1}{\Delta}\right)\right)-\\ \frac{3}{2}\left(x_1+r_2\right)\cdot\exp\left(-\frac{\left(r_2-x_1\right)^2}{\Delta^2}\right)+\frac{3}{2}\left(r_1+x_1\right)\cdot\exp\left(-\frac{\left(r_1-x_1\right)^2}{\Delta^2}\right)\end{array}\right)\end{array}\right]\beta\phi^2\cdot c_{N+M+1}^n exp\left(\gamma\left(1-\frac{1}{\theta_{N+M+1}}\right)\right)$$

(98)

$$\frac{dc_{N+M+3}}{d\tau}=\frac{1}{\varepsilon_3\zeta}\cdot\left[\frac{c_{N+M+4}-2c_{N+M+3}+c_{N+M+2}}{h_{III}^2}+\frac{2}{x_{N+M+3}}\frac{c_{N+M+4}-c_{N+M+2}}{2h_{III}}\right]$$

$$\frac{d\theta_{N+M+3}}{d\tau}=\frac{\psi_3}{\zeta}\cdot\left[\frac{\theta_{N+M+4}-2\theta_{N+M+3}+\theta_{N+M+2}}{h_{III}^2}+\frac{2}{x_{N+M+3}}\frac{\theta_{N+M+4}-\theta_{N+M+2}}{2h_{III}}\right]$$

$$\frac{dc_i}{d\tau}=\frac{1}{\varepsilon_3\zeta}\cdot\left[\frac{c_{i+1}-2c_i+c_{i-1}}{h_{III}^2}+\frac{2}{x_i}\frac{c_{i+1}-c_{i-1}}{2h_{III}}\right]$$

$$\frac{d\theta_i}{d\tau}=\frac{\psi_3}{\zeta}\cdot\left[\frac{\theta_{i+1}-2\theta_i+\theta_{i-1}}{h_{III}^2}+\frac{2}{x_i}\frac{\theta_{i+1}-\theta_{i-1}}{2h_{III}}\right],$$

$$i=N+M+4,\cdots,N+M+K+2$$

$$\frac{dc_{N+M+K+2}}{d\tau}=\frac{1}{\varepsilon_3\zeta}\cdot\left[\begin{array}{c}\frac{c_{N+M+K+3}-2c_{N+M+K+2}+c_{N+M+K+1}}{h_{III}^2}+\\ \frac{2}{x_{N+M+K+2}}\frac{c_{N+M+K+3}-c_{N+M+K+1}}{2h_{III}}\end{array}\right]$$

$$\frac{d\theta_{N+M+K+2}}{d\tau}=\frac{\psi_3}{\zeta}\cdot\left[\begin{array}{c}\frac{\theta_{N+M+K+3}-2\theta_{N+M+K+2}+\theta_{N+M+K+1}}{h_{III}^2}+\\ \frac{2}{x_{N+M+K+2}}\frac{\theta_{N+M+K+3}-\theta_{N+M+K+1}}{2h_{III}}\end{array}\right]$$

In the Python computer program, the concentrations and temperatures at boundary points are represented by variables $c0=c_0$, $\theta0=\theta_0$, $cN1=c_{N+1}$, $\theta N1=\theta_{N+1}$, $cNM1=c_{N+M+2}$, $\theta NM1=\theta_{N+M+2}$, $cNMK1=c_{N+M+K+3}$, and $\theta NMK1=\theta_{N+M+K+3}$. Additionally, an array denoted as $c[0,...,N+M+K-1]$ and

$\theta[0,...,N+M+K-1]$ are utilized to store the concentration at the internal mesh points as follows:

$$c[0]=\underline{c}_1,...,c[N-1]=\underline{c}_N,c[N]=\underline{c}_{N+2},...,c[N+M-1]=\underline{c}_{N+M+1},$$

$$c[N+M]=\underline{c}_{N+M+3},...,c[N+M+K-1]=\underline{c}_{N+M+K+2}.$$

$$\theta[0]=\theta_1,...,\theta[N-1]=\theta_N,\theta[N]=\theta_{N+2},...,\theta[N+M-1]=\theta_{N+M+1},$$

$$\theta[N+M]=\theta_{N+M+3},...,\theta[N+M+K-1]=\theta_{N+M+K+2}.$$

Chapter 5 – Results and Discussion

In this chapter, numerical schemes and computer programs are verified for pellets of various geometries with the non-uniform distribution of active catalytic material. Initially, a detailed comparison between analytical predictions and numerical outcomes is presented for isothermal catalytic pellets of slab and spherical geometries with a step distribution of active material. Subsequently, the effects of process parameters on concentration and temperature profiles of non-isothermal core-shell pellets with a Gaussian distribution of catalytic material in the active layer are described. Finally, an evaluation of the effectiveness of the catalyst is conducted for various process parameters for uniform and non-uniform distributions.

5.1 Catalytic pellets with step distribution of active material

Steady-state mass balance equations for an isothermal irreversible first-order reaction in catalytic pellets with step distribution of active material were derived by solving Eqs. (1), (2) , and (3) analytically and numerically. The method of separation of variables was employed to obtain an analytical solution and the numerical solution was obtained using the method of lines with a finite difference approximation for spatial derivatives. For numerical solution, the following uniform mesh is introduced, $N = 100$ is the number of interior mesh points in Region 1, $M = 100$ is the number of interior mesh points in Region 2, and $K = 100$ is the number of interior mesh points in Region 3. The mesh spacing in each region is given as $h_I = \frac{r_1}{N+1}, h_{II} = \frac{r_2 - r_1}{M+1}$, $h_{III} = \frac{1-r_2}{K+1}$, where $r_1 = 0.45$ is the position of the 1st layer and $r_2 = 0.55$ is the position of the 2nd layer.

Figures 5.1 and **5.2** illustrate the comparison of the results of the analytical solution summarized in **Table 4.1** and the numerical solution described in Section 4.1.2 for slab and spherical pellet geometries, respectively.

According to **Figure 5.1**, the reactant concentration profiles in all three regions of the slab-type catalyst pellet obtained numerically correspond to the analytical solution by Eqs. (49) which coincides with the solution provided by Cho [5].

For a spherical pellet, the analytical solutions provided in Appendix B differ from the analytical solution obtained by Cho [5]. The equations were verified for accuracy by solving them using Wolfram Mathematica, as detailed in Appendix C. Figure 5.2 illustrates that the

reactant concentration profiles in all three regions in a spherical pellet obtained numerically correspond to the analytical solution by Eqs. (50).

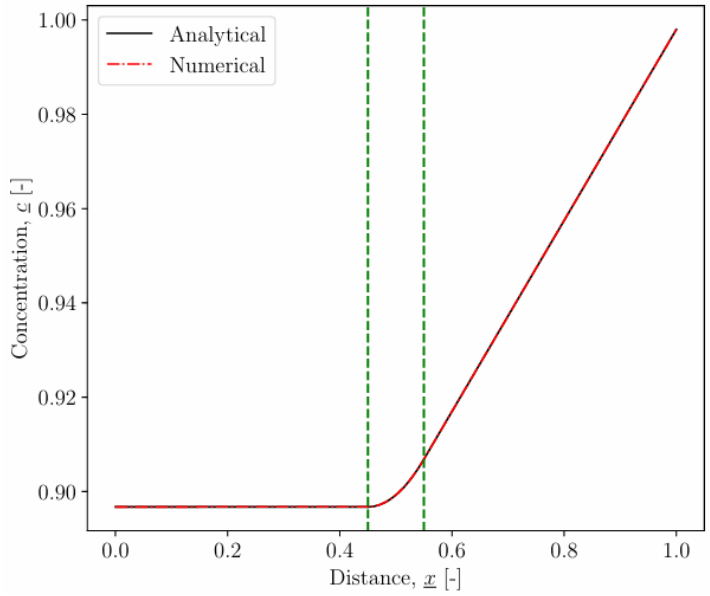

Figure 5.1: Concentration profile in the slab obtained by analytical and numerical solution.

$$Bi = 0.5,\ \phi = 1.5,\ \zeta = 1,\ r_1 = 0.45,\ r_2 = 0.55.$$

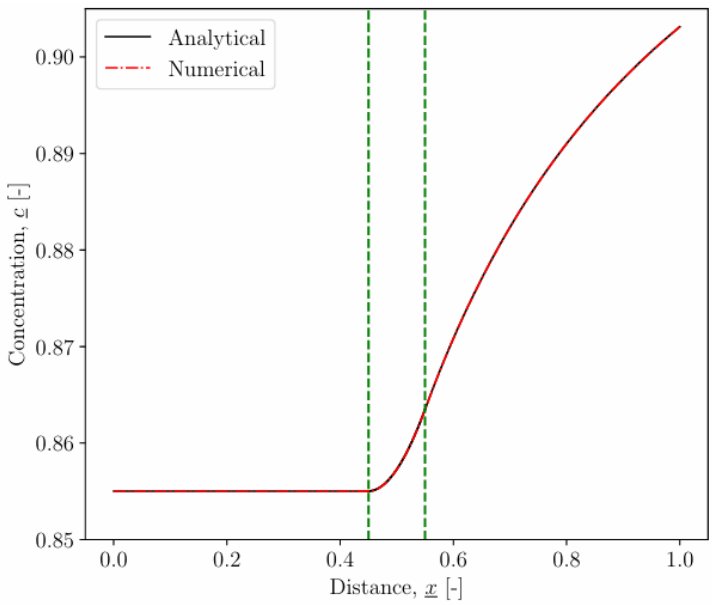

Figure 5.2: Concentration profile in the spherical pellet obtained by analytical and numerical solution.

$$Bi = 0.5,\ \phi = 1.5,\ \zeta = 1,\ r_1 = 0.45,\ r_2 = 0.55.$$

5.2 Catalytic pellets with non-uniform distribution of active material

5.2.1 Effect of process parameters on reactant concentration and temperature distributions in pellets

The set of model parameters used to plot concentration and temperature profiles at various parameters is listed in **Table 5.1.**

Table 5.1: The set of model parameters used for simulations of concentration and temperature profiles

z	ϕ	β	γ	n	Bi_m	Bi_h	r_1	r_2	$\underline{x}_1$	Δ	Fig
0	0.5	0.1	5	~	100	100	0.05	0.95	0.5	0.08	5.3a
2	0.5	0.1	5	~	100	100	0.05	0.95	0.5	0.08	5.3b
0	0.5	~	5	1	100	100	0.3	0.7	0.5	0.2	5.4a
2	0.5	~	5	1	100	100	0.3	0.7	0.5	0.2	5.4b
0	0.5	0.1	~	1	100	100	0.3	0.7	0.5	0.08	5.5a
2	0.5	0.1	~	1	100	100	0.3	0.7	0.5	0.08	5.5b
0	0.5	0.1	5	1	~	~	0.05	0.95	0.5	0.08	5.6a
2	0.5	0.1	5	1	~	~	0.05	0.95	0.5	0.08	5.6b
0	0.5	0.1	5	1	100	100	0.1	0.9	~	0.5	5.7a
2	0.5	0.1	5	1	100	100	0.1	0.9	~	0.5	5.7b

The symbols ~ indicates that simulations were performed for various values of parameters shown in the figure legend.

Figures 5.3 – 5.7 show the dimensionless concentration and temperature as a function of the dimensionless distance within the pellet. The different curves represent the concentration and temperature profiles for various parameters such as reaction order, Biot number, Arrhenius number, energy generation factor, and the position of the Gaussian distribution peak.

Figure 5.3 illustrates the profiles for slab-type and spherical geometry pellets, depicting how the concentration and temperature vary across the pellet at different reaction orders. A higher *n* value implies that the reaction rate is more sensitive to changes in the reactant concentration. Higher reaction orders result in faster consumption of reactants where their concentration is higher, leading to steeper gradients. Conversely, lower reaction orders yield

more gradual changes in concentration across the pellet. The concentration of the reactant decreases as it moves from 1 to 0, implying that the direction of mass transfer is from the particle surface to the center of the pellet and the reactant being consumed in the reaction process. Since the reaction is exothermic $\beta > 0$, the temperature profile starts to increase. For both slab-type and spherical pellet, the Gaussian distribution is centered at 0.5, meaning that the catalytic activity reaches its maximum here. For all three reaction orders, the changes in slope around this point are observed. As it approaches the center of the pellet, the concentration no longer changes significantly since there is less reactant available to be consumed after the peak, resulting in a linear or constant concentration profile. Due to the decrease of the reaction rate and heat generation, the temperature approaches an asymptote or a boundary value, determined by the external temperature conditions.

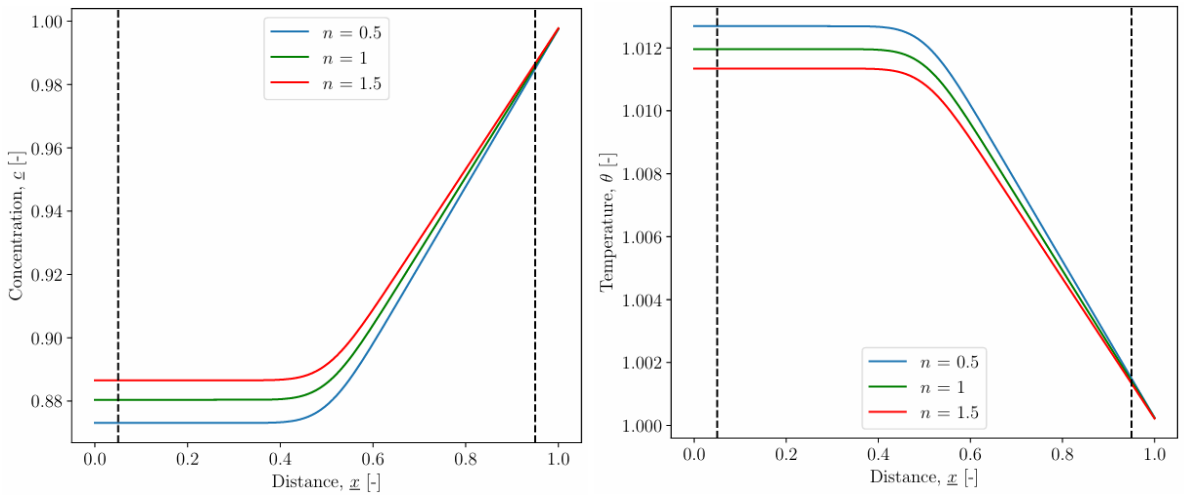

a)

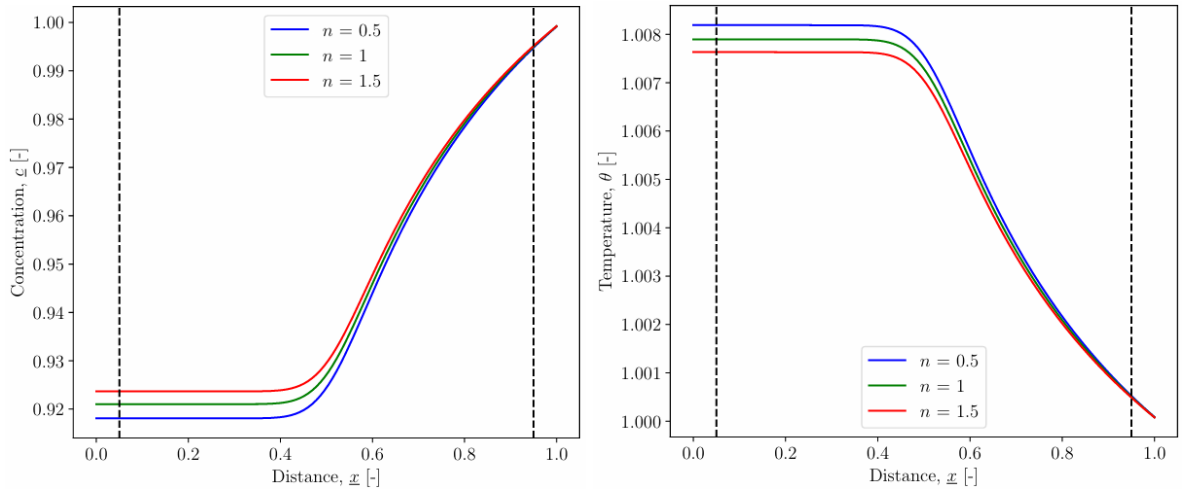

b)

Figure 5.3: Concentration and temperature profiles at different reaction orders n for various pellet geometries: a) slab-type and b) spherical:
$\phi = 0.5,\ \gamma = 5,\ r_1 = 0.05,\ r_2 = 0.95,\ x_1 = 0.5,\ \Delta = 0.08,\ \beta = 0.1,\ Bi_m = Bi_h = 100.$

The changes in the concentration and temperature profiles for different Arrhenius numbers are illustrated in **Figure 5.4**. In the case of exothermic reaction ($\beta > 0$), with an increasing Arrhenius number, the rate of reaction becomes larger, leading to a rapid consumption of reactants. This results in a steep concentration gradient, with lower concentrations of reactants in the hotter regions. Meanwhile, the opposite trend is observed for endothermic reactions with the negative value of β, since the reaction rate decreases due to the cooling of the catalytic reaction zone. The Arrhenius number significantly influences the temperature profile within a pellet during an exothermic reaction. It can be seen that a higher Arrhenius number correlates with faster heat production, leading to a notable rise in temperature from the outer boundary to the center of the pellet.

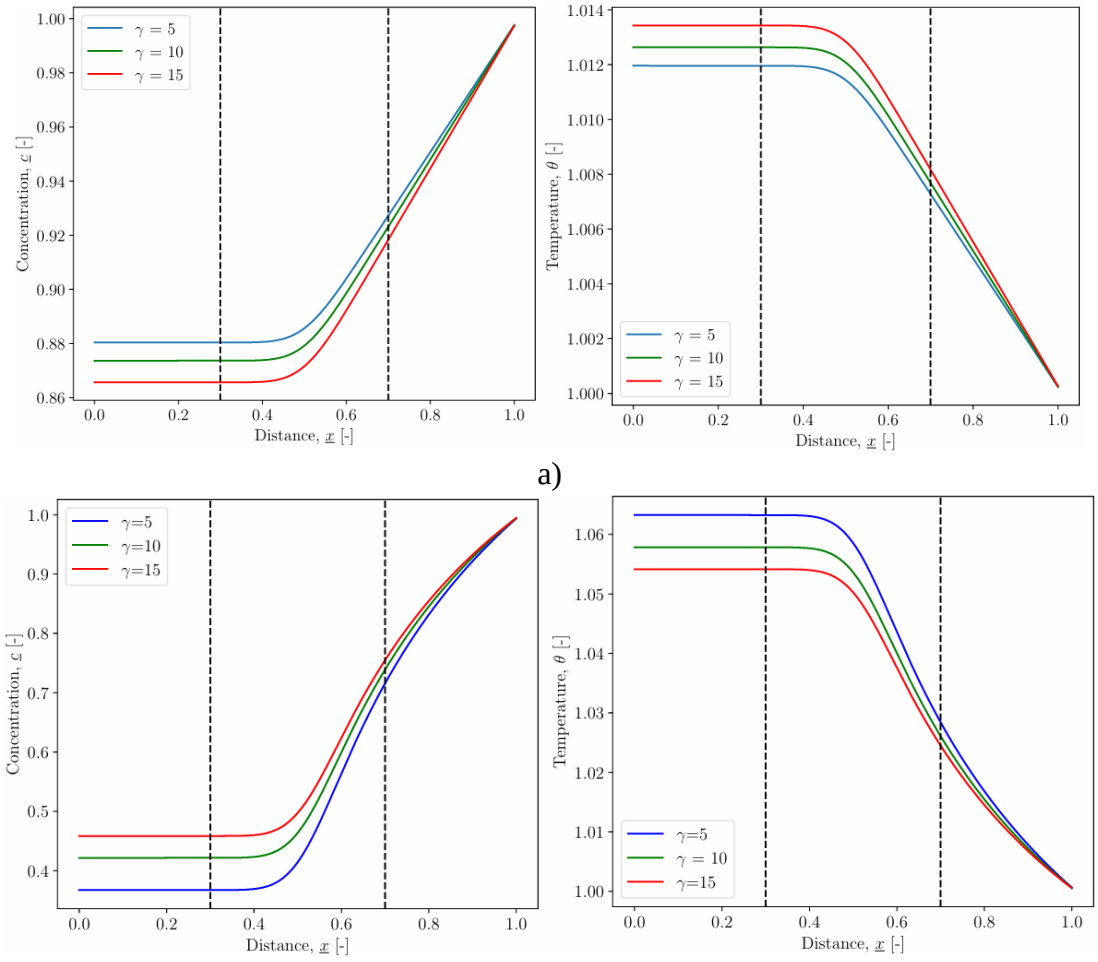

Figure 5.4: Concentration and temperature profiles at different Arrhenius numbers for various pellet geometries: a) slab-type and b) spherical:
$\phi = 1.5,\ \beta = 0.1,\ r_1 = 0.3,\ r_2 = 0.7,\ x_1 = 0.5,\ \Delta = 0.08,\ n = 1,\ Bi_m = Bi_h = 100.$

Figure 5.5 demonstrates concentration and temperature profiles for different values of Biot number for both slab-typed and spherical pellets. When *Bi* is equal to 1, the external transfer resistance is comparable to the internal diffusion resistance. This balance can lead to a relatively lower concentration and higher temperature within the pellet compared to a system with higher Biot numbers where internal resistance dominates.

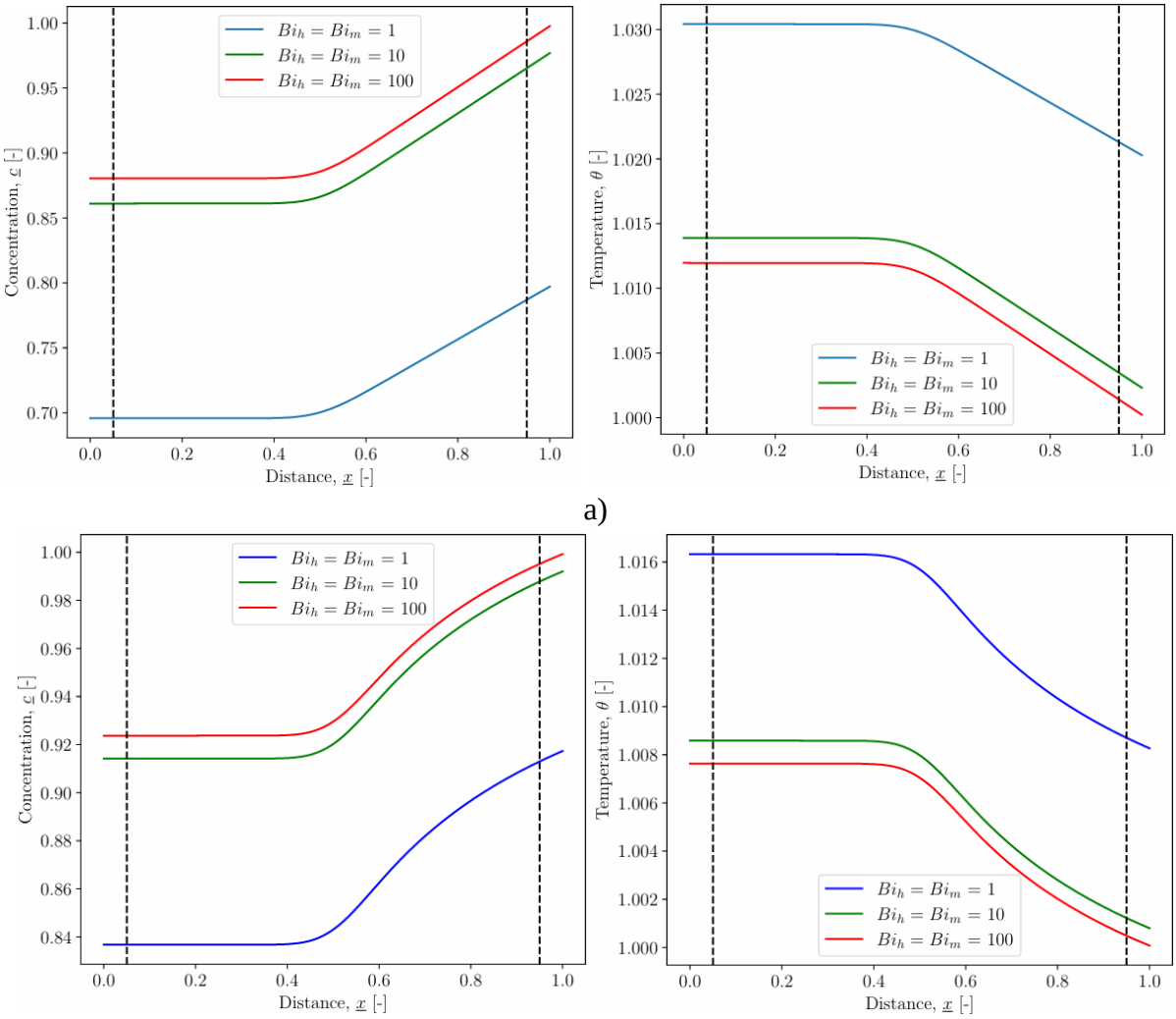

a)

b)

***Figure 5.5: Concentration and temperature profiles at different heat and mass Biot numbers for various pellet geometries: a) slab-type and b) spherical*:**

$\phi = 0.5,\ \beta = 0.1,\ r_1 = 0.05,\ r_2 = 0.95,\ x_1 = 0.5,\ \Delta = 0.08,\ n = 1,\ \gamma = 5.$

Figure 5.6 illustrates the concentration and temperature profiles within a catalytic pellet for different values of the energy generation factor for both slab-type and spherical pellets. The energy generation factor typically influences the rate at which heat is produced or consumed in the reaction, impacting both temperature and concentration profiles. For concentration profiles, when the reaction is exothermic and β is positive, a higher reaction rate, especially near the

center of activity distribution, is observed. The energy released during the reaction heats the porous pellet, leading to an increase in temperature. This temperature rise enhances the reactant consumption rate within the $\underline{x}_1$ range, reducing the amount of reactant species A that can diffuse into the region closer to the pellet's center, where the reaction rate is notably slower than near the Gaussian distribution center. A negative β indicates an endothermic reaction where the reaction absorbs heat. This can lead to an increase in the reaction rate with a decrease in temperature. The concentration profile in this case might show a less pronounced decline compared to the exothermic scenario because the absorption of heat could moderate the reaction rate. When β is zero, the reaction neither produces nor consumes energy, thus any changes in the temperature profile are not observed.

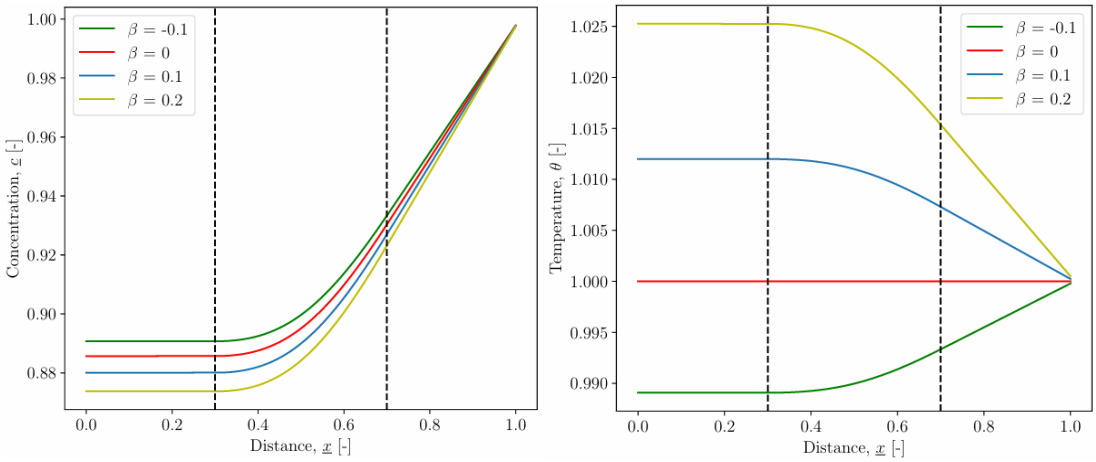

a)

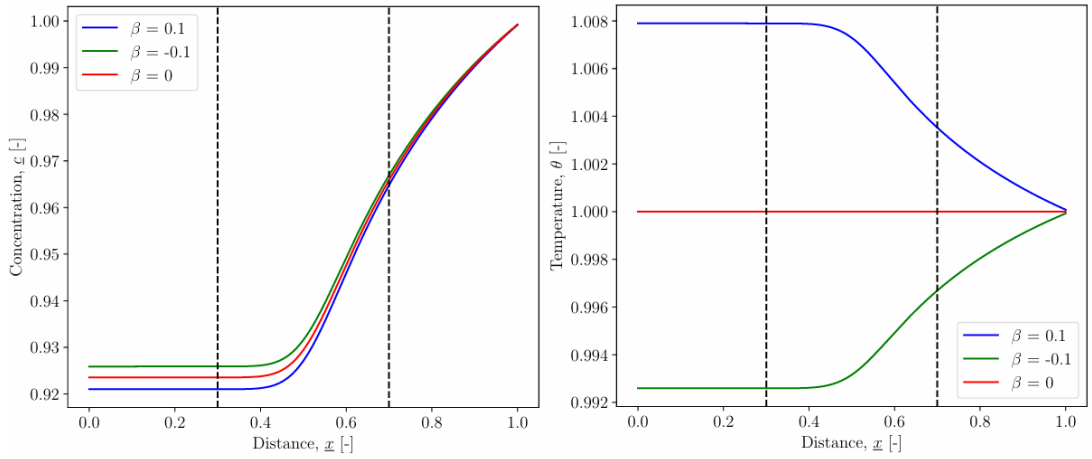

b)

***Figure 5.6: Concentration and temperature profiles at different beta for various pellet geometries: a) slab-type and b) spherical*:**

$\phi = 0.5,\ \gamma = 5,\ r_1 = 0.3,\ r_2 = 0.7,\ x_1 = 0.5,\ \Delta = 0.2,\ n = 1,\ Bi_m = Bi_h = 100.$

Figure 5.7 shows how the concentration and temperature profiles within a catalytic pellet are affected by varying the position of the peak in the Gaussian distribution. The position

of $\underline{x}_1$ affects where the reaction activity is most intense within the pellet. When $\underline{x}_1$ is closer to the center of the pellet, it leads to a sharper concentration gradient around that area. When the most amount of catalyst is located near the right boundary, the profile suggests a more uniform consumption of reactants throughout the pellet. This suggests that situating the peak reaction activity near the center of the pellet results in increased temperatures and reduced concentrations within the pellet.

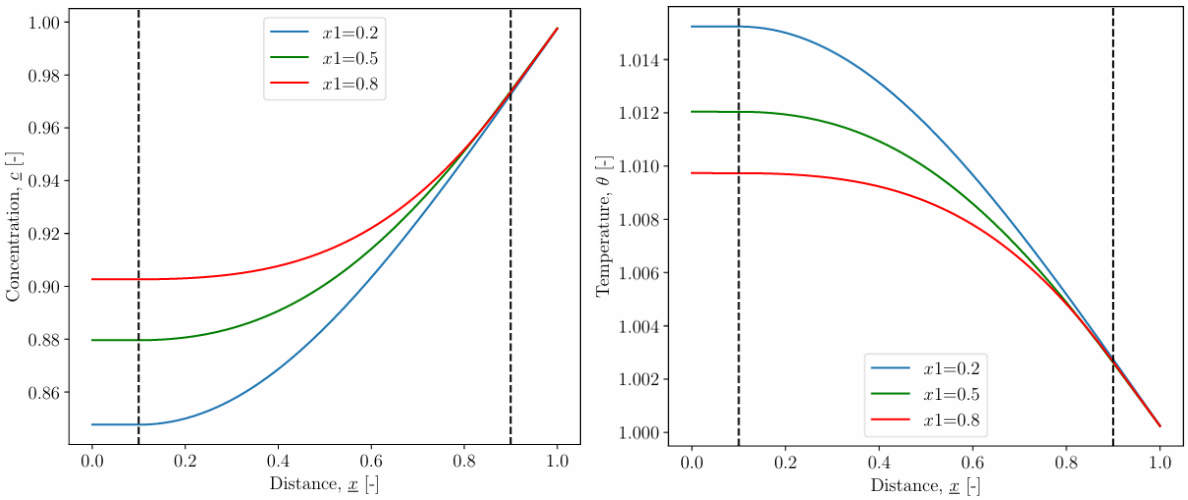

a)

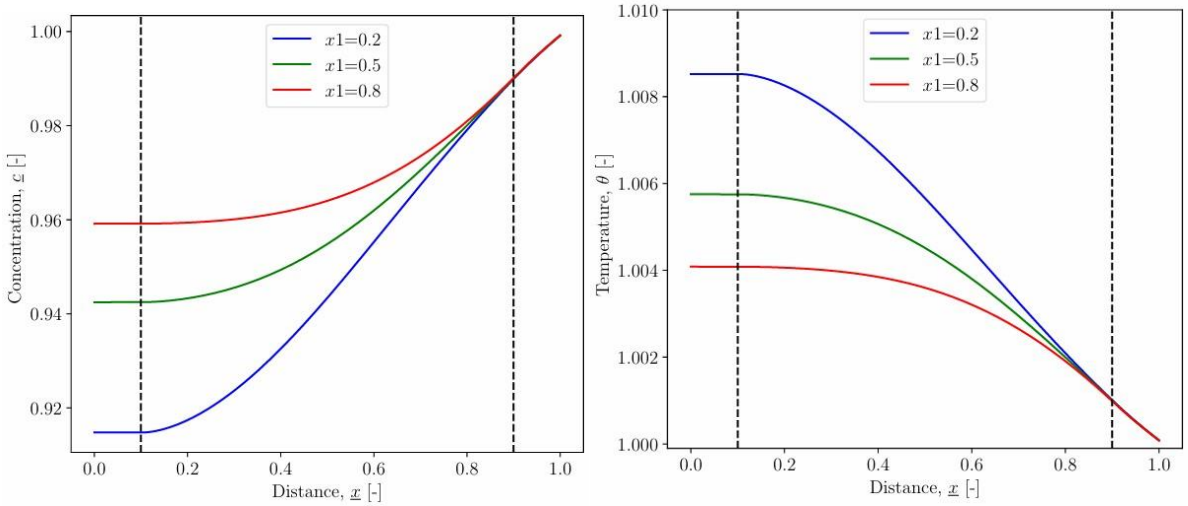

b)

Figure 5.7: Concentration and temperature profiles at different positions of Gaussian distribution of active species for various pellet geometries: a) slab-type and b) spherical: $\phi = 0.5,\ \beta = 0.1,\ \gamma = 5,\ r_1 = 0.1,\ r_2 = 0.9,\ \Delta = 0.5,\ n = 1,\ Bi_m = Bi_h = 100.$

5.2.2 Parametric analysis of catalyst effectiveness

The set of model parameters used to plot effectiveness factors at various parameters is listed in **Table 5.2.**

Table 5.2. The set of model parameters used for simulations of effectiveness factor

z	ϕ	β	γ	n	Bi_m	Bi_h	r_1	r_2	$\underline{x}_1$	Δ	Fig
0	$\vec{x}$	0.1	5	1	$\sim$	$\sim$	0.45	0.55	0.5	0.08	5.8a
2	$\vec{x}$	0.1	5	1	$\sim$	$\sim$	0.45	0.55	0.5	0.08	5.8b
0	$\vec{x}$	-0.1	5	1	$\sim$	$\sim$	0.45	0.55	0.5	0.08	5.9a
2	$\vec{x}$	-0.1	5	1	$\sim$	$\sim$	0.45	0.55	0.5	0.08	5.9b
0	0.5	0.1	$\vec{x}$	1	100	100	0.05	0.95	$\sim$	0.08	5.10a
2	0.5	0.1	$\vec{x}$	1	100	100	0.05	0.95	$\sim$	0.08	5.10b
0	0.5	-0.1	$\vec{x}$	1	100	100	0.05	0.95	$\sim$	0.08	5.11a
2	0.5	-0.1	$\vec{x}$	1	100	100	0.45	0.55	$\sim$	0.08	5.11b
0	0.5	$\vec{x}$	5	1	100	100	0.05	0.95	$\sim$	0.08	5.12a
2	0.5	$\vec{x}$	5	1	100	100	0.05	0.95	$\sim$	0.08	5.12b
0	0.5	0.1	5	1	100	100	0.05	0.95	$\vec{x}$	$\sim$	5.13a
2	0.5	0.1	5	1	100	100	0.05	0.95	$\vec{x}$	$\sim$	5.14b
0	0.5	-0.1	5	1	100	100	0.05	0.95	$\vec{x}$	$\sim$	5.15a
2	0.5	-0.1	5	1	100	100	0.05	0.95	$\vec{x}$	$\sim$	5.15b
0	0.5	0.1	5	1	100	100	0.05	0.95	$\sim$	$\vec{x}$	5.16a
2	0.5	0.1	5	1	100	100	0.05	0.95	$\sim$	$\vec{x}$	5.16b

The symbols $\vec{x}$ and $\sim$ denotes that simulations were performed for various values of parameters indicated on the x-axis and shown in the figure legend, respectively.

Figures 5.8 – 5.16 highlight the influence of various parameters on the effectiveness factor in catalytic reactions within slab-type pellets, offering insights into how different reaction and distribution conditions can impact catalytic performance.

From **Figs 5.8** and **5.9,** it can be observed that the large value of the Thiele modulus reduces the effectiveness factor in both endothermic and exothermic reactions for slab-type and spherical pellets. This is due to the concentration and temperature gradients within the pellet, which occur when diffusion is slow compared to the reaction rate. On the contrary, the effectiveness factor is high when the Thiele modulus is small since diffusion is fast compared to the reaction rate, leading to a uniform concentration and temperature profile within the pellet.

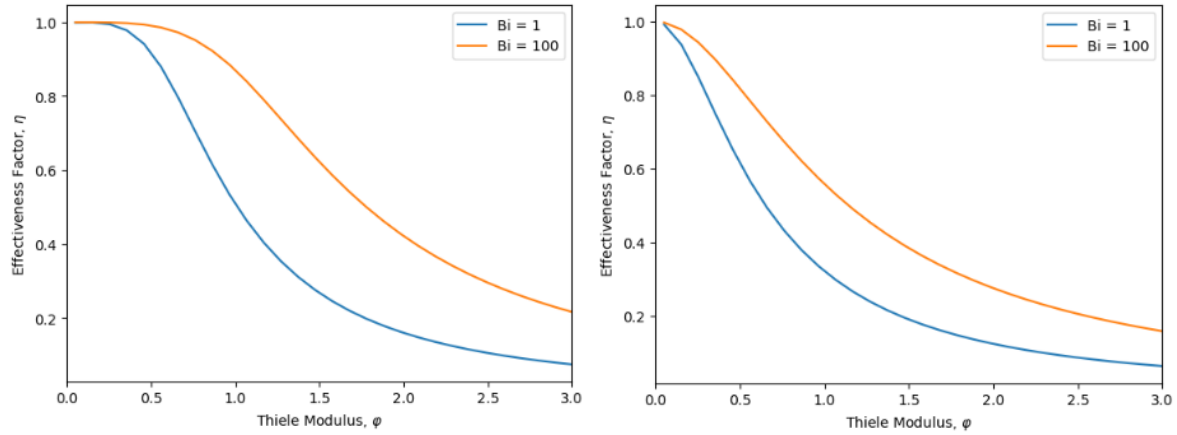

Figure 5.8: Effectiveness factor dependence on Thiele modulus for slab-type pellet: (a) exothermic reaction with $\beta = 0.1$ ***and (b) endothermic reaction with*** $\beta = -0.1$**.** $\gamma = 10,\ r_1 = 0.05,\ r_2 = 0.95,\ \underline{x}_1 = 0.5,\ \Delta = 0.08,\ n = 1.$

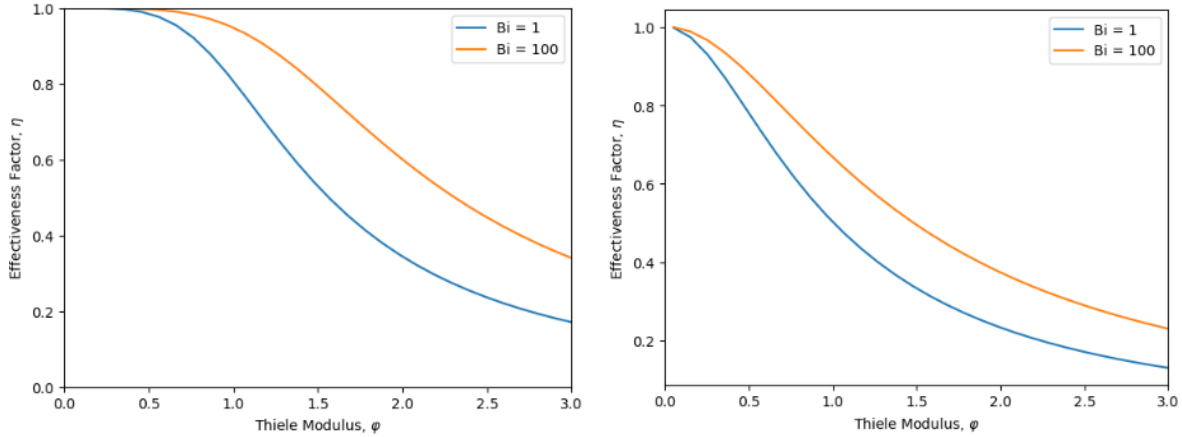

Figure 5.9: Effectiveness factor dependence on Thiele modulus for spherical pellet: (a) exothermic reaction with $\beta = 0.1$ ***and (b) endothermic reaction with*** $\beta = -0.1$**.** $\gamma = 10,\ r_1 = 0.05,\ r_2 = 0.95,\ \underline{x}_1 = 0.5,\ \Delta = 0.08,\ n = 1.$

In **Figs 5.10** and **5.11**, the effectiveness factor increases with a higher Arrhenius number in exothermic reactions for both pellet geometries, where temperature increase can significantly accelerate reaction rates at certain pellet regions, creating steep gradients. For endothermic reactions, a higher Arrhenius number reduces the reaction rate in cooler pellet regions, flattening the concentration profile and potentially decreasing the effectiveness factor. It can be seen that the effect of Arrhenius number is less pronounced when the peak of the Gaussian distribution is located at 0.9 which means that the most significant reaction activity is near the right boundary. This is because the boundary conditions can dominate the behavior at the edges, especially if fixed temperatures or concentrations are involved.

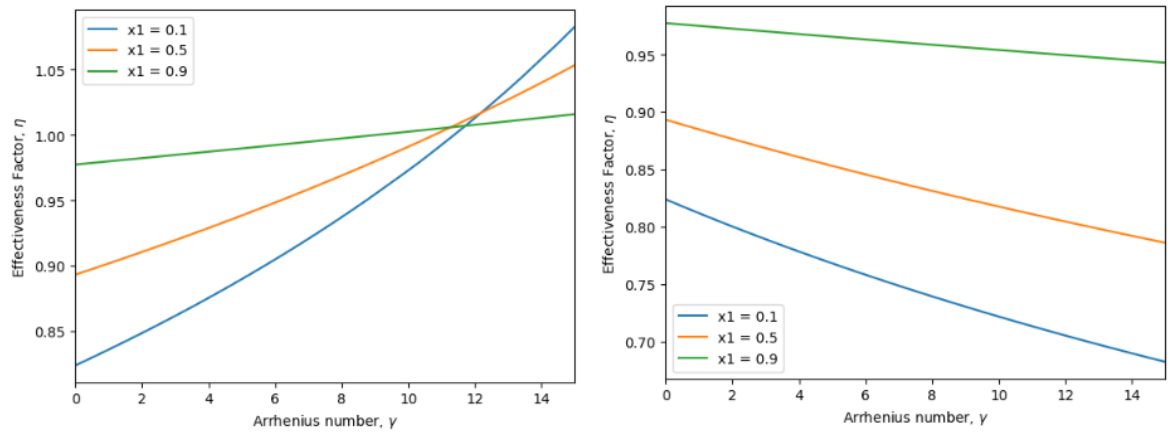

a) b)

Figure 5.10: Effectiveness factor dependence on Arrhenius number for slab-type pellet: (a) exothermic reaction with $\beta = 0.1$ ***and (b) endothermic reaction with*** $\beta = -0.1$.
$\phi = 0.5,\ r_1 = 0.05,\ r_2 = 0.95,\ \Delta = 0.08,\ n = 1,\ Bi_m = Bi_h = 100.$

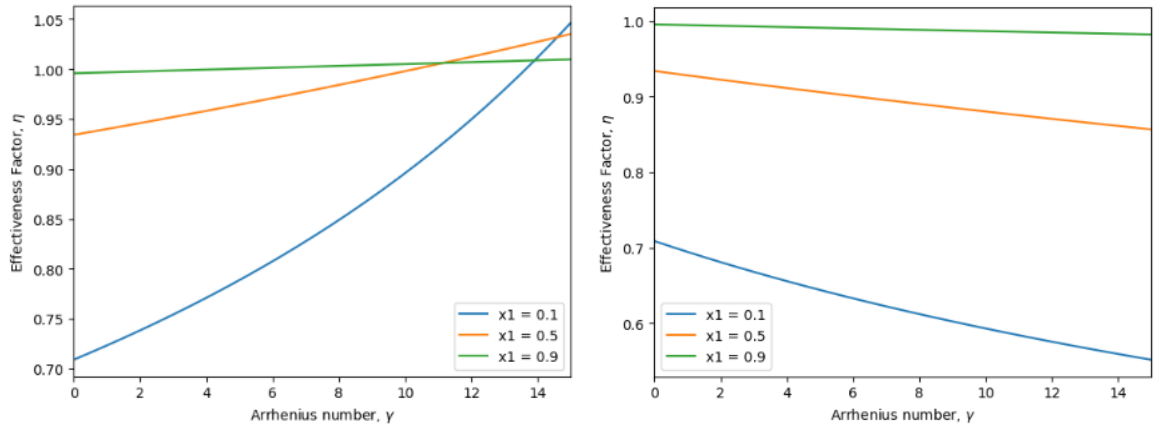

a) b)

Figure 5.11: Effectiveness factor dependence on Arrhenius number for spherical pellet: (a)exothermic reaction with $\beta = 0.1$ ***and (b) endothermic reaction with*** $\beta = -0.1$.
$\phi = 0.5,\ r_1 = 0.05,\ r_2 = 0.95,\ \Delta = 0.08,\ n = 1,\ Bi_m = Bi_h = 100.$

Figure 5.12 illustrates how the effectiveness factor changes with the Thiele modulus for different values of the energy generation factor. For all values of the energy generation factor, the effectiveness factor tends to decrease with increasing Thiele modulus because the reaction rate becomes increasingly limited by diffusion as the Thiele modulus increases. However, there is a more pronounced decline for $\beta = 0.2$, representing a highly exothermic reaction where significant heat generation occurs. The increased exothermicity enhances the reaction rates within the pellet, particularly at higher Thiele modulus, leading to a substantial increase in the effectiveness factor. The pronounced nature of this curve indicates that the effectiveness of the catalyst is significantly affected by the additional heat, which accelerates the reaction rate, overcoming diffusional limitations more effectively than in the less exothermic or isothermal cases.

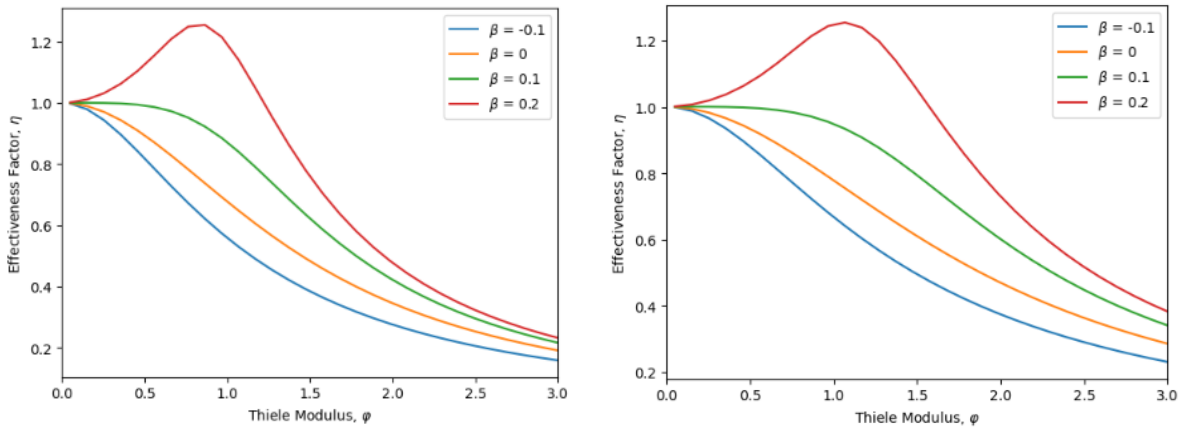

Figure 5.12: Effectiveness factor dependence on Thiele modulus for different values of energy generation factor: a) for slab-type pellet and b) for spherical pellet.
$\phi = 0.5,\ \gamma = 5,\ r_1 = 0.1,\ r_2 = 0.9,\ \underline{x}_1 = 0.5,\ \Delta = 0.08,\ n = 1,\ Bi_m = Bi_h = 100.$

Figures 5.13 and **5.14** investigate how the position of the Gaussian peak within a catalytic pellet affects the effectiveness factor for different widths of the Gaussian distribution. For both geometries, the green line represents the effectiveness factor for a Gaussian distribution with the largest width. The lack of change in the effectiveness factor as the peak position shifts indicates that the reaction intensity is almost uniformly distributed throughout the reactor. The fastest approach of effectiveness factor to 1 is observed when the center of distribution $\underline{x}_1$ is closer to the outer radius of the active layer. It can be explained by two factors. Firstly, with an increase in Δ, the region where the catalytic reaction takes place within the

pellet broadens. Secondly, when $\underline{x}_1$ approaches r_2, the active zone for the catalytic reaction migrates towards the pellet's outer surface. Despite the reduced concentration of catalytic sites in the pellet's core, the concentration of species A is also diminished there, leading to a lesser contribution from this central region to the overall efficiency of the porous catalyst. At the edges, the blue line demonstrates a sharp increase. This sharp rise indicates a sudden change in the effectiveness factor, which could be due to the boundary effects and the small width. When Δ is small, the Gaussian peak is narrow, which means that the effects of the reaction are concentrated in a smaller volume, intensifying the boundary effects.

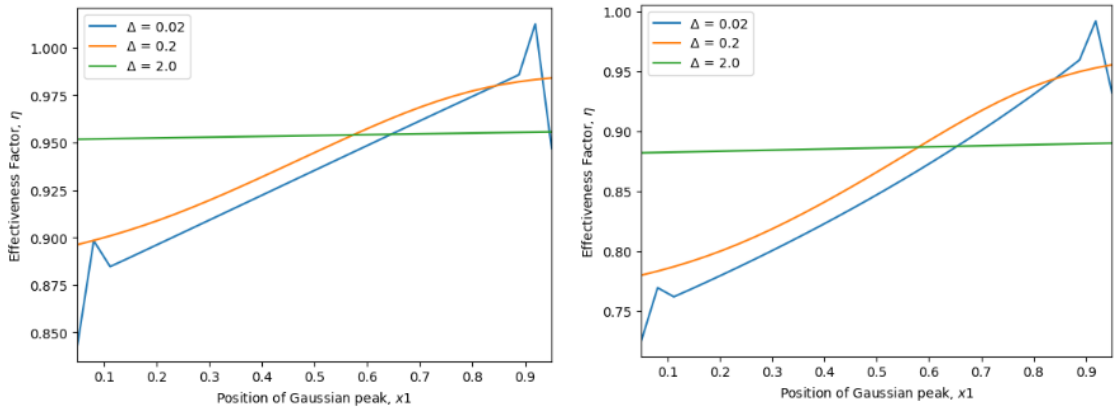

a) b)

Figure 5.13: Effect of varying the peak of Gaussian distribution on the effectiveness factor for slab-type pellet:

(a) exothermic reaction with $\beta = 0.1$ ***and (b) endothermic reaction with*** $\beta = -0.1$.

$\phi = 0.5,\ \gamma = 5,\ r_1 = 0.05,\ r_2 = 0.95,\ n = 1,\ Bi_m = Bi_h = 100.$

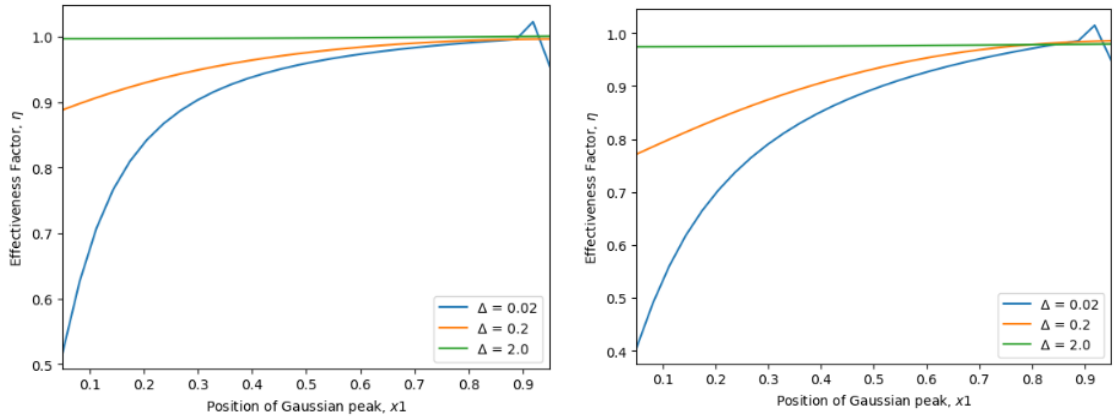

a) b)

Figure 5.14: Effect of varying the peak of Gaussian distribution on the effectiveness factor for spherical pellet:

(a) exothermic reaction with $\beta = 0.1$ ***and (b) endothermic reaction with*** $\beta = -0.1$.

$\phi = 0.5,\ \gamma = 5,\ r_1 = 0.05,\ r_2 = 0.95,\ n = 1,\ Bi_m = Bi_h = 100.$

Figures 5.15 and **5.16** illustrate how the effectiveness factor is affected by the width of activity distribution for different values of the peak. It is observed that the larger values of width lead to less effectiveness factor because as the width increases, the reactive zone becomes more spread out within the pellet. As the width increases, the effectiveness factor tends to increase for all curves, which implies that a broader distribution of catalytic activity within the pellet enhances its overall effectiveness. This effect is due to the increased area over which the reaction can occur, spreading out the catalytic sites more evenly throughout the pellet.

The green curve shows a more pronounced increase in the effectiveness factor compared to the other two. This suggests that when the peak of catalytic activity is closer to the outer radius of the active layer, the catalyst's effectiveness is more sensitive to changes in the width of the activity distribution. The closer proximity to the surface reduces diffusion limitations for reactants and products, making the catalyst more effective as the distribution of activity broadens. In contrast, when the peak is near the center the effectiveness factor is less sensitive to changes in Δ, as diffusion limitations play a more significant role in limiting the overall reaction rate, and the benefits of a broader activity distribution are less pronounced.

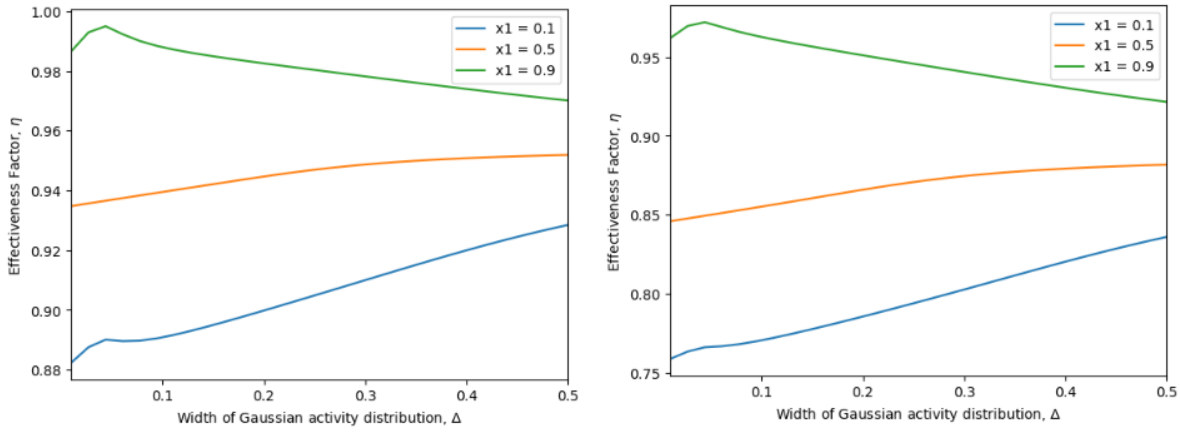

a) b)

Figure 5.15: Effect of varying the width of Gaussian distribution on the effectiveness factor for slab-type pellet:

(a) exothermic reaction with $\beta = 0.1$ ***and (b) endothermic reaction with*** $\beta = -0.1$.

$$\phi = 0.5,\ \gamma = 5,\ r_1 = 0.05,\ r_2 = 0.95,\ n = 1,\ Bi_m = Bi_h = 100.$$

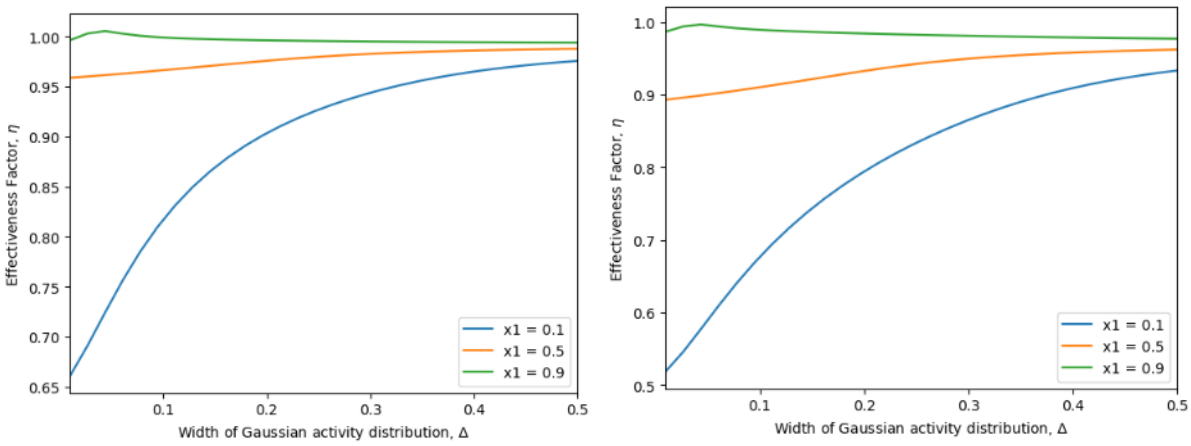

a) b)

Figure 5.16: Effect of varying the width of Gaussian distribution on the effectiveness factor for spherical pellet (a) exothermic reaction with $\beta = 0.1$ ***and (b) endothermic reaction with*** $\beta = -0.1$.

$$\phi = 0.5,\ \gamma = 5,\ r_1 = 0.05,\ r_2 = 0.95,\ n = 1,\ Bi_m = Bi_h = 100.$$

The values of effectiveness factor with uniform and non-uniform distribution of catalyst for slab-type and spherical pellet for other parameters are listed in **Table D.1** in **Appendix D.** It shows that a non-uniform distribution of active catalytic material gives a higher effectiveness factor than a uniform distribution.

Chapter 6 – Conclusion

Catalysts play a crucial role in enhancing the efficiency of chemical reactions, making the study of their distribution within catalytic pellets an important area of research. While there has been significant investigation into the impact of non-uniform catalyst distribution, less attention has been given to core-shell catalytic pellets. These pellets are particularly interesting because they offer a unique way to control reaction environments and improve catalyst effectiveness.

The core-shell structure, where the core is inert and the shell is catalytically active, presents a novel approach to catalyst design. This thesis aimed to explore how varying the catalyst distribution within the shell influences the overall reaction performance.

The objectives of this research were to develop a mathematical model for describing the reaction and diffusion processes in core-shell pellets and to analyze how Gaussian distributions affect the effectiveness of the catalyst. Thus, the mathematical model, including mass and heat balances in the spherical and slab pellets with Gaussian distribution of active material in the internal layer, was derived. The numerical algorithms and computer programs for solving model equations based on the method of lines were developed and successfully validated. The effects of dimensionless parameters, such as the Biot number, Thiele modulus, Arrhenius number, and energy generation factor, as well as model parameters like the thickness of the active core and the width and center of the Gaussian distribution, were investigated on the concentration and temperature profiles under steady-state conditions. The simulation results confirmed that the effectiveness factor increases with smaller values of Thiele modulus and higher Biot numbers. Moreover, it was demonstrated that the increase in Arrhenius number in exothermic and the decrease in endothermic reactions lead to a higher effectiveness factor. Finally, the analysis of the effectiveness factor showed better performance when the center of distribution is closer to the outer radius of the active layer.

The findings from this research demonstrate that non-uniform, particularly Gaussian, catalyst distribution within the shell of core-shell pellets can enhance catalytic performance compared to a uniform distribution. This improvement is attributed to the optimized interaction between the reactants and the catalyst.

For future improvements, investigation into the aspect of dead zone formation and the application of non-uniform catalyst distribution to more complex reaction systems hold great promise for advancing the field of catalysis and enabling the development of more efficient and sustainable chemical processes.

Bibliography

[1] Bizon, K., Continillo, G., "Determination of the optimal distribution of active centers in a multifunctional catalyst pellet using global searching combined with reduced-order modeling approach," Computer Aided Chemical Engineering, pp. 1015–1020, 2019.

[2] Bizon, K., Skrzypek-Markiewicz, K., Pędzich, D., Reczek, N., "Intensification of catalytic processes through the pellet structuring: Steady-state properties of a bifunctional catalyst pellet applied to generic chemical reactions and the direct synthesis of DME," Catalysts, vol. 9, no. 12, p. 1020, 2019.

[3] Boukezoula, T. F., Bencheikh, L., Belkhiat, D. E., "A heterogeneous mathematical model for a spherical fixed bed axial flow reactor applied to a naphtha reforming process: Enhancing performance challenge using a non-uniform catalyst distribution in the pellet," Reaction Kinetics, Mechanisms and Catalysis, vol. 135, no. 5, pp. 2323–2340, 2022.

[4] Bukur, D. B., Mandić, M., Todić, B., Nikačević, N., "Pore diffusion effects on catalyst effectiveness and selectivity of cobalt based Fischer-Tropsch catalyst," Catalysis Today, vol. 343, pp. 146–155, 2020.

[5] Cho, Y.-S., "Modeling of Core-shell Catalytic Pellets of Inert Shell with Various Morphologies for Series Reactions," Journal of Chemical Engineering of Japan, vol. 56, no. 1, 2205457, 2023, doi: 10.1080/00219592.2023.2205457.

[6] Cho, Y.-S., "Modelling of batch reactors and CSTRs containing core-shell catalytic pellets with various morphologies under non-iso-thermal condition," J Chem Eng Jpn, 56, 2023a, doi: 10.1080/00219592.2023.2172995.

[7] Cho, Y.-S., "Modelling of catalytic reactors containing core–shell pellets with various morphologies for series reactions," Can J Chem Eng, (in press), 2023b, doi: 10.1002/cjce.24776.

[8] Iglesias, I., Poggio-Fraccari, E., and Giunta, P., "Study of effectiveness factors with non-uniform catalyst distributions for methane steam reforming," Reaction Kinetics, Mechanisms and Catalysis, vol. 130, no. 2, pp. 713–726, 2020, doi: https://doi.org/10.1007/s11144-020-01822-8.

[9] Golman, B., "A Set of Jupyter Notebooks for the Analysis of Transport Phenomena and Reaction in Porous Catalyst Pellet," Computer Applications in Engineering Education, 27, pp. 531–542, 2019, doi: 10.1002/cae.22095.

[10] Golman, "Chemical Reaction Engineering with IPython Part I: Transport Processes and Reaction in Porous Pellets," Ventus Publishing, Copenhagen, Denmark, 2016.

[11] Kasaoka, S., Sakata, Y., "Effectiveness factors for non-uniform catalyst pellets," J. Chem. Eng. Japan, 1: 138–142, 1968.

[12] Le et al., "Core-shell and egg-shell zeolite catalysts for enhanced hydrocarbon processing," Journal of catalysis, vol. 405, pp. 664–675, Jan. 2022, doi: 10.1016/j.jcat.2021.11.004.

[13] Li, P., Xiu, G., Rodrigues, A.E., "Modelling diffusion and reaction for inert-core catalyst in batch and fixed bed reactors," The Canadian Journal of Chemical Engineering, 97(1), pp. 217–225, 2018, doi: 10.1002/cjce.23189.

[14] Martínez, V. A., Shadman, F., "Improving the performance of fixed-bed catalytic reactors by Innovative Catalyst Distribution," Journal of Applied Mathematics and Physics, vol. 08, no. 04, pp. 672–683, 2020.

[15] Martínez, V., Shadman, F., "Non-uniform catalyst distribution in fixed-bed reactors to improve dehydrogenation processes," Chemical Engineering Journal Advances, vol. 10, p. 100254, 2022.

[16] Ndagijimana, P., Liu, X., Li, Z., Yu, G., Wang, Y., "Optimized synthesis of a core-shell structure activated carbon and its adsorption performance for bisphenol A," Sci Total Environ, 689:457–468, 2019, doi: 10.1016/j.scitotenv.2019.06.235.

[17] Peters, B., "Secondary effectiveness factors and solubility effects for catalytic reactions in series," ACS Catal, 10:4319–4325, 2020, doi: 10.1021/acscatal.0c00185.

[18] Russo, V., Mastroianni, L., Tesser, R., Salmi, T., Di Serio, M., "Intraparticle modeling of Non-Uniform Active Phase Distribution Catalyst," Chem Engineering, vol. 4, no. 2, p. 24, 2020.

[19] Salucci, E., Russo, V., Salmi, T., Di Serio, M., Tesser, R., "Intraparticle model for non-uniform active phase distribution catalysts in a batch reactor," Chem Engineering, vol. 5, no. 3, p. 38, 2021.

[20] Schiesser, W. E., Griffiths, G. W., "A Compendium of Partial Differential Equations Models: Method of Lines Analysis with Matlab," Cambridge University Press, Oxford, UK, 2009.

[21] Servia, A., "Using modeling to select catalyst dilution methods for mass transfer intensification in lab gas–liquid fixed-bed reactors," Oil & Gas Science and Technology – Revue d'IFP Energies nouvelles, vol. 75, p. 74, 2020, doi: 10.2516/ogst/2020071.

[22] Verykios, X. E., Kluck, R. W., Johnson, D. L., "Fixed-bed reactor simulation with nonuniformly activated catalyst pellets," In Modeling and Simulation in Engineering, eds. Ames, W. F., and Vichnevetsky, R., pp. 3–10, Amsterdam: North-Holland, 1983.

[23] Virtanen, P., et al., "SciPy 1.0: Fundamental Algorithms for Scientific Computing in Python," Nature Methods, 17(3), 261-272, 2020, doi: 10.1038/s41592-019-0686-2.

[24] Xu et al., "Engineering an egg-shell structure for the Ag/SiO2 pellet catalyst for selective hydrogenation of dimethyl oxalate to methyl glycolate," New journal of chemistry, vol. 47, no. 13, pp. 6045–6049, Jan. 2023, doi: https://doi.org/10.1039/d3nj00542a.

[25] Zadeh, A. S., Peters, B., "Secondary effectiveness factors for catalytic reactions in series: extension to slab, cylindrical, and spherical geometries," React Chem Eng, 5:2003–2008, 2020, doi: 10.1039/D0RE00242A.

[26] Zimmermann, R. T., et al., "Core–shell catalyst pellets for effective reaction heat management," Chem. Eng J, 457:140921, 2023, doi: 10.1016/j.cej.2022.140921.

Appendices

Appendix A. Derivation of Gaussian activity distribution profiles

Slab-type pellet, ($z = 0$)

The integral in Eq. (13) is analytically evaluated for slab-type pellets as follows:

$$\int_{r_1}^{r_2} \exp\left(-\frac{\left(\underline{x}-\underline{x}_1\right)^2}{\Delta^2}\right) d\underline{x} = \Delta\frac{\sqrt{\pi}}{2}\left(erf\left(\frac{r_2-\underline{x}_1}{\Delta}\right) - erf\left(\frac{r_1-\underline{x}_1}{\Delta}\right)\right) \qquad (.99)$$

The integration is carried out by changing the integration variable.

$$\int_{r_1}^{r_2} \exp\left(-\frac{\left(\underline{x}-\underline{x}_1\right)^2}{\Delta^2}\right) d\underline{x} = \Delta\int_{r_1}^{r_2} \exp\left(-\frac{\left(\underline{x}-\underline{x}_1\right)^2}{\Delta^2}\right) d\left(\frac{\underline{x}-\underline{x}_1}{\Delta}\right). \qquad (.100)$$

Introduce a new variable $y = \frac{\underline{x}-\underline{x}_1}{\Delta}$, where $\underline{x} = y\cdot\Delta + \underline{x}_1$. To change the limits of the integral, the values of y are estimated at $\underline{x} = r_1$ and $\underline{x} = r_2$ as $y_1 = \frac{r_1-\underline{x}_1}{\Delta}$ and $y_2 = \frac{r_2-\underline{x}_1}{\Delta}$. Then, Eq. (.100) is rewritten as follows:

$$\Delta\int_{y_1}^{y_2} \exp\left(-y^2\right) dy\,. \qquad (.101)$$

Using the definition of the error function, the following expression is obtained:

$$\begin{aligned}\Delta\int_{y_1}^{y_2} \exp\left(-y^2\right) dz &= \Delta\frac{\sqrt{\pi}}{2}\left(erf(y_2) - erf(y_1)\right)\\ &= \Delta\frac{\sqrt{\pi}}{2}\left(erf\left(\frac{r_2-\underline{x}_1}{\Delta}\right) - erf\left(\frac{r_1-\underline{x}_1}{\Delta}\right)\right)\end{aligned}. \qquad (.102)$$

After substituting Eq. (.102) into Eq. (13), the normalizing factor is obtained as follows:

$$B = \frac{1}{\Delta\frac{\sqrt{\pi}}{2}\left(erf\left(\frac{r_2-\underline{x}_1}{\Delta}\right) - erf\left(\frac{r_1-\underline{x}_1}{\Delta}\right)\right)}. \qquad (.103)$$

The activity distribution in the slab pellet is derived by substituting Eq. (.103) into Eq. (12).

$$a\left(\underline{x}\right)=\frac{\exp\left(-\frac{\left(\underline{x}-\underline{x}_1\right)^2}{\Delta^2}\right)}{\Delta\frac{\sqrt{\pi}}{2}\left(erf\left(\frac{r_2-\underline{x}_1}{\Delta}\right)-erf\left(\frac{r_1-\underline{x}_1}{\Delta}\right)\right)} \qquad (.104)$$

Spherical pellet ($z=2$)

The integral in Eq. (13) is analytically evaluated for spherical pellet as follows:

$$\int_{r_1}^{r_2}\underline{x}^2\exp\left(-\frac{\left(\underline{x}-\underline{x}_1\right)^2}{\Delta^2}\right)d\underline{x}= \frac{1}{4}\Delta\left(\begin{array}{c}\sqrt{\pi}\left(\Delta^2+2\underline{x}_1^2\right)\left(erf\left(\frac{r_2-\underline{x}_1}{\Delta}\right)-erf\left(\frac{r_1-\underline{x}_1}{\Delta}\right)\right)+\\ \exp\left(-\frac{\left(r_2-\underline{x}_1\right)^2}{\Delta^2}\right)\left(-2\Delta\left(\underline{x}_1+r_2\right)\right)+\\ \exp\left(-\frac{\left(r_1-\underline{x}_1\right)^2}{\Delta^2}\right)\left(2\Delta\left(r_1+\underline{x}_1\right)\right)\end{array}\right) \qquad (.105)$$

The integral is obtained by changing the integration variable.

$$\int_{r_1}^{r_2}\underline{x}^2\exp\left(-\frac{\left(\underline{x}-\underline{x}_1\right)^2}{\Delta^2}\right)d\underline{x}=\Delta\int_{r_1}^{r_2}\underline{x}^2\exp\left(-\frac{\left(\underline{x}-\underline{x}_1\right)^2}{\Delta^2}\right)d\left(\frac{\underline{x}-\underline{x}_1}{\Delta}\right) \qquad (.106)$$

Using the variable y, the dimensionless distance $\underline{x}$ is given as $\underline{x}=y\cdot\Delta+\underline{x}_1$. Then, $\underline{x}^2$ is derived as follows:

$$\underline{x}^2=\left(y\cdot\Delta+\underline{x}_1\right)^2=y^2\Delta^2+2y\Delta\underline{x}+\underline{x}_1^2$$

Then, Eq. (.106) is rewritten as follows:

$$\Delta\int_{y_1}^{y_2}\left(y^2\Delta^2+2y\Delta\underline{x}_1+\underline{x}_1^2\right)\cdot\exp\left(-y^2\right)dy \qquad (.107)$$

Each term in the integral will be estimated separately:

$$\Delta\int_{y_1}^{y_2}y^2\Delta^2\exp\left(-y^2\right)dy+\Delta\int_{y_1}^{y_2}2y\Delta\underline{x}_1\exp\left(-y^2\right)dy+ \Delta\int_{y_1}^{y_2}\underline{x}_1^2\exp\left(-y^2\right)dy \qquad (.108)$$

1) first integral

$$\Delta\int_{y_1}^{y_2} y^2\Delta^2\exp(-y^2)dy = \Delta^3\int_{y_1}^{y_2} y\cdot y\cdot\exp(-y^2)dy = \frac{\Delta^3}{2}\int_{y_1}^{y_2} y\cdot\exp(-y^2)d(y^2) \quad (.109)$$

Using the method of integrating by parts, the integral in Eq. (.109) is evaluated as follows:

$$u = y \qquad dv = \exp(-y^2)d(y^2)$$

$$du = dy \qquad v = -\exp(-y^2)$$

$$u\cdot v - \int vdu = \frac{\Delta^3}{2}\left((-y\cdot\exp(-y^2))\Big|_{y_1}^{y_2} + \int_{y_1}^{y_2}\exp(-y^2)dy\right) \quad (.110)$$

$$\frac{\Delta^3}{2}\left(-y_2\cdot\exp(-{y_2}^2) + y_1\cdot\exp(-{y_1}^2) + \frac{\sqrt{\pi}}{2}(erf(y_2) - erf(y_1))\right) \quad (.111)$$

Thus, the solution to the first integral is obtained as follows:

$$\frac{\Delta^2}{2}\left(\underline{x}_1 - r_2\right)\exp\left(-\frac{\left(r_2-\underline{x}_1\right)^2}{\Delta^2}\right) + \frac{\Delta^2}{2}\left(r_1-\underline{x}_1\right)\exp\left(-\frac{\left(r_1-\underline{x}_1\right)^2}{\Delta^2}\right) + \frac{\sqrt{\pi}\,\Delta^3}{4}\left(erf\left(\frac{r_2-\underline{x}_1}{\Delta}\right) - erf\left(\frac{r_1-\underline{x}_1}{\Delta}\right)\right) \quad (.112)$$

2) second integral

$$\Delta^2\int_{y_1}^{y_2} 2y\,\Delta\underline{x}_1\exp(-y^2)dy =$$

$$\Delta^2\underline{x}_1\int_{y_1}^{y_2} 2y\exp(-y^2)dy = \Delta^2\underline{x}_1\int_{y_1}^{y_2}\exp(-y^2)d(y^2)$$

The integration results in the following expression:

$$-\Delta^2\underline{x}_1(\exp(-y^2))\Big|_{y_1}^{y_2} = -\Delta^2\underline{x}_1(\exp(-{y_2}^2) - \exp(-{y_1}^2))$$

$$= -\Delta^2\underline{x}_1\left(\exp\left(-\frac{\left(r_2-\underline{x}_1\right)^2}{\Delta^2}\right) - \exp\left(-\frac{\left(r_1-\underline{x}_1\right)^2}{\Delta^2}\right)\right)$$

The solution of the second integral is obtained as follows:

$$-\Delta^2 \underline{x}_1 \exp\left(-\frac{\left(r_2-\underline{x}_1\right)^2}{\Delta^2}\right)+\Delta^2 \underline{x}_1 \exp\left(-\frac{\left(r_1-\underline{x}_1\right)^2}{\Delta^2}\right) \qquad (.113)$$

3) Third integral

$$\Delta\int_{y_1}^{y_2} \underline{x}_1^2 \exp(-y^2)\,dy = \Delta \underline{x}_1^2 \int_{y_1}^{y_2} \exp(-y^2)\,dy$$

The solution of the third integral is derived as follows:

$$\Delta \underline{x}_1^2 \frac{\sqrt{\pi}}{2}\left(erf(y_2)-erf(y_1)\right)=\Delta \underline{x}_1^2 \frac{\sqrt{\pi}}{2}\left(erf\left(\frac{r_2-\underline{x}_1}{\Delta}\right)-erf\left(\frac{r_1-\underline{x}_1}{\Delta}\right)\right) \qquad (.114)$$

Combining the solutions to all three integrals through Eqs. (.112), (.113) and (.114) yields:

$$\frac{\Delta^3}{2}\left(-y_2\cdot\exp(-{y_2}^2)+y_1\cdot\exp(-{y_1}^2)+\frac{\sqrt{\pi}}{2}\left(erf(y_2)-erf(y_1)\right)\right)$$

$$-\Delta^2 \underline{x}_1\left(\exp(-{y_2}^2)-\exp(-{y_1}^2)\right) \;+\; \left\{\Delta \underline{x}_1^2 \frac{\sqrt{\pi}}{2}\left(erf(y_2)-erf(y_1)\right)\right\} \;=$$

$$\frac{\Delta}{4}\left(\Delta^2+2\underline{x}_1^2\right)\sqrt{\pi}\left(erf(y_2)-erf(y_1)\right) \;+$$

$$\frac{\Delta}{4}\left(\exp(-{y_2}^2)\cdot\left(-2\Delta^2 y_2-4\Delta \underline{x}_1\right) \;+\exp(-{y_1}^2)\left(2\Delta^2 y_1+4\Delta \underline{x}_1\right)\right)$$

and

$$\frac{\Delta}{4}\left(\begin{array}{c}\sqrt{\pi}\left(\Delta^2+2\underline{x}_1^2\right)\left(erf\left(\frac{r_2-\underline{x}_1}{\Delta}\right)-erf\left(\frac{r_1-\underline{x}_1}{\Delta}\right)\right)+\\ \exp\left(-\frac{\left(r_2-\underline{x}_1\right)^2}{\Delta^2}\right)\left(-2\Delta\left(\underline{x}_1+r_2\right)\right)+\\ \exp\left(-\frac{\left(r_1-\underline{x}_1\right)^2}{\Delta^2}\right)\left(2\Delta\left(r_1+\underline{x}_1\right)\right)\end{array}\right) \qquad (.115)$$

The normalizing factor is obtained by substituting Eq. (.115) into Eq. (13) as follows:

$$B=\left(\begin{array}{c}\frac{3\sqrt{\pi}}{4}\left(\Delta^3+2\underline{x}_1^2\Delta\right)\left(erf\left(\frac{r_2-\underline{x}_1}{\Delta}\right)-erf\left(\frac{r_1-\underline{x}_1}{\Delta}\right)\right)- \\ \frac{3}{2}\Delta^2\left(\underline{x}_1+r_2\right)\cdot\exp\left(-\frac{\left(r_2-\underline{x}_1\right)^2}{\Delta^2}\right)+\frac{3}{2}\Delta^2\left(r_1+\underline{x}_1\right)\cdot\exp\left(-\frac{\left(r_1-\underline{x}_1\right)^2}{\Delta^2}\right)\end{array}\right)^{-1} \quad (.116)$$

Then, the activity distribution in the spherical pellet is derived by substituting Eq. (.116) into Eq. (12) as follows:

$$a\left(\underline{x}\right)=\frac{\exp\left(-\frac{\left(\underline{x}-\underline{x}_1\right)^2}{\Delta^2}\right)}{\left(\begin{array}{c}\frac{3\sqrt{\pi}}{4}\left(\Delta^3+2\underline{x}_1^2\Delta\right)\left(erf\left(\frac{r_2-\underline{x}_1}{\Delta}\right)-erf\left(\frac{r_1-\underline{x}_1}{\Delta}\right)\right)- \\ \frac{3}{2}\Delta^2\left(\underline{x}_1+r_2\right)\cdot\exp\left(-\frac{\left(r_2-\underline{x}_1\right)^2}{\Delta^2}\right)+\frac{3}{2}\Delta^2\left(r_1+\underline{x}_1\right)\cdot\exp\left(-\frac{\left(r_1-\underline{x}_1\right)^2}{\Delta^2}\right)\end{array}\right)} \quad (.117)$$

Appendix B. Derivation of analytical solutions for steady-state mass balances

Slab-type pellet

The reactant concentration in each region of the slab-type pellet can be determined by solving the following equations, which were obtained by substituting z = 0 into Eqs. (1), (2), and (3):

$$\frac{d^2 \underline{c}_1}{d \underline{x}^2} = 0, \tag{B.1}$$

$$\frac{d^2 \underline{c}_2}{d \underline{x}^2} = \phi^2 \underline{c}_2, \tag{B.2}$$

$$\frac{d^2 \underline{c}_3}{d \underline{x}^2} = 0. \tag{B.3}$$

The solution of the second order linear ODE by Eq. (B.2) is given as:

$$\underline{c}_2 = C_3 e^{\phi \underline{x}} - C_4 e^{-\phi \underline{x}}. \tag{B.4}$$

The derivative of $\underline{c}_2$ by $\underline{x}$ is derived as:

$$\frac{d \underline{c}_2}{d \underline{x}} = \phi \left(C_3 e^{\phi \underline{x}} - C_4 e^{-\phi \underline{x}} \right). \tag{B.5}$$

The integration of Eq. (B.1) results in:

$$\frac{d \underline{c}_1}{d \underline{x}} = C_1 \tag{B.6}$$

The integration of Eq. (B.3) results in:

$$\frac{d \underline{c}_3}{d \underline{x}} = C_5 \tag{B.7}$$

where C_1, C_3, C_4 and C_5 are the integration constants.

After integrating Eqs. (B.6) and (B.7) for the second time, the reactant concentration distribution in each pellet region is obtained as follows:

$$\underline{c}_1 = C_1 \underline{x} + C_2, \tag{B.8}$$

$$\underline{c}_2 = C_3 e^{\phi \underline{x}} + C_4 e^{-\phi \underline{x}} \tag{B.9}$$

$$\underline{c}_3 = C_5 \underline{x} + C_6 \tag{B.10}$$

where C_2 and C_6 are the integration constants.

Substituting Eqs. (B.8) and (B.9) into the boundary condition given by Eq. (6) results in:

$$C_1 r_1 + C_2 = C_3 e^{\phi r_1} + C_4 e^{-\phi r_1}. \tag{B.11}$$

Inserting Eqs. (B.6) and (B.5) into the boundary condition given by Eq. (7) yields:

$$C_1 = \zeta' \phi \left(C_3 e^{\phi r_1} - C_4 e^{-\phi r_1} \right). \tag{B.12}$$

Introducing Eqs. (B.9) and (B.10) into the boundary condition by Eq. (8) results in:

$$C_3 e^{\phi r_2} + C_4 e^{-\phi r_2} = C_5 r_2 + C_6. \tag{B.13}$$

Substituting Eq. (B.5) and the derivative of $\underline{c}_3$ with respect to $\underline{x}$ given by the differentiation of Eq. (B.10) into the boundary condition by Eq. (9) yields:

$$\zeta \phi \left(C_3 e^{\phi r_2} - C_4 e^{-\phi r_2} \right) = C_5 \tag{B.14}$$

Given that from Eq. (B.10) $\underline{c}_3(1) = C_5 + C_6$, and using Eq. (B.7), after substituting these equations into the boundary condition given by Eq. (5), the following equation is obtained:

$$C_5 = Bi\left(1 - (C_5 + C_6)\right)$$

and

$$C_6 + \frac{C_5(1 + Bi)}{Bi} = 1. \tag{B.15}$$

The integration constant C_1 is equal to zero from the boundary condition by Eq. (4) and Eq. (B.6). Thus, Eq. (B.12) can be rewritten as:

$$0 = \zeta' \phi \left(C_3 e^{\phi r_1} - C_4 e^{-\phi r_1} \right); \quad C_3 e^{\phi r_1} = C_4 e^{-\phi r_1}.$$

Then, the constant C_4 is derived as:

$$C_4 = C_3 e^{2\phi r_1}. \tag{B.16}$$

The integration constant C_2 is obtained by substituting Eq. (B.16) and $C_1 = 0$ into Eq. (B.11) as:

$$C_2 = C_3 e^{\phi r_1} + C_3 e^{2\phi r_1} e^{-\phi r_1}$$

and

$$C_2 = 2C_3 e^{\phi r_1} \tag{B.17}$$

The integration constant C_5 is derived by substituting Eq. (B.16) into Eq. (B.14) as:

$$C_5 = \zeta\phi\left(C_3 e^{\phi r_2} - C_3 e^{2\phi r_1} e^{-\phi r_2}\right) = C_3\zeta\phi e^{\phi r_1}\left(e^{\phi r_2} e^{-\phi r_1} - e^{-\phi r_2} e^{\phi r_1}\right)$$
$$= C_3\zeta\phi e^{\phi r_1}\left(e^{\phi(r_2 - r_1)} - e^{-\phi(r_2 - r_1)}\right),$$

and

$$C_5 = 2C_3\zeta\phi e^{\phi r_1} sinh\left(\phi(r_2 - r_1)\right), \tag{B.18}$$

where $sinh$ is the hyperbolic sine defined as:

$$sinh(x) = \frac{e^x - e^{-x}}{2}. \tag{B.19}$$

The integration constant C_6 is determined by substituting Eqs. (B.16) and (B.18) into Eq. (B.13) as:

$$C_3 e^{\phi r_2} + C_3 e^{2\phi r_1} e^{-\phi r_2} = C_3 e^{\phi r_1}\left(e^{\phi(r_2 - r_1)} + e^{-\phi(r_2 - r_1)}\right) = 2C_3 e^{\phi r_1} cosh\left(\phi(r_2 - r_1)\right) = C_5 r_2 + C_6$$

$$C_6 = 2C_3 e^{\phi r_1} cosh\left(\phi(r_2 - r_1)\right) - 2C_3\zeta\phi e^{\phi r_1} sinh\left(\phi(r_2 - r_1)\right) r_2,$$

$$C_6 = 2C_3 e^{\phi r_1}\left(cosh\left(\phi(r_2 - r_1)\right) - \zeta\phi r_2 sinh\left(\phi(r_2 - r_1)\right)\right), \tag{B.20}$$

where $cosh$ is the hyperbolic cosine defined as:

$$cosh(x) = \frac{e^x + e^{-x}}{2} \tag{B.21}$$

Substituting Eqs. (B.18) and (B.20) into Eq. (B.15) yields:

$$2C_3 e^{\phi r_1}\left(cosh\left(\phi(r_2 - r_1)\right) - \zeta\phi r_2 sinh\left(\phi(r_2 - r_1)\right)\right) +$$
$$\frac{2C_3\zeta\phi e^{\phi r_1} sinh\left(\phi(r_2 - r_1)\right)(1 + Bi)}{Bi} = 1$$

and

$$2C_3 Bi e^{\phi r_1}\left(cosh\left(\phi(r_2 - r_1)\right) - \zeta\phi r_2 sinh\left(\phi(r_2 - r_1)\right)\right) +$$
$$2C_3\zeta\phi e^{\phi r_1} sinh\left(\phi(r_2 - r_1)\right)(1 + Bi) =$$
$$2C_3 Bi e^{\phi r_1} cosh\left(\phi(r_2 - r_1)\right) - 2C_3 Bi e^{\phi r_1}\zeta\phi r_2 sinh\left(\phi(r_2 - r_1)\right) +$$
$$2C_3\zeta\phi e^{\phi r_1} sinh\left(\phi(r_2 - r_1)\right) + 2C_3 Bi e^{\phi r_1}\zeta\phi sinh\left(\phi(r_2 - r_1)\right) = Bi$$

Dividing all terms by *Bi* and factoring out $2C_3 e^{\phi r_1}$ results in:

$$2C_3 e^{\phi r_1}\left(cosh\left(\phi(r_2-r_1)\right)+\zeta\,\phi\;sinh\left(\phi(r_2-r_1)\right)\left(1-r_2+\frac{1}{Bi}\right)\right)=1.$$

Then, the integration constant C_3 is obtained as:

$$C_3=\frac{1}{2e^{\phi r_1}\left(cosh\left(\phi(r_2-r_1)\right)+\zeta\,\phi\;sinh\left(\phi(r_2-r_1)\right)\left(1-r_2+\frac{1}{Bi}\right)\right)}. \qquad \text{(B.22)}$$

The constant C_4 is derived by substituting Eq. (B.22) into Eq. (B.16) as:

$$C_4=\frac{1}{2e^{\phi r_1}\left(cosh\left(\phi(r_2-r_1)\right)+\zeta\,\phi\;sinh\left(\phi(r_2-r_1)\right)\left(1-r_2+\frac{1}{Bi}\right)\right)}e^{2\phi r_1}$$

and

$$C_4=\frac{e^{\phi r_1}}{2\left(cosh\left(\phi(r_2-r_1)\right)+\zeta\,\phi\;sinh\left(\phi(r_2-r_1)\right)\left(1-r_2+\frac{1}{Bi}\right)\right)} \qquad \text{(B.23)}$$

The constant C_2 is obtained by substituting Eq. (B.22) into Eq. (B.17) as:

$$C_2=2e^{\phi r_1}\frac{1}{2e^{\phi r_1}\left(cosh\left(\phi(r_2-r_1)\right)+\zeta\,\phi\;sinh\left(\phi(r_2-r_1)\right)\left(1-r_2+\frac{1}{Bi}\right)\right)}$$

and

$$C_2=\frac{1}{cosh\left(\phi(r_2-r_1)\right)+\zeta\,\phi\;sinh\left(\phi(r_2-r_1)\right)\left(1-r_2+\frac{1}{Bi}\right)}. \qquad \text{(B.24)}$$

The constant C_5 is recovered by substituting Eq. (B.22) into Eq. (B.18) as:

$$C_5=\frac{2\zeta\phi e^{\phi r_1}sinh\left(\phi(r_2-r_1)\right)}{2e^{\phi r_1}\left(cosh\left(\phi(r_2-r_1)\right)+\zeta\,\phi\;sinh\left(\phi(r_2-r_1)\right)\left(1-r_2+\frac{1}{Bi}\right)\right)},$$

and

$$C_5=\frac{\zeta\,\phi\;sinh\left(\phi(r_2-r_1)\right)}{cosh\left(\phi(r_2-r_1)\right)+\zeta\,\phi\;sinh\left(\phi(r_2-r_1)\right)\left(1-r_2+\frac{1}{Bi}\right)} \qquad \text{(B.25)}$$

The constant C_6 is derived by substituting Eq. (B.22) into Eq. (B.20) as:

$$C_6=2\frac{1}{2e^{\phi r_1}\left(cosh\left(\phi(r_2-r_1)\right)+\zeta\,\phi\;sinh\left(\phi(r_2-r_1)\right)\left(1-r_2+\frac{1}{Bi}\right)\right)}\times,$$

$$e^{\phi r_1}\left(cosh\left(\phi(r_2-r_1)\right)-\zeta\phi r_2 sinh\left(\phi(r_2-r_1)\right)\right)$$

and

$$C_6 = \frac{cosh(\phi(r_2 - r_1)) - \zeta\phi r_2 sinh(\phi(r_2 - r_1))}{cosh(\phi(r_2 - r_1)) + \zeta\ \phi\ sinh(\phi(r_2 - r_1))\left(1 - r_2 + \frac{1}{Bi}\right)} \tag{B.26}$$

Finally, by substituting the value of constant C_2 by Eq. (B.24) and $C_1 = 0$ into Eq. (B.8), the reactant concentration in the first region for the slab-type pellet can be determined using the following equation:

$$\underline{c}_1 = \frac{1}{cosh(\phi(r_2 - r_1)) + \zeta\ \phi\ sinh(\phi(r_2 - r_1))\left(1 - r_2 + \frac{1}{Bi}\right)} \tag{B.27}$$

The reactant concentration distribution in the second region is obtained by substituting the values of constant C_3 by Eq. (B.22) and constant C_4 by Eq. (B.23) into Eq. (B.9).

$$\underline{c}_2(\underline{x}) = C_3 e^{\phi\underline{x}} + C_4 e^{-\phi\underline{x}}$$

$$= \frac{e^{-\phi r_1}}{2\left(cosh(\phi(r_2 - r_1)) + \zeta\ \phi\ sinh(\phi(r_2 - r_1))\left(1 - r_2 + \frac{1}{Bi}\right)\right)} e^{\phi\underline{x}} +$$

$$\frac{e^{\phi r_1}}{2\left(cosh(\phi(r_2 - r_1)) + \zeta\ \phi\ sinh(\phi(r_2 - r_1))\left(1 - r_2 + \frac{1}{Bi}\right)\right)} e^{-\phi\underline{x}}$$

Using the definition of the hyperbolic sine and cosine, the following expression is derived:

$$cosh(\phi\underline{x})\,cosh(\phi r_1) - sinh(\phi\underline{x})\,sinh(\phi r_1) =$$

$$\left(e^{\phi\underline{x}} + e^{-\phi\underline{x}}\right)\left(e^{\phi r_1} + e^{-\phi r_1}\right) - \left(e^{\phi\underline{x}} - e^{-\phi\underline{x}}\right)\left(e^{\phi r_1} - e^{-\phi r_1}\right) =$$

$$\left(e^{\phi\underline{x}} e^{\phi r_1} + e^{-\phi\underline{x}} e^{\phi r_1} + e^{\phi\underline{x}} e^{-\phi r_1} + e^{-\phi\underline{x}} e^{-\phi r_1}\right) -$$

$$\left(e^{\phi\underline{x}} e^{\phi r_1} - e^{-\phi\underline{x}} e^{\phi r_1} - e^{\phi\underline{x}} e^{-\phi r_1} + e^{-\phi\underline{x}} e^{-\phi r_1}\right) =$$

$$2 \cdot \left(e^{-\phi\underline{x}} e^{\phi r_1} + e^{\phi\underline{x}} e^{-\phi r_1}\right)$$

Thus, the reactant concentration distribution in the second region is obtained as follows:

$$\underline{c}_2(\underline{x}) = \frac{cosh(\phi\underline{x})\,cosh(\phi r_1) - sinh(\phi\underline{x})\,sinh(\phi r_1)}{cosh(\phi(r_2 - r_1)) + \zeta\ \phi\ sinh(\phi(r_2 - r_1))\left(1 - r_2 + \frac{1}{Bi}\right)} \tag{B.28}$$

The reactant concentration distribution in the third region is obtained by substituting the values of constant C_5 by Eq. (B.25) and constant C_6 by Eq. (B.26) into Eq. (B.10).

$$\underline{c}_3 = C_5\,\underline{x} + C_6 = \frac{\zeta\,\phi\,sinh\left(\phi(r_2-r_1)\right)}{cosh\left(\phi(r_2-r_1)\right)+\zeta\,\phi\,sinh\left(\phi(r_2-r_1)\right)\left(1-r_2+\frac{1}{Bi}\right)}\underline{x} +$$

$$\frac{cosh\left(\phi(r_2-r_1)\right)-\zeta\phi r_2 sinh\left(\phi(r_2-r_1)\right)}{cosh\left(\phi(r_2-r_1)\right)+\zeta\,\phi\,sinh\left(\phi(r_2-r_1)\right)\left(1-r_2+\frac{1}{Bi}\right)} =$$

$$\frac{\zeta\,\phi\,sinh\left(\phi(r_2-r_1)\right)\underline{x}\;+\;cosh\left(\phi(r_2-r_1)\right)-\zeta\phi r_2 sinh\left(\phi(r_2-r_1)\right)}{cosh\left(\phi(r_2-r_1)\right)+\zeta\,\phi\,sinh\left(\phi(r_2-r_1)\right)\left(1-r_2+\frac{1}{Bi}\right)} =$$

$$1-\frac{\zeta\,\phi\,sinh\left(\phi(r_2-r_1)\right)\left(1-\underline{x}+\frac{1}{Bi}\right)}{cosh\left(\phi(r_2-r_1)\right)+\zeta\,\phi\,sinh\left(\phi(r_2-r_1)\right)\left(1-r_2+\frac{1}{Bi}\right)}$$

Thus, the reactant concentration in the third region is derived as:

$$\underline{c}_3(\underline{x}) = 1-\frac{\zeta\,\phi\,sinh\left(\phi(r_2-r_1)\right)\left(1-\underline{x}+\frac{1}{Bi}\right)}{cosh\left(\phi(r_2-r_1)\right)+\zeta\,\phi\,sinh\left(\phi(r_2-r_1)\right)\left(1-r_2+\frac{1}{Bi}\right)} \tag{B.29}$$

Spherical pellet

The concentration of reactant in each region of spherical pellet can be determined by solving the following equations, which were obtained by substituting *z* = 2 into Eqs. (1), (2), and (3):

$$\underline{x}\frac{d^2\underline{c}_1}{d\underline{x}^2}+2\frac{d\underline{c}_1}{d\underline{x}}=0 \tag{B.30}$$

$$\frac{d^2\underline{c}_2}{d\underline{x}^2}+\frac{2}{\underline{x}}\frac{d\underline{c}_2}{d\underline{x}}=\phi^2\underline{c}_2 \tag{B.31}$$

$$\underline{x}\frac{d^2\underline{c}_3}{d\underline{x}^2}+2\frac{d\underline{c}_3}{d\underline{x}}=0 \tag{B.32}$$

After introducing a new variable $u=\underline{c}_1\cdot\underline{x}$, the first and second derivatives of u with respect to $\underline{x}$ are as follows:

$$\frac{du}{d\underline{x}}=\underline{x}\frac{d\underline{c}_1}{d\underline{x}}+\underline{c}_1 \tag{B.33}$$

$$\frac{d^2u}{d\underline{x}^2}=\underline{x}\frac{d^2\underline{c}_1}{d\underline{x}^2}+2\frac{d\underline{c}_1}{d\underline{x}} \tag{B.34}$$

Substituting Eq. (B.34) into (B.30) yields:

$$\frac{d^2u}{d\underline{x}^2} = 0 \tag{B.35}$$

Two times integration of Eq. (B.35) results in:

$$u = C_1\underline{x} + C_2, \tag{B.36}$$

where C_1 and C_2 are the integration constants.

Since $\underline{c}_1 = \frac{u}{\underline{x}}$, dividing Eq. (B.36) by $\underline{x}$ yields:

$$\underline{c}_1 = C_1 + \frac{C_2}{\underline{x}} \tag{B.37}$$

The first derivative of $\underline{c}_1$ with respect to $\underline{x}$ will be as follows:

$$\frac{d\underline{c}_1}{d\underline{x}} = -\frac{C_2}{\underline{x}^2} \tag{B.38}$$

Upon the introduction of a new variable $m = \underline{c}_2\underline{x}$, the first and the second derivative of m with respect to $\underline{x}$ are as follows:

$$\frac{dm}{d\underline{x}} = \underline{x}\frac{d\underline{c}_2}{d\underline{x}} + \underline{c}_2 \tag{B.39}$$

$$\frac{d^2m}{d\underline{x}^2} = \underline{x}\frac{d^2\underline{c}_2}{d\underline{x}^2} + 2\frac{d\underline{c}_2}{d\underline{x}} \tag{B.40}$$

After multiplying Eq. (B.31) by $\underline{x}$ and substituting Eq. (B.40) into (B.31), the following result is obtained:

$$\frac{d^2m}{d\underline{x}^2} = \phi^2 m \tag{B.41}$$

The solution of the second-order linear ODE by Eq. (B.41) is given as:

$$m = C_3e^{\phi\underline{x}} + C_4e^{-\phi\underline{x}} \tag{B.42}$$

where C_3 and C_4 are the integration constants.

Since $\underline{c}_2 = \frac{m}{\underline{x}}$, dividing Eq. (B.42) by $\underline{x}$ will result in:

$$\underline{c}_2 = \frac{C_3 e^{\phi \underline{x}} + C_4 e^{-\phi \underline{x}}}{\underline{x}} \tag{B.43}$$

The first derivative of $\underline{c}_2$ with respect to $\underline{x}$ will be as follows:

$$\frac{d\underline{c}_2}{d\underline{x}} = \frac{\phi\left(C_3 e^{\phi \underline{x}} - C_4 e^{-\phi \underline{x}}\right)\underline{x} - \left(C_3 e^{\phi \underline{x}} + C_4 e^{-\phi \underline{x}}\right)}{\underline{x}^2} \tag{B.44}$$

After introducing a new variable $k = \underline{c}_3 \underline{x}$, the first and the second derivative of k with respect to $\underline{x}$ are as follows:

$$\frac{dk}{d\underline{x}} = \underline{x}\frac{d\underline{c}_3}{d\underline{x}} + \underline{c}_3 \tag{B.45}$$

$$\frac{d^2 k}{d\underline{x}^2} = \underline{x}\frac{d^2 \underline{c}_3}{d\underline{x}^2} + 2\frac{d\underline{c}_3}{d\underline{x}} \tag{B.46}$$

By substituting Eq. (B.46) into (B.32), the following expression is derived:

$$\frac{d^2 k}{d\underline{x}^2} = 0 \tag{B.47}$$

Two times integration of Eq. (B.47) results in:

$$k = C_5 \underline{x} + C_6 \tag{B.48}$$

where C_5 and C_6 are the integration constants.

Since $\underline{c}_3 = \frac{k}{\underline{x}}$, dividing Eq. (B.48) by $\underline{x}$ yields:

$$\underline{c}_3 = C_5 + \frac{C_6}{\underline{x}} \tag{B.49}$$

The first derivative of $\underline{c}_3$ with respect to $\underline{x}$ will be as follows:

$$\frac{d\underline{c}_3}{d\underline{x}} = -\frac{C_6}{\underline{x}^2} \tag{B.50}$$

Substituting Eqs. (B.37) and (B.43) into the boundary condition given by Eq. (6) results in:

$$C_1 + \frac{C_2}{r_1} = \frac{C_3 e^{\phi r_1} + C_4 e^{-\phi r_1}}{r_1} \tag{B.51}$$

Inserting Eqs. (B.38) and (B.44) into the boundary condition given by Eq. (7) yields:

$$-\frac{C_2}{{r_1}^2}=\zeta'\left(\frac{\phi\left(C_3e^{\phi r_1}-C_4e^{-\phi r_1}\right)r_1-\left(C_3e^{\phi r_1}+C_4e^{-\phi r_1}\right)}{{r_1}^2}\right) \tag{B.52}$$

Introducing Eqs. (B.43) and (B.49) into the boundary condition by Eq. (8) results in:

$$\frac{C_3e^{\phi r_2}+C_4e^{-\phi r_2}}{r_2}=C_5+\frac{C_6}{r_2} \tag{B.53}$$

Substituting Eqs. (B.44) and (B.50) into the boundary condition given by Eq. (9) and multiplying by r_2^2, we obtain the following:

$$\zeta\phi r_2\left(C_3e^{\phi r_2}-C_4e^{-\phi r_2}\right)-\zeta\left(C_3e^{\phi r_2}+C_4e^{-\phi r_2}\right)=-C_6 \tag{B.54}$$

Given that $\underline{c}_3(1)=C_5+C_6$ from Eq. (B.49) and using Eqs. (B.50), after substituting these equations into the boundary condition given by Eq. (5), the following equation is obtained:

$$-C_6=Bi\left(1-\left(C_5+C_6\right)\right)$$

and

$$C_6\left(1-\frac{1}{Bi}\right)+C_5=1 \tag{B.55}$$

The integration constant C_2 is equal to zero from the boundary condition by Eq. (4) and Eq. (B.38). Thus, Eq. (B.52) can be rewritten as:

$$0=\zeta'\left(\frac{\phi\left(C_3e^{\phi r_1}-C_4e^{-\phi r_1}\right)r_1-\left(C_3e^{\phi r_1}+C_4e^{-\phi r_1}\right)}{{r_1}^2}\right),$$

and

$$\phi r_1\left(C_3e^{\phi r_1}-C_4e^{-\phi r_1}\right)-\left(C_3e^{\phi r_1}+C_4e^{-\phi r_1}\right)=0,$$

$$\phi r_1C_3e^{\phi r_1}-\phi r_1C_4e^{-\phi r_1}-C_3e^{\phi r_1}-C_4e^{-\phi r_1}=0,$$

$$C_3e^{\phi r_1}(\phi r_1-1)-C_4e^{-\phi r_1}(\phi r_1+1)=0.$$

Thus, the relationship between constant C_3 and C_4 is derived as follows:

$$C_3=\left(\frac{\phi r_1+1}{\phi r_1-1}\right)C_4e^{-2\phi r_1}. \tag{B.56}$$

The integration constant C_1 is obtained by substituting Eq. (B.56) and $C_2=0$ into Eq. (B.51) as:

$$C_1 = \frac{\left(\frac{\phi r_1 + 1}{\phi r_1 - 1}\right) C_4 e^{-2\phi r_1} e^{\phi r_1} + C_4 e^{-\phi r_1}}{r_1},$$

and

$$C_1 = \frac{C_4 e^{-\phi r_1}\left(\frac{\phi r_1 + 1 + \phi r_1 - 1}{\phi r_1 - 1}\right)}{r_1},$$

$$C_1 = \frac{C_4 e^{-\phi r_1} 2\phi r_1}{r_1(\phi r_1 - 1)}.$$

Thus, the relationship between constant C_1 and C_4 is obtained as follows:

$$C_1 = \frac{2C_4 \phi\, e^{-\phi r_1}}{\phi r_1 - 1}. \tag{B.57}$$

The integration constant C_5 is derived by substituting Eq. (B.56) into Eq. (B.53) as:

$$C_5 = \frac{\left(\frac{\phi r_1 + 1}{\phi r_1 - 1}\right) C_4 e^{-2\phi r_1} e^{\phi r_2} + C_4 e^{-\phi r_2}}{r_2} - \frac{C_6}{r_2},$$

$$C_5 = \frac{C_4 e^{-\phi r_1}(\phi r_1 e^{\phi(r_2 - r_1)} + e^{\phi(r_2 - r_1)} + \phi r_1 e^{-\phi(r_2 - r_1)} - e^{-\phi(r_2 - r_1)})}{r_2(\phi r_1 - 1)} - \frac{C_6}{r_2},$$

$$C_5 = \frac{2C_4 e^{-\phi r_1}(\phi r_1 cosh(\phi(r_2 - r_1)) + sinh(\phi(r_2 - r_1)))}{r_2(\phi r_1 - 1)} - \frac{C_6}{r_2},$$

$$C_5 = \frac{2C_4 e^{-\phi r_1} cosh(\phi(r_2 - r_1))(\phi r_1 + tanh(\phi(r_2 - r_1)))}{r_2(\phi r_1 - 1)} - \frac{C_6}{r_2} \tag{B.58}$$

where $sinh$, $cosh$, $tanh$ are the hyperbolic sine, cosine, and tangent, respectively, defined as:

$$sinh(\phi(r_2 - r_1)) = \frac{e^{\phi(r_2 - r_1)} - e^{-\phi(r_2 - r_1)}}{2} \tag{B.59}$$

$$cosh(\phi(r_2 - r_1)) = \frac{e^{\phi(r_2 - r_1)} + e^{-\phi(r_2 - r_1)}}{2} \tag{B.60}$$

$$tanh(\phi(r_2 - r_1)) = \frac{sinh(\phi(r_2 - r_1))}{cosh(\phi(r_2 - r_1))} \tag{B.61}$$

The integration constant C_6 is obtained by substituting Eq. (B.56) into (B.54):

$$C_6 = \zeta\left(C_3 e^{\phi r_2} + C_4 e^{-\phi r_2}\right) - \zeta\phi r_2\left(C_3 e^{\phi r_2} - C_4 e^{-\phi r_2}\right),$$

and

$$C_6 = \zeta\left(\left(\frac{\phi r_1 + 1}{\phi r_1 - 1}\right)C_4 e^{-2\phi r_1} e^{\phi r_2} + C_4 e^{-\phi r_2}\right) - \zeta\phi r_2\left(\left(\frac{\phi r_1 + 1}{\phi r_1 - 1}\right)C_4 e^{-2\phi r_1} e^{\phi r_2} - C_4 e^{-\phi r_2}\right),$$

$$C_6 = \zeta C_4 e^{-\phi r_1}\left(e^{\phi(r_2 - r_1)}\left(\frac{\phi r_1 + 1}{\phi r_1 - 1}\right) + e^{-\phi(r_2 - r_1)}\right) - \zeta\phi r_2 C_4 e^{-\phi r_1}\left(e^{\phi(r_2 - r_1)}\left(\frac{\phi r_1 + 1}{\phi r_1 - 1}\right) - e^{-\phi(r_2 - r_1)}\right),$$

$$C_6 = \zeta C_4 e^{-\phi r_1}\frac{\phi r_1 e^{\phi(r_2 - r_1)} + e^{\phi(r_2 - r_1)} + \phi r_1 e^{-\phi(r_2 - r_1)} - e^{-\phi(r_2 - r_1)}}{\phi r_1 - 1} - \zeta\phi r_2 C_4 e^{-\phi r_1}\frac{\phi r_1 e^{\phi(r_2 - r_1)} + e^{\phi(r_2 - r_1)} - \phi r_1 e^{-\phi(r_2 - r_1)} + e^{-\phi(r_2 - r_1)}}{\phi r_1 - 1},$$

$$C_6 = 2\zeta C_4 e^{-\phi r_1}\frac{\phi r_1 cosh(\phi(r_2 - r_1)) + sinh(\phi r(r_2 - r_1))}{\phi r_1 - 1} - 2\zeta\phi r_2 C_4 e^{-\phi r_1}\frac{\phi r_1 sinh(\phi(r_2 - r_1)) + cosh(\phi(r_2 - r_1))}{\phi r_1 - 1},$$

$$C_6 = \frac{2\zeta C_4 e^{-\phi r_1} cosh(\phi(r_2 - r_1))\begin{pmatrix} tanh(\phi(r_2 - r_1)) - \phi^2 r_1 r_2\ tanh(\phi(r_2 - r_1)) \\ -\phi r_2 + \phi r_1 \end{pmatrix}}{\phi r_1 - 1},$$

$$C_6 = \frac{2\zeta C_4 e^{-\phi r_1} cosh(\phi(r_2 - r_1))\left(tanh(\phi(r_2 - r_1))(1 - \phi^2 r_1 r_2) + \phi(r_1 - r_2)\right)}{\phi r_1 - 1}.$$

(B.62)

Inserting Eq. (B.58) into (B.55):

$$C_6\left(1 - \frac{1}{Bi}\right) + \frac{2C_4 e^{-\phi r_1} cosh(\phi(r_2 - r_1))(\phi r_1 + tanh(\phi(r_2 - r_1)))}{r_2(\phi r_1 - 1)} - \frac{C_6}{r_2} = 1,$$

$$C_6\left(1 - \frac{1}{Bi} - \frac{1}{r_2}\right) + \frac{2C_4 e^{-\phi r_1} cosh(\phi(r_2 - r_1))(\phi r_1 + tanh(\phi(r_2 - r_1)))}{r_2(\phi r_1 - 1)} = 1$$

(B.63)

Then the constant C_4 is obtained by substituting Eq. (B.62) into (B.63):

$$\frac{2\zeta C_4 e^{-\phi r_1} cosh(\phi(r_2 - r_1))\left(tanh(\phi(r_2 - r_1))(1 - \phi^2 r_1 r_2) + \phi(r_1 - r_2)\right)}{\phi r_1 - 1} \times \left(1 - \frac{1}{Bi} - \frac{1}{r_2}\right) + \frac{2C_4 e^{-\phi r_1} cosh(\phi(r_2 - r_1))(\phi r_1 + tanh(\phi(r_2 - r_1)))}{r_2(\phi r_1 - 1)} = 1 \quad \text{(B.64)}$$

$$\frac{2\zeta C_4 e^{-\phi r_1} cosh(\phi(r_2-r_1))\,(tanh(\phi(r_2-r_1))(1-\phi^2 r_1 r_2)+\phi(r_1-r_2))r_2\left(1-\frac{1}{Bi}-\frac{1}{r_2}\right)}{r_2(\phi r_1-1)}+$$

$$\frac{2C_4 e^{-\phi r_1} cosh(\phi(r_2-r_1))(\phi r_1+tanh(\phi(r_2-r_1)))}{r_2(\phi r_1-1)}=1$$

$$2\zeta e^{-\phi r_1} cosh(\phi(r_2-r_1))\,(tanh(\phi(r_2-r_1))(\phi^2 r_1 r_2-1)+\phi(r_2-r_1))\left(1-r_2+\frac{r_2}{Bi}\right)\;+$$

$$2e^{-\phi r_1} cosh(\phi(r_2-r_1))(\phi r_1+tanh(\phi(r_2-r_1)))=\frac{r_2(\phi r_1-1)}{C_4}$$

$$C_4=\frac{r_2(\phi r_1-1)/2e^{-\phi r_1} cosh(\phi(r_2-r_1))}{\left\{(tanh(\phi(r_2-r_1))(\phi^2 r_1 r_2-1)+\phi(r_2-r_1))\zeta\left(1-r_2+\frac{r_2}{Bi}\right)\right\}+\{\phi r_1+tanh(\phi(r_2-r_1))\}}$$

(B.65)

The integration constant C_3 is recovered by substituting Eq. (B.65) into (B.56):

$$C_3=\left(\frac{\phi r_1+1}{\phi r_1-1}\right)e^{-2\phi r_1}\times$$

$$\frac{r_2(\phi r_1-1)/2e^{-\phi r_1} cosh(\phi(r_2-r_1))}{\left\{(tanh(\phi(r_2-r_1))(\phi^2 r_1 r_2-1)+\phi(r_2-r_1))\zeta\left(1-r_2+\frac{r_2}{Bi}\right)\right\}+\{\phi r_1+tanh(\phi(r_2-r_1))\}}$$

$$C_3=\frac{r_2(\phi r_1+1)e^{-\phi r_1}/2cosh(\phi(r_2-r_1))}{\left\{(tanh(\phi(r_2-r_1))(\phi^2 r_1 r_2-1)+\phi(r_2-r_1))\zeta\left(1-r_2+\frac{r_2}{Bi}\right)\right\}+\{\phi r_1+tanh(\phi(r_2-r_1))\}} \quad \text{(B.66)}$$

The integration constant C_1 is determined by substituting Eq. (B.65) into (B.57):

$$C_1=\frac{2e^{-\phi r_1}\phi}{\phi r_1-1}\cdot\frac{r_2(\phi r_1-1)/2e^{-\phi r_1} cosh(\phi(r_2-r_1))}{\left\{(tanh(\phi(r_2-r_1))(\phi^2 r_1 r_2-1)+\phi(r_2-r_1))\zeta\left(1-r_2+\frac{r_2}{Bi}\right)\right\}+\{\phi r_1+tanh(\phi(r_2-r_1))\}}$$

$$C_1=\frac{\phi r_2/cosh(\phi(r_2-r_1))}{\left\{(tanh(\phi(r_2-r_1))(\phi^2 r_1 r_2-1)+\phi(r_2-r_1))\zeta\left(1-r_2+\frac{r_2}{Bi}\right)\right\}+\{\phi r_1+tanh(\phi(r_2-r_1))\}}$$

(B.67)

The integration constant C_6 is determined by inserting Eq. (B.65) into (B.62):

$$C_6=\frac{2\zeta e^{-\phi r_1} cosh(\phi(r_2-r_1))\,(tanh(\phi(r_2-r_1))(\phi^2 r_1 r_2-1)+\phi(r_2-r_1))}{\phi r_1-1}\times$$

$$\frac{r_2(\phi r_1-1)/2e^{-\phi r_1} cosh(\phi(r_2-r_1))}{\left\{(tanh(\phi(r_2-r_1))(\phi^2 r_1 r_2-1)+\phi(r_2-r_1))\zeta\left(1-r_2+\frac{r_2}{Bi}\right)\right\}+\{\phi r_1+tanh(\phi(r_2-r_1))\}}$$

$$C_6 = \frac{\zeta r_2 \left(tanh(\phi(r_2 - r_1))(\phi^2 r_1 r_2 - 1) + \phi(r_2 - r_1)\right)}{\left\{(tanh(\phi(r_2 - r_1))(\phi^2 r_1 r_2 - 1) + \phi(r_2 - r_1))\zeta\left(1 - r_2 + \frac{r_2}{Bi}\right)\right\} + \{\phi r_1 + tanh(\phi(r_2 - r_1))\}}$$

(B.68)

Finally, by substituting the value of constant C_1 by Eq. (B.67) and $C_2 = 0$ into Eq.(B.37), the reactant concentration in the first region for the spherical pellet can be determined using the following equation:

$$\underline{c}_1 = \frac{\phi r_2 / cosh(\phi(r_2 - r_1))}{\left\{(tanh(\phi(r_2 - r_1))(\phi^2 r_1 r_2 - 1) + \phi(r_2 - r_1))\zeta\left(1 - r_2 + \frac{r_2}{Bi}\right)\right\} + \{\phi r_1 + tanh(\phi(r_2 - r_1))\}}$$

(B.69)

The reactant concentration distribution in the second region is obtained by substituting the values of constant C_3 by Eq. (B.56) and constant C_4 by Eq. (B.65) into Eq. (B.43) as:

$$\underline{c}_2\left(\underline{x}\right) = \frac{e^{\phi \underline{x}}}{\underline{x}} \frac{r_2(\phi r_1 + 1)e^{-\phi r_1}/2cosh(\phi(r_2 - r_1))}{\left\{(tanh(\phi(r_2 - r_1))(\phi^2 r_1 r_2 - 1) + \phi(r_2 - r_1))\zeta\left(1 - r_2 + \frac{r_2}{Bi}\right)\right\} + \{\phi r_1 + tanh(\phi(r_2 - r_1))\}} +$$

$$\frac{e^{-\phi \underline{x}}}{\underline{x}} \frac{r_2(\phi r_1 - 1)/2e^{-\phi r_1}cosh(\phi(r_2 - r_1))}{\left\{(tanh(\phi(r_2 - r_1))(\phi^2 r_1 r_2 - 1) + \phi(r_2 - r_1))\zeta\left(1 - r_2 + \frac{r_2}{Bi}\right)\right\} + \{\phi r_1 + tanh(\phi(r_2 - r_1))\}}$$

$$= \frac{1}{\underline{x}} \frac{e^{\phi \underline{x}} r_2(\phi r_1 + 1)e^{-\phi r_1}/2cosh(\phi(r_2 - r_1)) \; + \; e^{-\phi \underline{x}} r_2(\phi r_1 - 1)/2e^{-\phi r_1}cosh(\phi(r_2 - r_1))}{\left\{(tanh(\phi(r_2 - r_1))(\phi^2 r_1 r_2 - 1) + \phi(r_2 - r_1))\zeta\left(1 - r_2 + \frac{r_2}{Bi}\right)\right\} + \{\phi r_1 + tanh(\phi(r_2 - r_1))\}}$$

$$\underline{c}_2\left(\underline{x}\right) = \frac{r_2}{\underline{x}\ cosh(\phi(r_2 - r_1))} \times$$

$$\frac{e^{\phi \underline{x}}(\phi r_1 + 1)e^{-\phi r_1}/2 \; + \; e^{-\phi \underline{x}}(\phi r_1 - 1)e^{\phi r_1}/2}{\left\{(tanh(\phi(r_2 - r_1))(\phi^2 r_1 r_2 - 1) + \phi(r_2 - r_1))\zeta\left(1 - r_2 + \frac{r_2}{Bi}\right)\right\} + \{\phi r_1 + tanh(\phi(r_2 - r_1))\}}$$

$$= \frac{r_2}{\underline{x}\ cosh(\phi(r_2 - r_1))} \times$$

$$\frac{\phi r_1\left(e^{\phi \underline{x}}e^{-\phi r_1} + e^{-\phi \underline{x}}e^{\phi r_1}\right)/2 \; + \; \left(e^{\phi \underline{x}}e^{-\phi r_1} - e^{-\phi \underline{x}}e^{\phi r_1}\right)/2}{\left\{(tanh(\phi(r_2 - r_1))(\phi^2 r_1 r_2 - 1) + \phi(r_2 - r_1))\zeta\left(1 - r_2 + \frac{r_2}{Bi}\right)\right\} + \{\phi r_1 + tanh(\phi(r_2 - r_1))\}}$$

Using the definition of the hyperbolic sine and cosine, the following expression is derived:

$$cosh\left(\phi \underline{x}\right)\left(\phi r_1 cosh\left(\phi r_1\right)-sinh\left(\phi r_1\right)\right)+sinh\left(\phi \underline{x}\right)\left(cosh\left(\phi r_1\right)-\phi r_1 sinh\left(\phi r_1\right)\right)=$$

$$\phi r_1 cosh\left(\phi \underline{x}\right)cosh\left(\phi r_1\right)-cosh\left(\phi \underline{x}\right)sinh\left(\phi r_1\right)+sinh\left(\phi \underline{x}\right)cosh\left(\phi r_1\right)-\phi r_1 sinh\left(\phi \underline{x}\right)sinh\left(\phi r_1\right)=$$

$$\phi r_1 \frac{\left(e^{\phi \underline{x}}+e^{-\phi \underline{x}}\right)}{2}\frac{\left(e^{\phi r_1}+e^{-\phi r_1}\right)}{2}-\frac{\left(e^{\phi \underline{x}}+e^{-\phi \underline{x}}\right)}{2}\frac{\left(e^{\phi r_1}-e^{-\phi r_1}\right)}{2}+$$

$$\frac{\left(e^{\phi \underline{x}}-e^{-\phi \underline{x}}\right)}{2}\frac{\left(e^{\phi r_1}+e^{-\phi r_1}\right)}{2}-\phi r_1 \frac{\left(e^{\phi \underline{x}}-e^{-\phi \underline{x}}\right)}{2}\frac{\left(e^{\phi r_1}-e^{-\phi r_1}\right)}{2}=$$

$$\phi r_1 \frac{\left(e^{\phi \underline{x}}e^{\phi r_1}+e^{-\phi \underline{x}}e^{\phi r_1}+e^{\phi \underline{x}}e^{-\phi r_1}+e^{-\phi \underline{x}}e^{-\phi r_1}\right)}{4}-\frac{\left(e^{\phi \underline{x}}e^{\phi r_1}+e^{-\phi \underline{x}}e^{\phi r_1}-e^{\phi \underline{x}}e^{-\phi r_1}-e^{-\phi \underline{x}}e^{-\phi r_1}\right)}{4}+$$

$$\frac{\left(e^{\phi \underline{x}}e^{\phi r_1}-e^{-\phi \underline{x}}e^{\phi r_1}+e^{\phi \underline{x}}e^{-\phi r_1}-e^{-\phi \underline{x}}e^{-\phi r_1}\right)}{4}-\phi r_1 \frac{\left(e^{\phi \underline{x}}e^{\phi r_1}-e^{-\phi \underline{x}}e^{\phi r_1}-e^{\phi \underline{x}}e^{-\phi r_1}+e^{-\phi \underline{x}}e^{-\phi r_1}\right)}{4}=$$

$$\phi r_1 \frac{\left(\cancel{e^{\phi \underline{x}}e^{\phi r_1}}+e^{-\phi \underline{x}}e^{\phi r_1}+e^{\phi \underline{x}}e^{-\phi r_1}+\cancel{e^{-\phi \underline{x}}e^{-\phi r_1}}\cancel{-e^{\phi \underline{x}}e^{\phi r_1}}+e^{-\phi \underline{x}}e^{\phi r_1}+e^{\phi \underline{x}}e^{-\phi r_1}-\cancel{e^{-\phi \underline{x}}e^{-\phi r_1}}\right)}{4}-$$

$$\frac{\cancel{-e^{\phi \underline{x}}e^{\phi r_1}}-e^{-\phi \underline{x}}e^{\phi r_1}+e^{\phi \underline{x}}e^{-\phi r_1}+\cancel{e^{-\phi \underline{x}}e^{-\phi r_1}}+\cancel{e^{\phi \underline{x}}e^{\phi r_1}}-e^{-\phi \underline{x}}e^{\phi r_1}+e^{\phi \underline{x}}e^{-\phi r_1}-\cancel{e^{-\phi \underline{x}}e^{-\phi r_1}}}{4}=$$

$$\phi r_1\left(\frac{e^{-\phi \underline{x}}e^{\phi r_1}+e^{\phi \underline{x}}e^{-\phi r_1}}{2}\right)+\left(\frac{e^{\phi \underline{x}}e^{-\phi r_1}-e^{-\phi \underline{x}}e^{\phi r_1}}{2}\right)$$

Thus, the reactant concentration distribution in the second region is obtained as follows:

$$\underline{c}_2\left(\underline{x}\right)=\frac{r_2}{\underline{x}\ cosh\left(\phi\left(r_2-r_1\right)\right)}\times$$

$$\frac{cosh\left(\phi \underline{x}\right)\left(\phi r_1 cosh\left(\phi r_1\right)-sinh\left(\phi r_1\right)\right)+sinh\left(\phi \underline{x}\right)\left(cosh\left(\phi r_1\right)-\phi r_1 sinh\left(\phi r_1\right)\right)}{\left\{\left(tanh\left(\phi\left(r_2-r_1\right)\right)\left(\phi^2 r_1 r_2-1\right)+\phi\left(r_2-r_1\right)\right)\zeta\left(1-r_2+\frac{r_2}{Bi}\right)\right\}+\left\{\phi r_1+tanh\left(\phi\left(r_2-r_1\right)\right)\right\}} \tag{B.70}$$

The reactant concentration distribution in the third region is obtained by substituting the values of constant C_6 by Eq. (B.68) into Eq.(B.49), where from Eq. (B.55):

$$C_6\left(1-\frac{1}{Bi}\right)+C_5=1,\ C_5=1-C_6\left(1-\frac{1}{Bi}\right)$$

$$\underline{c}_3=C_5+\frac{C_6}{\underline{x}}=\ 1-C_6\left(1-\frac{1}{Bi}\right)+\frac{C_6}{\underline{x}}=1-C_6\left(1-\frac{1}{Bi}+\frac{1}{\underline{x}}\right)$$

Thus, the reactant concentration in the third region is derived as:

$$\underline{c}_3 = 1 - \frac{\zeta r_2 \left(tanh\left(\phi(r_2 - r_1)\right)(\phi^2 r_1 r_2 - 1) + \phi(r_2 - r_1)\right)}{\left\{\left(tanh\left(\phi(r_2 - r_1)\right)(\phi^2 r_1 r_2 - 1) + \phi(r_2 - r_1)\right)\zeta\left(1 - r_2 + \frac{r_2}{Bi}\right)\right\} + \left\{\phi r_1 + tanh\left(\phi(r_2 - r_1)\right)\right\}} \times \left(\frac{1}{Bi} + \frac{1}{\underline{x}} - 1\right) \tag{B.71}$$

Appendix C. Wolfram Mathematica implementation

$$\underline{c}_1 = -\frac{2Bie^{r_1\phi+(r_1+r_2)\phi}(r_1+r_2)\zeta\phi}{\left(\begin{array}{c} -Bie^{2r_1\phi}+Bie^{2(r_1+r_2)\phi}-e^{2r_1\phi}r_1+Bie^{2r_1\phi}r_1+e^{2(r_1+r_2)\phi}r_1-Bie^{2(r_1+r_2)\phi}r_1- \\ e^{2r_1\phi}r_2+Bie^{2r_1\phi}r_2+e^{2(r_1+r_2)\phi}r_2-Bie^{2(r_1+r_2)\phi}r_2+Bie^{2r_1\phi}\zeta-Bie^{2(r_1+r_2)\phi}\zeta-Bie^{2r_1\phi}r_2\phi- \\ Bie^{2(r_1+r_2)\phi}r_2\phi-e^{2r_1\phi}r_1r_2\phi+Bie^{2r_1\phi}r_1r_2\phi-e^{2(r_1+r_2)\phi}r_1r_2\phi+Bie^{2(r_1+r_2)\phi}r_1r_2\phi-e^{2r_1\phi}r_2^2\phi+ \\ Bie^{2r_1\phi}r_2^2\phi-e^{2(r_1+r_2)\phi}r_2^2\phi+Bie^{2(r_1+r_2)\phi}r_2^2\phi-Bie^{2r_1\phi}r_1\zeta\phi-Bie^{2(r_1+r_2)\phi}r_1\zeta\phi+Bie^{2r_1\phi}r_1^2\phi^2- \\ Bie^{2(r_1+r_2)\phi}r_1^2\phi^2+e^{2r_1\phi}r_1^3\phi^2-Bie^{2r_1\phi}r_1^3\phi^2-e^{2(r_1+r_2)\phi}r_1^3\phi^2+Bie^{2(r_1+r_2)\phi}r_1^3\phi^2+Bie^{2r_1\phi}r_1r_2\phi^2- \\ Bie^{2(r_1+r_2)\phi}r_1r_2\phi^2+2e^{2r_1\phi}r_1^2r_2\phi^2-2Bie^{2r_1\phi}r_1^2r_2\phi^2-2e^{2(r_1+r_2)\phi}r_1^2r_2\phi^2+2Bie^{2(r_1+r_2)\phi}r_1^2r_2\phi^2+ \\ e^{2r_1\phi}r_1r_2^2\phi^2-Bie^{2r_1\phi}r_1r_2^2\phi^2-e^{2(r_1+r_2)\phi}r_1r_2^2\phi^2+Bie^{2(r_1+r_2)\phi}r_1r_2^2\phi^2 \end{array}\right)}$$

$$\underline{c}_2(\underline{x}) = \frac{-\left(Bie^{(r_1+r_2)\phi-\underline{x}\phi}(r_1+r_2)\zeta(-e^{2r_1\phi}+e^{2\underline{x}\phi}+e^{2r_1\phi}r_1\phi+e^{2\underline{x}\phi}r_1\phi)\right)}{\underline{x}\left(\begin{array}{c} -Bie^{2r_1\phi}+Bie^{2(r_1+r_2)\phi}-e^{2r_1\phi}r_1+Bie^{2r_1\phi}r_1+e^{2(r_1+r_2)\phi}r_1-Bie^{2(r_1+r_2)\phi}r_1- \\ e^{2r_1\phi}r_2+Bie^{2r_1\phi}r_2+e^{2(r_1+r_2)\phi}r_2-Bie^{2(r_1+r_2)\phi}r_2+Bie^{2r_1\phi}\zeta-Bie^{2(r_1+r_2)\phi}\zeta-Bie^{2r_1\phi}r_2\phi- \\ Bie^{2(r_1+r_2)\phi}r_2\phi-e^{2r_1\phi}r_1r_2\phi+Bie^{2r_1\phi}r_1r_2\phi-e^{2(r_1+r_2)\phi}r_1r_2\phi+Bie^{2(r_1+r_2)\phi}r_1r_2\phi-e^{2r_1\phi}r_2^2\phi+ \\ Bie^{2r_1\phi}r_2^2\phi-e^{2(r_1+r_2)\phi}r_2^2\phi+Bie^{2(r_1+r_2)\phi}r_2^2\phi-Bie^{2r_1\phi}r_1\zeta\phi-Bie^{2(r_1+r_2)\phi}r_1\zeta\phi+Bie^{2r_1\phi}r_1^2\phi^2- \\ Bie^{2(r_1+r_2)\phi}r_1^2\phi^2+e^{2r_1\phi}r_1^3\phi^2-Bie^{2r_1\phi}r_1^3\phi^2-e^{2(r_1+r_2)\phi}r_1^3\phi^2+Bie^{2(r_1+r_2)\phi}r_1^3\phi^2+Bie^{2r_1\phi}r_1r_2\phi^2- \\ Bie^{2(r_1+r_2)\phi}r_1r_2\phi^2+2e^{2r_1\phi}r_1^2r_2\phi^2-2Bie^{2r_1\phi}r_1^2r_2\phi^2-2e^{2(r_1+r_2)\phi}r_1^2r_2\phi^2+2Bie^{2(r_1+r_2)\phi}r_1^2r_2\phi^2+ \\ e^{2r_1\phi}r_1r_2^2\phi^2-Bie^{2r_1\phi}r_1r_2^2\phi^2-e^{2(r_1+r_2)\phi}r_1r_2^2\phi^2+Bie^{2(r_1+r_2)\phi}r_1r_2^2\phi^2 \end{array}\right)}$$

$$\underline{c}_3(\underline{x}) = \frac{\left(\begin{array}{c} (-Bie^{2r_1\phi}r_1+Bie^{2(r_1+r_2)\phi}r_1-Bie^{2r_1\phi}r_2+Bie^{2(r_1+r_2)\phi}r_2+Bie^{2r_1\phi}\underline{x}-Bie^{2(r_1+r_2)\phi}\underline{x}- \\ Bie^{2r_1\phi}\underline{x}\zeta+Bie^{2(r_1+r_2)\phi}\underline{x}\zeta-Bie^{2r_1\phi}r_1r_2\phi-Bie^{2(r_1+r_2)\phi}r_1r_2\phi-Bie^{2r_1\phi}r_2^2\phi-Bie^{2(r_1+r_2)\phi}r_2^2\phi+ \\ Bie^{2r_1\phi}r_2\underline{x}\phi+Bie^{2(r_1+r_2)\phi}r_2\underline{x}\phi+Bie^{2r_1\phi}r_1\underline{x}\zeta\phi+Bie^{2(r_1+r_2)\phi}r_1\underline{x}\zeta\phi+Bie^{2r_1\phi}r_1^3\phi^2-Bie^{2(r_1+r_2)\phi}r_1^3\phi^2+ \\ 2Bie^{2r_1\phi}r_1^2r_2\phi^2-2Bie^{2(r_1+r_2)\phi}r_1^2r_2\phi^2+Bie^{2r_1\phi}r_1r_2^2\phi^2-Bie^{2(r_1+r_2)\phi}r_1r_2^2\phi^2- \\ Bie^{2r_1\phi}r_1^2\underline{x}\phi^2+Bie^{2(r_1+r_2)\phi}r_1^2\underline{x}\phi^2-Bie^{2r_1\phi}r_1r_2\underline{x}\phi^2+Bie^{2(r_1+r_2)\phi}r_1r_2\underline{x}\phi^2) \end{array}\right)}{\underline{x}\left(\begin{array}{c} Bie^{2r_1\phi}-Bie^{2(r_1+r_2)\phi}+e^{2r_1\phi}r_1-Bie^{2r_1\phi}r_1-e^{2(r_1+r_2)\phi}r_1+Bie^{2(r_1+r_2)\phi}r_1+ \\ e^{2r_1\phi}r_2-Bie^{2r_1\phi}r_2-e^{2(r_1+r_2)\phi}r_2+Bie^{2(r_1+r_2)\phi}r_2-Bie^{2r_1\phi}\zeta+Bie^{2(r_1+r_2)\phi}\zeta+Bie^{2r_1\phi}r_2+ \\ Bie^{2(r_1+r_2)\phi}r_2\phi+e^{2r_1\phi}r_1r_2\phi-Bie^{2r_1\phi}r_1r_2\phi+e^{2(r_1+r_2)\phi}r_1r_2\phi-Bie^{2(r_1+r_2)\phi}r_1r_2\phi+e^{2r_1\phi}r_2^2\phi- \\ Bie^{2r_1\phi}r_2^2\phi+e^{2(r_1+r_2)\phi}r_2^2\phi-Bie^{2(r_1+r_2)\phi}r_2^2\phi+Bie^{2r_1\phi}r_1\zeta\phi+Bie^{2(r_1+r_2)\phi}r_1\zeta\phi-Bie^{2r_1\phi}r_1^2\phi^2+ \\ Bie^{2(r_1+r_2)\phi}r_1^2\phi^2-e^{2r_1\phi}r_1^3\phi^2+Bie^{2r_1\phi}r_1^3\phi^2+e^{2(r_1+r_2)\phi}r_1^3\phi^2-Bie^{2(r_1+r_2)\phi}r_1^3\phi^2-Bie^{2r_1\phi}r_1r_2\phi^2+ \\ Bie^{2(r_1+r_2)\phi}r_1r_2\phi^2-2e^{2r_1\phi}r_1^2r_2\phi^2+2Bie^{2r_1\phi}r_1^2r_2\phi^2+2e^{2(r_1+r_2)\phi}r_1^2r_2\phi^2-2Bie^{2(r_1+r_2)\phi}r_1^2r_2\phi^2- \\ e^{2r_1\phi}r_1r_2^2\phi^2+Bie^{2r_1\phi}r_1r_2^2\phi^2+e^{2(r_1+r_2)\phi}r_1r_2^2\phi^2-Bie^{2(r_1+r_2)\phi}r_1r_2^2\phi^2 \end{array}\right)}$$

Appendix D. The values of the effectiveness factor for different parameters

Table D.1: The values of the effectiveness factor for different parameters

z	ϕ	β	γ	n	Bi_m	Bi_h	r_1	r_2	$\underline{x}_1$	Δ	η (non-uniform)	η (uniform)
0	0.5	0.1	5	0.5 1.5	100	100	0.45	0.55	0.5	0.08	0.99523 0.88708	0.09999 0.09877
2	0.5	0.1	5	0.5 1.5	100	100	0.45	0.55	0.5	0.08	0.99825 0.92601	0.07525 0.07481
0	0.5	0.1	5	1	100	100	0.1	0.9	0.5	0.02 0.2 2.0	0.93531 0.94458 0.95156	0.76917 0.76917 0.76917
2	0.5	0.1	5	1	100	100	0.1	0.9	0.5	0.02 0.2 2.0	0.95821 0.97421 0.98545	0.72036 0.72036 0.72036
0	0.5	0.1	5	1	100	100	0.1	0.9	0.2 0.8	0.02	0.89600 0.97434	0.76917 0.76917
2	0.5	0.1	5	1	100	100	0.1	0.9	0.2 0.8	0.02	0.83665 0.98946	0.72036 0.72036
0	0.5	0.1	5	1	100	100	0.05 0.3 0.45	0.95 0.7 0.55	0.5	0.2	0.94466 0.94201 0.93646	0.86264 0.39100 0.09938
2	0.5	0.1	5	1	100	100	0.05 0.3 0.45	0.95 0.7 0.55	0.5	0.2	0.97436 0.96948 0.96014	0.84881 0.31316 0.07503

Appendix E. Python code implementation

E.1. Code for concentration and temperature profiles for reaction with the non-uniform distribution of active catalytic material and calculating effectiveness factor

```
import numpy as np
import math
import matplotlib.pyplot as plt
from sympy import sqrt, pi
from scipy import integrate
from scipy.integrate import solve_ivp
#
# dimwnsionless distance from the center to the inner radius of the
intermediate active shell
r1 = 0.05
# dimwnsionless distance from the center to the outer radius of the
intermediate active shell
r2 = 0.95
# Number of interior mesh points
N = 100
M = 100
K = 100
# Thiele modulus
Th = 0.5
# Biot number for mass and heat transfer
Bi=1
# ratio of effective diffusivities of 2 and 3 regions
Y=1
# ratio of effective diffusivities of 1 and 2 regions
Y1=1
# Porosity of the ith region
E1=1
E2=1
E3=1
# reaction exponent n in (0,1) means strong absorption
n=1
# energy generation function
beta = 0.1
# Arrhenius number
gamma = 5
# Ratio of of effective conductivities in regions II and III
k23=1
# Ratio of of effective conductivities in regions II and I
k21=1
# the ratios of characteristic times of diffusion and heat conduction for ith
region
```

```
ψ1=1
ψ2=1
ψ3=1
# Time-independent bulk concentration
Cs=0
# Time-independent bulk temperature
θs=0
# dimensionless center of Gaussian function
x1=0.5
# dimensionless width of Gaussian distribution
Δ=0.08

# The mesh spacing in each region
hI = r1/(N+1)
hII = (r2-r1)/(M+1)
hIII = (1-r2)/(K+1)
#
c = np.zeros(N+M+K)
θ = np.zeros(N+M+K)
dcdt = np.zeros(len(c))
dθdt = np.zeros(len(θ))
x = np.zeros(len(c))

NMK = N+M+K
#
def mol(t, u):
    c[:] = u[0:NMK]     ####################################
    θ[:] = u[NMK:]      ####################################
# left boundary
    c0=4*c[0]/3-c[1]/3
    dcdt[0] = (c[1] - 2.*c[0] + c0)/(hI**2*E1*Y1)
    θ0=4*θ[0]/3-θ[1]/3
    dθdt[0] = ψ1*(θ[1] - 2.*θ[0] + θ0)/(hI**2*Y1)
    for i in range(1,N-1):
        dcdt[i] = (c[i+1] - 2.*u[i] + c[i-1])/(hI**2*E1*Y1)
        dθdt[i] = ψ1*(θ[i+1] - 2.*θ[i] + θ[i-1])/(hI**2*Y1)
#
    cN1 = ((4*c[N]-c[N+1])*Y1*hI-(c[N-2]-4*c[N-1])*hII)/(3.*(Y1*hI+hII))
    θN1 = ((4*θ[N]-θ[N+1])*k21*hI-(θ[N-2]-4*θ[N-1])*hII)/(3.*(k21*hI+hII))
#
    dcdt[N-1] = (cN1 - 2.*c[N-1] + c[N-2])/(hI**2*E1*Y1)
    dθdt[N-1] = ψ1*(θN1 - 2.*θ[N-1] + θ[N-2])/(hI**2*Y1)
#
    x[N]=r1+hII
    dcdt[N] = (c[N+1] - 2.*c[N] + cN1)/(hII**2*E2) - (1/E2)*(np.exp(-((x[N]-
x1)**2)/Δ**2)/(0.8862269254*Δ*(math.erf((r2-x1)/Δ)-math.erf((r1-
x1)/Δ))))*Th**2*c[N]**n*np.exp(gamma*(1-(1/θ[N])))
```

```
    dθdt[N] = ψ2*(θ[N+1] - 2.*θ[N] + θN1)/(hII**2) + ψ2*(np.exp(-((x[N]-
x1)**2)/Δ**2)/(0.8862269254*Δ*(math.erf((r2-x1)/Δ)-math.erf((r1-
x1)/Δ))))*beta*Th**2*c[N]**n*np.exp(gamma*(1-(1/θ[N])))
    for i in range(N+1,N+M-1):
        x[i]=r1+(i-N+1)*hII
        dcdt[i] = (c[i+1] - 2.*c[i] + c[i-1])/(hII**2*E2) - (1/E2)*(np.exp(-
((x[i]-x1)**2)/Δ**2)/(0.8862269254*Δ*(math.erf((r2-x1)/Δ)-math.erf((r1-
x1)/Δ))))*Th**2*c[i]**n*np.exp(gamma*(1-(1/θ[i])))
        dθdt[i] = ψ2*(θ[i+1] - 2.*θ[i] + θ[i-1])/(hII**2) + ψ2*(np.exp(-
((x[i]-x1)**2)/Δ**2)/(0.8862269254*Δ*(math.erf((r2-x1)/Δ)-math.erf((r1-
x1)/Δ))))*beta*Th**2*c[i]**n*np.exp(gamma*(1-(1/θ[i])))
#
    θNM1 = ((4*θ[N+M]-θ[N+M+1])*hII-((θ[N+M-2]-4*θ[N+M-
1])*k23*hIII))/(3.*(hII+k23*hIII))
    cNM1 = ((4*c[N+M]-c[N+M+1])*hII-((c[N+M-2]-4*c[N+M-
1])*Y*hIII))/(3.*(hII+Y*hIII))
    x[N+M-1]=r2-hII
    dcdt[N+M-1] = (cNM1 - 2.*c[N+M-1] + c[N+M-2])/(hII**2*E2) -
(1/E2)*(np.exp(-((x[N+M-1]-x1)**2)/Δ**2)/(0.8862269254*Δ*(math.erf((r2-x1)/Δ)-
math.erf((r1-x1)/Δ))))*Th**2*c[N+M-1]**n*np.exp(gamma*(1-(1/θ[N+M-1])))
    dθdt[N+M-1] = ψ2*(θNM1 - 2.*θ[N+M-1] + θ[N+M-2])/(hII**2) + ψ2*(np.exp(-
((x[N+M-1]-x1)**2)/Δ**2)/(0.8862269254*Δ*(math.erf((r2-x1)/Δ)-math.erf((r1-
x1)/Δ))))*beta*Th**2*c[N+M-1]**n*np.exp(gamma*(1-(1/θ[N+M-1])))
#
    dcdt[N+M]=(c[N+M+1] - 2.*c[N+M] + cNM1)/(hIII**2*E3*Y)
    dθdt[N+M]=ψ3*(θ[N+M+1] - 2.*θ[N+M] + θNM1)/(hIII**2*Y)
    for i in range(N+M+1, N+M+K-1):
        dcdt[i] = (c[i+1] - 2.*c[i] + c[i-1])/(hIII**2*E3*Y)
        dθdt[i] = ψ3*(θ[i+1] - 2.*θ[i] + θ[i-1])/(hIII**2*Y)
#
    cNMK1 = (2*hIII*Bi + 2*hIII*Bi*Cs + 4*c[N+M+K-1]-c[N+M+K-2])/(3. +
2*hIII*Bi)
    θNMK1 = (2*hIII*Bi + 2*hIII*Bi*θs + 4*θ[N+M+K-1]-θ[N+M+K-2])/(3. +
2*hIII*Bi)
#
    dcdt[N+M+K-1] = (cNMK1 - 2.*c[N+M+K-1] + c[N+M+K-2])/(hIII**2*E3*Y)
    dθdt[N+M+K-1] = ψ3*(θNMK1 - 2.*θ[N+M+K-1] + θ[N+M+K-2])/(hIII**2*Y)
    dudt = np.concatenate([dcdt,
dθdt])  ########################################
    return [dudt]
# initial conditions
c_in = np.ones(len(c))
θ_in = np.ones(len(θ))
u_in = np.concatenate([c_in, θ_in])
u_in=u_in*0.001
t_span = (0.0, 30)
sol = solve_ivp(mol, t_span, u_in, method='LSODA')
# Extract results for c and θ
c_result = sol.y[0:NMK]
```

```
θ_result = sol.y[NMK:]
#
x = np.zeros(N+M+K+4)

for ii in range (1,N+1):
    x[ii] = ii*hI
x[N+1] = r1
for ii in range (1, M+1):
    x[ii+N+1] = r1 + ii*hII
x[N+M+2] = r2
for ii in range (1,K+1) :
    x[ii+N+M+2] = r2 + ii*hIII
x[N+M+K+3]=1.

Y = np.zeros(len(x))

c0=4*sol.y[0,len(sol.t)-1]/3-sol.y[1,len(sol.t)-1]/3
c_1layer_boundary1 =((4*sol.y[N,len(sol.t)-1]-sol.y[N+1,len(sol.t)-1])*hI-
(sol.y[N-2,len(sol.t)-1]-4*sol.y[N-1,len(sol.t)-1])*hII)/(3.*(hI*Y1+hII))
c_2layer_boundary1 =((4*sol.y[N+M,len(sol.t)-1]-sol.y[N+M+1,len(sol.t)-
1])*hII-(sol.y[N+M-2,len(sol.t)-1]-4*sol.y[N+M-1,len(sol.t)-
1])*hIII)/(3.*(hII+hIII))
c_right_boundary = (2*hIII*Bi + 2*hIII*Bi*Cs + 4*sol.y[N+M+K-1,len(sol.t)-1]-
sol.y[N+M+K-2,len(sol.t)-1])/(3. + 2*hIII*Bi)

#effectiveness factor by dc/dx
#dC_dx_1=(3*c_right_boundary-4*sol.y[N+M+K-1,len(sol.t)-1]+sol.y[N+M+K-
2,len(sol.t)-1])/(2*hIII)
#print(dC_dx_1)
effectivenessfactor=(1/Th**2)*Bi*(1-c_right_boundary)
print(effectivenessfactor)

#effectiveness factor by integration
xx=np.zeros(M+2)
xx[0]=r1
xx[M+1]=r2
for i in range (1, M+1):
    xx[i] = r1 + i*hII
    #cc[i] = sol.y[N+i-1,len(sol.t)-1]

Y = np.hstack([c0, sol.y[0:N,len(sol.t)-
1],c_1layer_boundary1,sol.y[N:N+M,len(sol.t)-
1],c_2layer_boundary1,sol.y[N+M:N+M+K,len(sol.t)-1],c_right_boundary])
cc=np.zeros(M+2)
cc[0]=c_1layer_boundary1
cc[1:M+1]=Y[N+2:N+M+2]
cc[M+1]=c_2layer_boundary1

plt.plot(x,Y)
```

```
plt.plot(xx,cc,'o')
plt.xlabel('Dimensionless distance, x[-]')
plt.ylabel('Dimensionless concentration $c_A$[-]')
plt.show()

plt.savefig('Figure1_power.png', dpi=600)
plt.savefig('Figure1.pdf', dpi=600)
plt.show()
#
Y = np.zeros(len(x))

θ0=4*sol.y[NMK+0,len(sol.t)-1]/3-sol.y[NMK+1,len(sol.t)-1]/3
θ_1layer_boundary1 =((4*sol.y[NMK+N,len(sol.t)-1]-sol.y[NMK+N+1,len(sol.t)-
1])*k21*hI-(sol.y[NMK+N-2,len(sol.t)-1]-4*sol.y[N-1+NMK,len(sol.t)-
1])*hII)/(3.*(hI*k21+hII))
θ_2layer_boundary1 =((4*sol.y[NMK+N+M,len(sol.t)-1]-
sol.y[NMK+N+M+1,len(sol.t)-1])*hII-(sol.y[NMK+N+M-2,len(sol.t)-1]-
4*sol.y[NMK+N+M-1,len(sol.t)-1])*k23*hIII)/(3.*(hII+k23*hIII))
θ_right_boundary = (2*hIII*Bi + 2*hIII*Bi*θs + 4*sol.y[NMK+N+M+K-1,len(sol.t)-
1]-sol.y[NMK+N+M+K-2,len(sol.t)-1])/(3. + 2*hIII*Bi)

Y = np.hstack([θ0, sol.y[NMK+0:NMK+N,len(sol.t)-
1],θ_1layer_boundary1,sol.y[NMK+N:NMK+N+M,len(sol.t)-
1],θ_2layer_boundary1,sol.y[NMK+N+M:NMK+N+M+K,len(sol.t)-1],θ_right_boundary])
θθ=np.zeros(M+2)
θθ[0]=θ_1layer_boundary1
θθ[1:M+1]=Y[N+2:N+M+2]
θθ[M+1]=θ_2layer_boundary1
plt.plot(x,Y)
plt.plot(xx,θθ,'o')
plt.xlabel('Dimensionless distance, x[-]')
plt.ylabel('Dimensionless temperature, θ[-]')

plt.show()

a=np.zeros(len(xx))
f=np.zeros(len(xx))
kk=np.zeros(len(f))
for i in range (0, M+2):
    a[i] = np.exp(-((xx[i]-x1)**2)/Δ**2)/(0.8862269254*Δ*(math.erf((r2-x1)/Δ)-
math.erf((r1-x1)/Δ)))
    f[i] = (cc[i])**n*np.exp(gamma*(1-(1/θθ[i])))
    kk[i]=a[i]*f[i]
int=integrate.cumtrapz(kk, xx, initial=0)
print("f=", int)

plt.savefig('Figure1_power.png', dpi=600)
plt.savefig('Figure1.pdf', dpi=600)
plt.show()
```

E.2. Code for comparison of analytical and numerical solutions for the first order reaction with a step-distribution of active material

```
import numpy as np
import scipy.sparse
import scipy.sparse.linalg
import matplotlib.pyplot as plt
from scipy.integrate import solve_ivp
#
plt.rc('font', family='serif')
plt.rc('figure',figsize=(7, 6))
plt.rc('text', usetex=True)
plt.rc('xtick', labelsize=14)
plt.rc('ytick', labelsize=14)
plt.rc('axes', labelsize=14)
#
#for sphere
# analytical
# Thiele modulus
Th = 1.5
# dimensionless distance from center to inner radius of intermediate active
shell
r1 = 0.45
# dimensionless distance from center to outer radius of intermediate active
shell
r2 =  0.55
# Biot number
Bi = 100
# ratio of effective diffusivities of 2 and 3 regions
Y=1
#
x=np.linspace(0,r1,304)
var1=(Th*(r2))/np.cosh(Th*(r2-r1))
var2=Th*r1+np.tanh(Th*(r2-r1))
var3=(Y)*(1-(r2) + (r2)/Bi)
var4=(Th**2*r1*(r2)-1)*np.tanh(Th*(r2-r1))+Th*(r2-r1)
c1=var1/(var2+var3*var4) # concentration c1
print(c1)
plt.plot([0,r1], [c1,c1], '-k', linewidth = 1.2, label = 'Analytical')
x = np.linspace(r1,r2,304)
var2=Th*r1+np.tanh(Th*(r2-r1))
var3=(Y)*(1-(r2) + (r2)/Bi)
var4=(Th**2*r1*(r2)-1)*np.tanh(Th*(r2-r1))+Th*(r2-r1)
var5 = ((Th*r1*np.cosh(Th*r1)-np.sinh(Th*r1))*np.cosh(Th*x))/np.cosh(Th*(r2-
r1))
```

```
var6=((np.cosh(Th*r1)-Th*r1*np.sinh(Th*r1))*np.sinh(Th*x))/np.cosh(Th*(r2-r1))
c2 = ((r2)*(var5+var6))/((var2+var3*var4)*x)  # concentration c2
plt.plot(x,c2, '-k', linewidth = 1.2)
plt.plot(x,c2, '-k', linewidth = 1.2)
x = np.linspace(r2,1,304)
var2=Th*r1+np.tanh(Th*(r2-r1))
var3=(Y)*(1-(r2) + (r2)/Bi)
var4=(Th**2*r1*(r2)-1)*np.tanh(Th*(r2-r1))+Th*(r2-r1)
var7=Th*(r2-r1)+(Th**2*r1*(r2)-1)*np.tanh(Th*(r2-r1))
c3 = 1-(((r2)*Y)*((1/x)-1+(1/Bi))*(var7/(var2+var3*var4))) # concentration c3
plt.plot(x,c3, '-k', linewidth = 1.2)
#
# numerical
# dimensionless distance from center to inner radius of intermediate active
shell
r1 = 0.45
# dimensionless distance from center to outer radius of intermediate active
shell
r2 =  0.55
# Number of interior mesh points
N = 100
M = 100
K = 100
# Thiele modulus
Th = 1.5
# Biot number
Bi=100
# The mesh spacing in each region
hI = r1/(N+1)
hII = (r2-r1)/(M+1)
hIII = (1-r2)/(K+1)
#
u = np.zeros(N+M+K)
dudt = np.zeros(len(u))
x = np.zeros(len(u))
#
def mol(t, u):
# left boundary
    u0=4*u[0]/3-u[1]/3
    x[0]=hI
    dudt[0] = (u[1] - 2.*u[0] + u0)/(hI**2) + (2./x[0])*((u[1] - u0)/(2.*hI))
#
    for i in range(1,N-1):
        x[i]=(i+1)*hI
        dudt[i] = (u[i+1] - 2.*u[i] + u[i-1])/(hI**2) + (2./x[i])*((u[i+1] -
u[i-1])/(2.*hI))
#
    uN1 = ((4*u[N]-u[N+1])*hI-(u[N-2]-4*u[N-1])*hII)/(3.*(hI+hII))
#
```

```
    x[N-1]=r1-hI
    dudt[N-1] = (uN1 - 2.*u[N-1] + u[N-2])/(hI**2) + (2/x[N-1])*((uN1 - u[N-
2])/(2.*hI))
#
    x[N]=r1+hII
    dudt[N] = (u[N+1] - 2.*u[N] + uN1)/(hII**2) + (2./x[N])*((u[N+1] -
uN1)/(2*hII)) - Th**2*u[N]
    for i in range(N+1,N+M-1):
        x[i]=r1+(i-N+1)*hII
        dudt[i] = (u[i+1] - 2.*u[i] + u[i-1])/(hII**2) + (2./x[i])*((u[i+1] -
u[i-1])/(2*hII)) - Th**2*u[i]
    uNM1 = ((4*u[N+M]-u[N+M+1])*hII-(u[N+M-2]-4*u[N+M-
1])*hIII)/(3.*(hII+hIII))
    x[N+M-1]=r2-hII
    dudt[N+M-1] = (uNM1 - 2.*u[N+M-1] + u[N+M-2])/(hII**2) + (2./x[N+M-
1])*((uNM1 - u[N+M-2])/(2.*hII)) - Th**2*u[N+M-1]
#
    x[N+M]=r2+hIII
    dudt[N+M]=(u[N+M+1] - 2.*u[N+M] + uNM1)/(hIII**2) + (2./x[N+M])*((u[N+M+1]
- uNM1)/(2.*hIII))
    for i in range(N+M+1, N+M+K-1):
        x[i]=r2+(i-N-M+1)*hIII
        dudt[i] = (u[i+1] - 2.*u[i] + u[i-1])/(hIII**2) + (2./x[i])*((u[i+1] -
u[i-1])/(2.*hIII))
#
    uNMK1 = (2*hIII*Bi + 4*u[N+M+K-1]-u[N+M+K-2])/(3. + 2.*hIII*Bi)
    x[N+M+K-1]=1.-hIII
    dudt[N+M+K-1] = (uNMK1 - 2.*u[N+M+K-1] + u[N+M+K-2])/(hIII**2) +
(2./x[N+M+K-1])*((uNMK1 - u[N+M+K-2])/(2.*hIII))
    return dudt
# initial conditions
u_in = np.zeros(len(u))
t_span = (0.0, 30)
#t = np.arange(0.0, 0.001, 0.0001)
sol = solve_ivp(mol, t_span, u_in, method='LSODA')
#
x = np.zeros(N+M+K+4)
for ii in range (1,N+1):
    x[ii] = ii*hI
x[N+1] = r1
for ii in range (1, M+1):
    x[ii+N+1] = r1 + ii*hII
x[N+M+2] = r2
for ii in range (1,K+1) :
    x[ii+N+M+2] = r2 + ii*hIII
x[N+M+K+3]=1.

Y = np.zeros(len(x))
#print(sol.y[N-1,len(sol.t)-1])
```

```
#print(c_layer_boundary)
c0=4*sol.y[0,len(sol.t)-1]/3-sol.y[1,len(sol.t)-1]/3
c_1layer_boundary1 =((4*sol.y[N,len(sol.t)-1]-sol.y[N+1,len(sol.t)-1])*hI-
(sol.y[N-2,len(sol.t)-1]-4*sol.y[N-1,len(sol.t)-1])*hII)/(3.*(hI+hII))
c_2layer_boundary1 =((4*sol.y[N+M,len(sol.t)-1]-sol.y[N+M+1,len(sol.t)-
1])*hII-(sol.y[N+M-2,len(sol.t)-1]-4*sol.y[N+M-1,len(sol.t)-
1])*hIII)/(3.*(hII+hIII))
c_right_boundary = (2*hIII*Bi + 4*sol.y[N+M+K-1,len(sol.t)-1]-sol.y[N+M+K-
2,len(sol.t)-1])/(3. + 2*hIII*Bi)
Y = np.hstack([c0, sol.y[0:N,len(sol.t)-
1],c_1layer_boundary1,sol.y[N:N+M,len(sol.t)-
1],c_2layer_boundary1,sol.y[N+M:N+M+K,len(sol.t)-1],c_right_boundary])

plt.ylim(0.85, 0.905)
plt.plot(x,Y, 'r', linestyle='-.' , linewidth = 1.2, label = 'Numerical')
plt.xlabel(r'Distance, $\underline{x}$ [-]',fontsize = 14)
plt.ylabel(r'Concentration, $\underline{c}$ [-]',fontsize = 14)
plt.legend(loc='upper left',fontsize=14)

#
plt.savefig('Figure8.png', dpi=600, bbox_inches='tight')
plt.savefig('Figure8.pdf', dpi=600, bbox_inches='tight')
plt.show()
```